Analysis of Managed Lanes on Freeway Facilities

Xiaoyue Liu

A dissertation submitted in partial fulfillment of the

requirements for the degree of

Doctor of Philosophy

University of Washington

2013

Reading Committee:

Yinhai Wang, Chair

Edward McCormack

Patty Rubstello

Program Authorized to Offer Degree:
Department of Civil and Environmental Engineering

University of Washington

Abstract

Analysis of Managed Lanes on Freeway Facilities

Xiaoyue Liu

Chair of the Supervisory Committee:

Professor Yinhai Wang

Department of Civil and Environmental Engineering

Roadway agencies face growing challenges to expand freeway capacity. Under consideration of rising construction costs, right-of-way limitations, and environmental constraints, transportation agencies are seeking solutions to efficiently manage the demand on existing freeway facilities and to provide options for travelers. The concept of Managed Lanes (MLs) is an increasingly popular countermeasure that aims to make the most efficient use of freeway facilities, by restricting access to one or more lanes, and to certain vehicle classes on a facility that is parallel to existing General Purpose (GP) lanes. With limited work being documented for analytical evaluation of ML facilities, transportation agencies often rely heavily on time-consuming and cost-ineffective simulation experiments for ML performance analysis. Therefore, there is an urging need for a framework to guide the practitioners for a systematic evaluation of ML system. This research aims at filling this gap by developing a methodological framework for analyzing freeway facilities with ML and GP lanes operated in parallel. The framework acknowledges that the composition and behavior characteristics of the ML traffic stream are expected to be quite different from those for the GP

lanes in terms of traffic volume, free-flow speed, capacity, vehicles type, etc. The framework further considers that there may still be certain levels of interactions between these two lane groups, especially for those facilities do not have physical (barrier) separations, either en route or at access points, between them. Within that framework, different modules were developed based on sensor-measured or simulation-generated data, including the characterization of ML speed-flow relationship, the frictional effect of adjacent lane traffic speed, the adjustment for cross-weave effects, and the development of side-by-side facility-wide ML and GP performance measures. Thus, the proposed methodology is sensitive to different GP and ML segment types (basic, weaving, etc.) and separation styles (stripe, buffer, barrier), and is capable of analyzing extended facilities across multiple time periods. The methodology is further implemented in a computational engine for testing and application. Furthermore, a mesoscopic simulation model, entitled twin-cell modeling approach, on the basis of Cell Transmission Model (CTM), is developed in this research to describe the traffic evolution of parallel facilities. The twin-cell modeling approach quantifies the frictional effect, which is unique to the parallel facilities, via data mining techniques, and also incorporates a weaving component that extends the original CTM model to the grid-level parallel facility modeling.

In summary, this research attempts to develop an analytical methodology for evaluating freeways with parallel GP lanes and MLs. The methodology is supported by extensive field data collected at ML facilities in several states of the U.S. The developed methodological framework presents an important, new approach for the performance analysis of ML-enabled freeway segments, which is valuable in providing guidance for analysts in evaluating freeway segments in the presence of concurrent GP lanes and MLs.

Table of Contents

Table of Contents 5

List of Tables 1

List of Figures 3

ACKNOWLEDGEMENT 7

CHAPTER 1 INTRODUCTION 9

1.1 Problem Statement 9

1.1.1 Methodological Framework for Analyzing ML Facilities 10

1.1.2 Data Needs for Quantifying MLs Performance 10

1.1.3 Traffic Flow Models for Modeling the Dynamics on ML Facilities 12

1.1.4 ML Demand Control Capability 12

1.2 Research Background 13

1.2.1 Operational Strategy 14

1.2.2 Separation Type 17

1.2.3 Number of Lanes 17

1.2.4 Access Points 18

1.3 Research Objectives and Originality 19

1.4 Research Scope 22

1.5 Dissertation Organization 23

CHAPTER 2 LITERATURE REVIEW 24

2.1 Methodology for ML Performance Analysis 24
2.1.1 Methodological Framework for Analyzing ML Facilities - Supply-side of roadway infrastructure 24
2.1.2 Demand Analysis for HOT Lane Facilities 27
2.2 ML Traffic Flow Characteristics 29
2.3 ML Weaving Analysis 32
2.4 Traffic Simulation Models and Traffic Flow Theory 33
CHAPTER 3 ML ANALYSIS METHODOLOGY FOR PERFORMANCE ASSESSMENT . 38
3.1 Brief Introduction 38
3.2 HOT Lane Demand Modeling 39
3.2.1 Case Study Site Description 39
3.2.2 Field Data Collection for Modeling HOT Lane Demand 40
3.2.3 Modeling Approach for Quantifying SOVs Response to Tolling 42
3.3 Analysis Methodology for ML Facility Performance (Supply-Side) 46
3.3.1 Methodological Framework for ML Facility 46
3.3.2 Defining ML Analysis Segment 48
3.3.3 Speed-Flow Models Developed for ML Basic Segments 50
3.3.4 Access Point Analysis 55
3.4 Mesoscopic Approach of Twin-Cell Modeling for Parallel Freeway Facilities 55
3.4.1 Basic ML Segment Modeling 56

3.4.2 Weaving Segment Modeling 66

CHAPTER 4 OPERATIONAL CONCEPTS AND TRAFFIC FLOW PRINCIPLES IN MANAGED LANES 69

4.1 Segment Type 69

4.1.1 The Lane Group Concept 69

4.2 Speed-Flow Model Development for Basic ML Segments 71

4.2.1 Different Separation Type Characteristics 72

4.2.2 Data Acquisition 76

4.2.3 Observed Traffic Flow Characteristics of Basic ML Segments 83

4.3 ML Access Points 97

4.3.1 Access Point Configurations for ML facilities 97

4.3.2 Simulation Test Scenario 101

CHAPTER 5 EMPIRICAL AND MODELING RESULTS 104

5.1 HOT Demand Modeling 104

5.1.1 VOT Distribution Analysis for Infrequent Users and Frequent Users 104

5.1.2 Modeling SOV Response to Tolling and Traffic Conditions 108

5.2 Slow Car Following Effect Validation 111

5.3 Speed-Flow Models for Basic ML Segment 114

5.3.1 Continuous Access 114

5.3.2 Buffer 1 117

5.3.3 Buffer 2 119
5.3.4 Barrier 1 120
5.3.5 Barrier 2 122
5.3.6 Comparison of Speed-Flow Models amongst Different Basic ML Types 124
5.4 Modeling of Cross-Weave Effect 126
5.4.1 Simulation Model Calibration 126
5.4.2 Simulation Scenario Setup 128
5.4.3 Simulation Result Analysis 131
5.5 Twin-Cell based Modeling Approach 138
5.5.1 Basic Segment Modeling Result 138
5.5.2 Weaving Segment Modeling 143
CHAPTER 6 CONCLUSIONS AND FUTURE RESEARCH 146
6.1 Summary of Research 147
6.1.1 Identify Incentives for SOVs to Use the HOT Lane Facilities 147
6.1.2 Methodological Framework for Analyzing the ML Facilities 148
6.1.3 Twin-Cell Modeling Approach for Parallel Freeway Facilities 150
6.2 Research Contribution 152
6.3 Future Research 153
REFERENCES 155
REPRINT PERMISSIONS 164

APPENDICES 165

Appendix A..... 165

List of Tables

TABLE 1.1 HOT Lane Projects Open to Traffic in the U.S. as of January 2012 15

TABLE 3.1 CTM Parameters for the Freeway Segment 60

TABLE 3.2 Sensor Data for Calibrating the Friction Model 62

TABLE 3.3 Means of Variables for Each Cluster 64

TABLE 3.4 Robust Regression Result for Friction 66

TABLE 4.1 Continuous Access Data Site, I-5 & I-405 Washington State 77

TABLE 4.2 Continuous Access Data Sites, I-95 Florida 78

TABLE 4.3 Buffer 1 sites at I-405 California 78

TABLE 4.4 Buffer 1 Data Sites, SR-167 Washington State 79

TABLE 4.5 Buffer 1 Data Sites, I-394 Minnesota 79

TABLE 4.6 Buffer 2 Data Site, I-110, Los Angeles, California 80

TABLE 4.7 Barrier 1 Data Site, I-5 Orange County, California 80

TABLE 4.8 Barrier 2 Sites, I-394 Minneaplois, Minnesota 81

TABLE 4.9 Data Site Summary 82

TABLE 4.10 Number of Sample Points for FFSs by Separation Type 83

TABLE 4.11 Operational Parameters Estimated Using Van Aerde's Model 95

TABLE 4.12 Stochastic Capacity Estimation using Weibull Distribution Function 96

TABLE 5.1 Statistic Result for Modeling SOVs Demand to Tolling and Traffic Conditions 110

TABLE 5.2 t-Test Results for Slow Car Following Effect 113

TABLE 5.3 Continuous Access Speed-Flow Model Parameters 116

TABLE 5.4 Speed-Flow Equations for Continuous Access 116

TABLE 5.5 Buffer 1 Speed-Flow Model Parameters 118

TABLE 5.6 Buffer 1 Speed-Flow Equations 118

TABLE 5.7 Buffer 2 Speed-Flow Curve Variable Values..... 120

TABLE 5.8 Buffer 2 Speed-Flow Equations 120

TABLE 5.9 Barrier 1 Speed-Flow Curve Parameters..... 122

TABLE 5.10 Barrier 1 Speed-Flow Equations 122

TABLE 5.11 Barrier 2 Speed-Flow Curve Parameters..... 123

TABLE 5.12 Barrier 2 Speed Flow Equations..... 124

TABLE 5.13 Field Data Reference for $L_{CW\text{-}Min}$ and $L_{CW\text{-}Max}$..... 130

TABLE 5.14 CRF for Each Configuration Scenario 135

TABLE 5.15 Linear Regression Output for CRI and the Corresponding Variables 138

List of Figures

FIGURE 1.1 Time Series of Speed and Flow Plots for SR 91 HOT Lane System in Orange County, California 16

FIGURE 1.2 Schematic of At-Grade Access with Limited Access Point 19

FIGURE 2.1 Existing Methodology Flow Chart based on Chapter 10 in HCM 2010 25

FIGURE 2.2 Flow-Density Relationship for the Basic CTM 35

FIGURE 2.3 Representation of a Merge Area 36

FIGURE 2.4 Network Topology Representation 37

FIGURE 3.1 Location of SR 167 HOT Lane and Segmentation Information (S:segment) 41

FIGURE 3.2 Revised Methodological Flow Chart Incorporating MLs 48

FIGURE 3.3 Different Segment Types for ML and GP Lanes 50

FIGURE 3.4 The Speed-flow Curve Family for Buffer-separated Single ML Facility 57

FIGURE 3.5 Cell Representation of Buffer-separated ML Facility 58

FIGURE 3.6 Flow-density Curves Calibrated for GP Lanes and Buffer-separated ML 59

FIGURE 3.7 Framework of the Traffic Flow Model 60

FIGURE 3.8 Sum of *Within Cluster Sum of Squares* for Different Number of Clusters 63

FIGURE 3.9 Box Plot of Variables *GP Density* and *Friction* for the Six Clusters 65

FIGURE 3.10 A Weaving Representation 66

FIGURE 4.1 Schematic of Continuous Access and Examples at I-5 Seattle, Washington and I-95 in Broward County, Florida (Source: Google Earth) 73

FIGURE 4.2 Schematic of Buffer 1 and Example at I-394 Minneapolis, Minnesota (Source: Google Earth) 74

FIGURE 4.3 Schematic of Buffer 2 and Example at I-110 Los Angeles, California (Source: Google

Earth)..... 74

FIGURE 4.4 Schematic of Barrier 1 and Example at I-5 Orange County, California (Source: Google Earth)..... 75

FIGURE 4.5 Schematic of Barrier 2 and Example at I-5 Seattle, Washington (Source: Google Earth) 76

FIGURE 4.6 Speed Flow Plots for FFS=65 mph for the Five Facility Types 86

FIGURE 4.7 Slow Car Following Effect Observations..... 88

FIGURE 4.8 Speed-Flow Data for Buffer-Separated Facility at SR 167 HOT Lane System in Washington..... 90

FIGURE 4.9 Time Series of Speed and Volume Plot for Buffer-Separated HOV Facility for SR 91 in Orange County, California..... 94

FIGURE 4.10 Speed-Flow Diagram and Van Aerde's Curve Fitting 95

FIGURE 4.11 Estimated Capacity Distribution Functions using PLM and Weibull Method 96

FIGURE 4.12 Illustrated of Access Point Designs 99

FIGURE 4.13 Defining Dimensions of APIA through Minimum and Maximum Cross-Weave Lengths..... 100

FIGURE 5.1 Histogram of SOV Usage on HOT Lane Based on Transponder Record 105

FIGURE 5.2 VOT Histogram for (a) Infrequent Users and (b) Frequent Users, and (c) VOT Cumulative Probability for Infrequent Users and Frequent Users..... 107

FIGURE 5.3 Time Series of Speed Plot for SR 167 NB @ Segment 3..... 109

FIGURE 5.4 Snap Shot of Platoon Effect from Video Data at I-635, Dallas, Texas (Source: University of Texas at Arlington).....112

FIGURE 5.5 Relationship Between Average Speed vs. Platoon Size 113

FIGURE 5.6 Continuous Access Speed-Flow Curves 115

FIGURE 5.7 Buffer 1 Speed-Flow Curves 117

FIGURE 5.8 Buffer 2 Speed Flow Curves 119

FIGURE 5.9 Barrier 1 Speed-Flow Curve 121

FIGURE 5.10 Barrier 2 Speed-Flow Curves 123

FIGURE 5.11 Sample ML Speed-Flow Relationships for FFS=60mph 125

FIGURE 5.12 Lane Configuration of the ML Access Point at IH 635 Dallas, Texas 127

FIGURE 5.13 Video Image for IH 635 ML Access Point 127

FIGURE 5.14 Configuration Used in VISSIM Simulation 129

FIGURE 5.15 Speed-Flow Diagrams from Simulation Output and Van Aerde's Curve Fitting for 4-lane GP Scenarios 133

FIGURE 5.16 CRF as Response to Cross Weave Flow and Lcw-min under 4-Lane GP Scenarios 135

FIGURE 5.17 Cumulative Lane Change Intensity for Different GP Lanes Scenarios with Cross-Weave Flow 300 pcph, and GP Input Demand of 2400 pcphpl 136

FIGURE 5.18 Cumulative Lane Change Intensity for Different $L_{CW\text{-}Min}$ Scenarios with Cross Weave Flow 300 pcph, and GP Input Demand of 2400 pcphpl 137

FIGURE 5.19 Temporal-Spatial Traffic Evolution using HCM-based Approach 139

FIGURE 5.20 Temporal-Spatial Traffic Evolution under Bottleneck Scenario using HCM-based Method 140

FIGURE 5.21 Temporal-Spatial Traffic Evolution under Bottleneck Scenario for Various ML Demand using the Unsupervised Machine Learning Method 142

FIGURE 5.22 Numerical Example 144

FIGURE 5.23 The Weaving Segment with Extended Lateral Building Blocks 145

ACKNOWLEDGEMENT

It has been such a wonderful journey for me to complete this Ph.D. study. I have been given the privilege to spend the past three and a half years in the Department of Civil & Environmental Engineering at the University of Washington, and the opportunity to work with the greatest talents of my field. The department and its people are so influential to me and will always be dear to my heart.

My first and foremost gratitude goes to my supervisor, Dr. Yinhai Wang. His dedication and enthusiasm towards academia have been so empowering that made me simply want to follow his path. Never in my wildest dream would I believe I can become who I am today. It is Dr. Wang that has always pushed me into doing things that I normally would not do myself, that oftentimes turned out to be such a transformation on me.

Special thanks to my Ph.D. committee members, Dr. Qing Shen, Dr. Edward McCormack, and Ms. Patty Rubstello, for their support, guidance and valuable inputs on my research work. My deepest heartful thanks and appreciation for their time and help in reviewing my work.

My sincere thanks to all the STAR Lab members at the University of Washington. Your friendship and support has been the driven force for me to complete my study. I have grown up so much through this learning process. Special thanks goes to Dr. Runze Yu, for all the craziness we had and all the joyful moments we shared; and Ms. Sa Xiao, for your tech-savvy geniuses, and your unconditional help on my research. It is such a privilege to know you two, and I am sure we all have a brilliant future ahead of us. I am also grateful to Dr. Guohui Zhang, former member of

STAR Lab, who has been guiding me through every single step of my study and career. You have paved the way for me and I am so blessed to know you as a friend and as a role model.

My deepest appreciation goes to Dr. Nagui Rouphail and Dr. Bastian Schroeder, who worked with me on the NCHRP 03-96 project, which is the main sponsor of my Ph.D. research. Their vast experience and knowledge base on traffic operations related research have just blown me away. I am also so indebted for their help and guidance on my career search.

My gratitude to all my friends is just beyond words. Thanks for sharing all the joy and laughter, and always being there for me through my high and low. Special thanks go to Kari Watkins, Erica Wygonik, Kelly Pitera, Yen-Yu Lin, Yegor Malinovskiy, Timothy Thomson, and Xiaoyi Liu for all your help, support, and advice.

Lastly and most importantly, I want to thank my family. My husband Xin Chen is my best friend, and the love of my life. I cannot tell you how lucky I am to find you, and thank you for the tremendous love and support you give me every single day. My parents, Jingang Liu and Zhimei Gao, I thank you for your unconditional love, and I dedicate this dissertation to you.

CHAPTER 1 INTRODUCTION

1.1 Problem Statement

According to the 2012 Urban Mobility Report, urban congestion costs about $121.2 billion dollars and a total of 5.52 billion-hour delay in 2011 (Schrank *et al*., 2012). Congestion has surely been massively greater than that in 1982, when the congestion data started being documented. It has also been growing gradually over the past years. Transportation agencies are therefore seeking for alternatives to mitigate the negative impacts of traffic congestion other than roadway expansion. One of the solutions towards this problem is the concept of Managed Lane (ML) and it is becoming more prevalent on freeway facilities. The goal of ML is to make the most efficient use of a freeway facility by combining a variety of operational strategies coupled with limited capacity expansion to manage travel demand.

MLs, as defined by the Federal Highway Administration (FHWA), are *"Highway facilities or a set of lanes in which operational strategies are implemented and managed (in real time) in response to changing conditions"* (Obenberger, 2004). It encompasses a wide range of operational and design practices including High-Occupancy Vehicle (HOV) lanes, express lanes or High-Occupancy Toll (HOT) lanes, and exclusive-use lanes such as Truck-Only Toll (TOT) lanes, etc. (Kuhn, *et al.*, 2005). In general, ML follows the operating philosophy of "active management", where the operating agency proactively manages demand and available capacity by applying restrictions on the existing facility (FHWA, 2012). The restrictions imposed on user groups often include the number of occupants, types of vehicles, and tolling. Obviously, the operational strategies and geometric characteristics of MLs may vary greatly from site to site.

1.1.1 Methodological Framework for Analyzing ML Facilities

Highway Capacity Manual (HCM) has been widely accepted as the guidelines for designing and analyzing freeway facilities. However, its current version, HCM 2010 (TRB, 2010), contains no methodology for MLs, although HOV facilities have been in use since 1970s and many HOT lanes facilities are in operations or under design/deployment. The current HCM freeway methodologies are not applicable to MLs due to the following reasons: (1) ML access control patterns and associated driver behaviors; (2) significant speed differentials between MLs and GP lanes; (3) interaction between tolling and traffic flow dynamics; and (4) slow vehicle constraint on single MLs. Therefore, a methodological framework dedicated to MLs is needed. Development of such a framework requires great efforts for modeling and understanding of the operational strategies and geometric characteristics of freeway facilities with MLs. Given the increasing popularity of MLs, including performance assessment and capacity analysis methods of MLs in HCM is highly desirable and would also greatly enhance its usefulness to engineers, designers, planners, and decision makers.

1.1.2 Data Needs for Quantifying MLs Performance

High quality data are always key to successful analysis. The selected data collection sites should be representative of existing ML facilities covering different operational maneuvers, separation types, number of lanes, as well as operational strategies. The selected sites should have well-functioning traffic sensors to provide quality data for capacity analysis and performance measurement.

In the process of identifying high priority ML sites for field data collection, three guiding criteria are applied:

1. The type of ML should occur frequently on ML facilities throughout the U.S. The key is to capture representative samples of the most common ones. Rare and unusual configurations may have to be examined in the simulation analysis only.
2. The ML operations cannot be captured or described by the current HCM 2010 procedures for GP lanes. For example, a right-hand ramp exit from the GP lanes that then merges with ML from a flyover bridge structure is fully covered by existing HCM methodologies. It is therefore not necessary to analyze this type of access point to MLs.
3. The ML data collection sites should have well-functioning traffic sensors.

Besides the sensor data, the design of access points can have important effects on the operations of both GP lanes and MLs. For example, a weaving access maneuver to the ML can cause friction in the GP lanes. Similarly, a poorly designed ML ramp or weave lane may impose constraints on traffic volumes into the ML facility. For this reason, data collection on quantifying the weaving behavior and other characteristics of access point is considered crucial. Surveillance camera or video recording will help facilitate the analysis of weaving behavior. Therefore, sites with surveillance camera or capable of enabling video-based data collection need to be identified.

Meanwhile, although field data available from the existing ML facilities are desirable for analysis of MLs on freeway facilities, field observations may not be sufficient to cover all analytical scenarios of interest. Well-calibrated, microscopic simulation models will be used to generate synthetic data when adequate field data are not available or feasible to collect. Simulation-based

investigation provides a cost-effective, risk free, and potentially fruitful means of exploring and examining ML system operations.

1.1.3 Traffic Flow Models for Modeling the Dynamics on ML Facilities

It is noted from previous studies (Liu *et al.,* 2011) that the composition and behavior of the ML traffic stream is different from those of traffic in the GP lanes. The dichotomy of geometric and behavioral attributes of parallel MLs and GP lanes, as well as the interaction between traffic operations in the two lane groups, makes it necessary to develop an updated methodology/model, suited particularly to the ML facility. The developed traffic flow model should be capable of analyzing both GP and ML segments on parallel facilities, successfully simulating the traffic evolution dynamics, taking into account the individuality of the two lane groups, as well as the interaction between the two. It is thus imperative to develop such a model functioning as an underlying traffic flow model of ML facilities in evaluation of the performance for freeway segment with MLs.

1.1.4 ML Demand Control Capability

MLs, especially HOT lanes, have the demand control capability. That is because tolling, as the pricing component, can dynamically manage the demand to prevent breakdown in the ML and assure toll-paying drivers a high degree of travel-time reliability (Liu *et al*., 2011). The methodological framework developed in this study restrains the demand as a user input when evaluating the ML performance, due to the fact that different agencies may use different tolling strategies for their HOT lane system operation, and demand is tied directly to those strategies. It

would thus be hard to generalize a demand model without considering specific cases. For example, it is hard to provide a general conclusion on how Single-Occupancy Vehicles (SOVs) choose the type of lane to use under the effect of tolling and the flow friction between HOT and GP lanes. Therefore, it would be intriguing to use a case study to reveal the heterogeneity among the SOV users of HOT lanes and to determine the contributing factors that had driven their lane choices.

1.2 Research Background

The ML concept encompasses a series of operational strategies to efficiently manage the traffic demand by altering pricing, vehicle eligibility, and access control. In the Managed Lane Handbook, ML facilities are defined as a "freeway within freeway" where a set of lanes are physically separated from GP lanes within a freeway cross section to allow a certain degree of operational flexibility over time in response to changing traffic conditions (Kuhn *et al.*, 2005). In this study, the scope of ML is limited to three categories of operational strategies: HOV lanes, HOT lanes, and express toll lanes. A major difference between HOT lanes and express toll lanes is that HOVs do not pay for use of HOT lanes but all kinds of vehicles need to pay to use express toll lanes. However, operation-wise express toll lanes are often considered as a special case of HOT lanes because both require tolling and access control, and express toll lanes are simpler in operations by tolling both HOVs and SOVs. This research, therefore, focuses on the methodology development for only on two of the three facility types, i.e. HOV and HOT lanes. Some important operating characteristics of existing ML facilities that may affect the performance of the MLs are reviewed as follows:

1.2.1 Operational Strategy

HOV lanes are by far the best documented among all the ML facilities in terms of design, implementation, and performance monitoring (TTI, 2001). The development of HOV facilities in the United States has evolved over 30 years. An HOV pooled fund study initiated by FHWA in 2002 continuously assembles information on existing HOV facilities in the United States, which by 2008 identified 345 HOV facilities in operation across the U.S. (Chang *et al*., 2008). The two longest active HOV facilities are I-95 between SR 112 and Gateway Blvd in Miami, Florida (116.0 lane-miles, 58.0 route miles) and I-405 in Los Angeles County, California (105.2 lane-miles, 52.6 route miles) with more under construction. The main intent of implementing HOV lanes is to improve person-throughput rather than vehicle-throughput on congested freeway corridors. Accessing an HOV facility often requires two or more persons (HOV 2+) per vehicle. Some agencies require three or more occupants per vehicle to assure reliable travel conditions in those lanes. Of the HOV facilities listed by the FHWA compendium (Chang *et al.,* 2008), 185 (54 percent) are purely HOV 2+. Fourteen facilities (4 percent) are purely HOV 3+. Two facilities, the I-10 HOV facility in Los Angeles, California and the Nimitz Highway in Honolulu, Hawaii, are HOV 3+ during certain time periods of the day and HOV 2+ otherwise.

In locations where HOV lanes are underutilized, a conversion to HOT lanes is considered an effective way to increase the overall throughput by providing SOVs or Low-Occupancy Vehicles (LOVs) the ability to choose the MLs as an alternative to the GP lanes. Pricing constitutes a core element of this practice. SOVs are allowed to use the HOT lanes by paying a toll in exchange for travel time savings or improved trip reliability. The toll is either dynamically-changed based on

real-time traffic conditions or scheduled by time of day. Table 1.1 shows the HOT lane projects in operation as of January 2012 (GAO, 2012).

TABLE 1.1 HOT Lane Projects Open to Traffic in the U.S. as of January 2012

Name	Location	Length	Pricing Began
SR 91	Orange County, CA	10 miles	December, 1995
I-15	San Diego County, CA	16 miles	December, 1996
I-680	Alameda/S. Clara, CA	14 miles	September, 2010
I-10	Houston, TX	12 miles	January, 1998
US 290	Houston, TX	15 miles	November, 2000
I-95	Miami-Ft. Lauderdale, FL	7 miles	December, 2008
I-394	Minneapolis-St. Paul, MN	11 miles	May, 2005
I-35W	Minneapolis-St. Paul, MN	16 miles	September, 2009
I-25	Denver, CO	7 miles	June, 2006
I-15	Salt Lake City, UT	40 miles	September, 2006
SR 167	Seattle, WA	9 miles South/11 miles North	May, 2008
I-85	Atlanta, GA	15.5 miles	October, 2011

Tolling policy may be customized for different facilities to achieve their specific objectives, whether it is to reduce emissions, to collect revenue, or to increase the overall throughput. This will greatly affect how the users respond to the pricing. However, in general HOT lanes are operated as a reliability control valve for the overall system. When the GP lane is experiencing congestion, some SOV drivers may opt to pay to use the HOT lane in exchange for travel time savings. As those SOVs divert to the HOT lane, the level of GP lane congestion is expected to decrease as a result of the drop in demand. Thus theoretically the HOT strategy can improve the overall throughput and operations of the freeway facilities with MLs. To demonstrate the HOT lane's demand control capability, Figure 1.1 illustrates a representative time series plot of speed and volume for data samples collected on September 3, 2009 at SR 91 HOT lanes in Orange County, California. The period of GP lane breakdown is easily identifiable from the figure, where a sudden speed drop below 60 mph is observed. Before 2:15 P.M., the average speed across the GP lane is relatively high, maintaining at 70 mph. However, at 2:15 P.M., it is experiencing a sharp speed

drop to below 50 mph, and generally remains below that threshold until 7:10 P.M., after which speeds recover to the pre-congestion stage. During that congested period, the speed of the dual HOT lanes is maintained at non-breakdown levels, although a slight speed drop to around 55 mph in average is observed. By looking at the corresponding time series volume plot, it is easy to identify that as the GP lanes are experiencing traffic breakdown, more people opt to pay to use the HOT lane to avoid the congestion. However, tolling is playing a key role during that period to dynamically manage the demand, so the HOT lanes can help alleviate part of GP lane traffic by directing those paid customers to use the "express road".

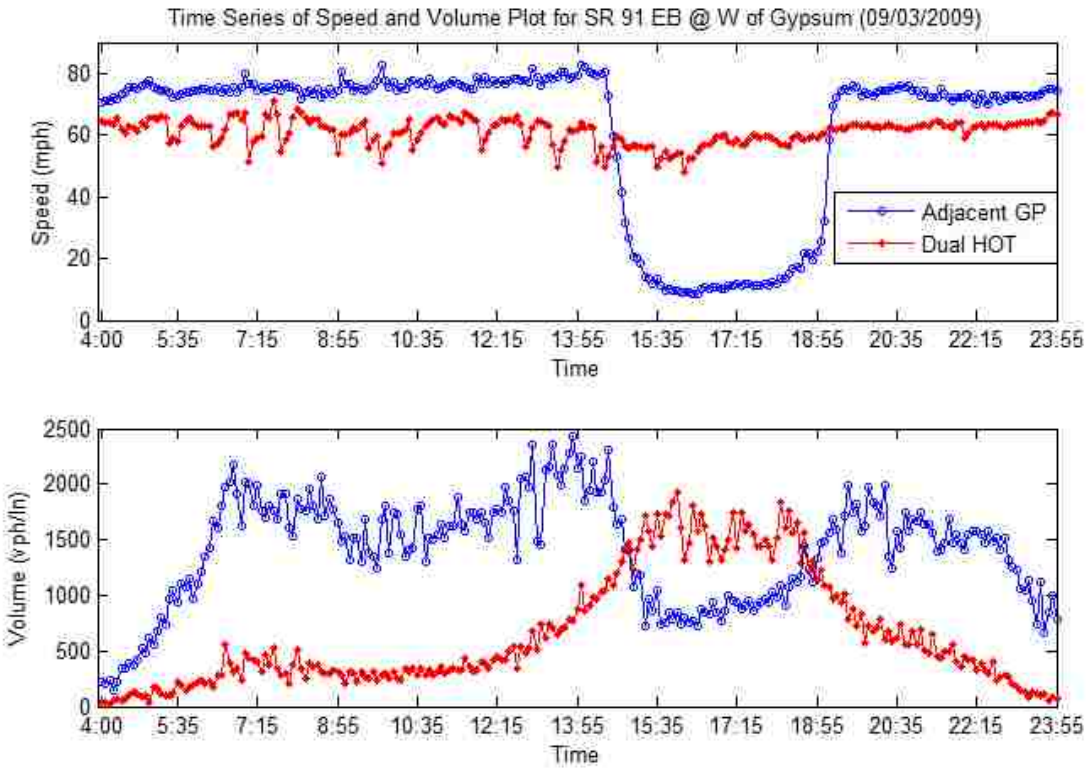

FIGURE 1.1 Time Series of Speed and Flow Plots for SR 91 HOT Lane System in Orange County, California

The increasing number of ML projects across the U.S. demonstrates the strong need of a robust and consistent analysis methodology to quantify the operational performance of these types of

facilities.

1.2.2 Separation Type

Most concurrent-flow MLs are separated from GP lanes by painted stripe or narrow buffer (at least 2 feet or 0.6m wide). According to Chang *et al*. (2008), 118 (34 percent) of U.S. HOV facilities are stripe-separated. Sixty HOV facilities (17 percent) use buffers. Forty-five HOV facilities (13 percent) have barrier separations. The remaining facilities do not have their separation type specified. Because of this proximity of GP and ML traffic, increasing congestion levels on GP lanes may have an adverse effect on ML operations, well before the ML demand reaches breakdown levels. This adverse effect on ML operations is referred to as frictional effect in this study. The reason for frictional effect is that drivers in the stripe or buffer separated MLs can readily observe the slow traffic on the adjacent lanes, and feel uncomfortable passing congested GP traffic at a high speed differential. While the effect of narrow lanes and freeway shoulders are documented to result in a reduction in free-flow speed according to HCM 2010 (TRB, 2010), this ML-GP frictional effect has not been well documented to date. To increase the capacity of the ML facility by avoiding this potential frictional effect, many two-lane or reversible ML facilities chose to use concrete barrier separations. Some facilities use soft barriers (plastic pylon) for separation and frictional effect can be reduced. Intuitively, a wider and more permanent separation between the GP lanes and MLs is hypothesized to reduce the interaction between the two parallel lane groups.

1.2.3 Number of Lanes

Most ML facilities in operation or being planned in the United States are one-lane facilities, which means that they have a single ML in each direction. Two-lane ML facilities can be found only in California, Northern Virginia, Minnesota, Florida, Texas, and Washington. Similar to the GP lane facilities, the number of lanes within an ML facility affects its performance. For a single ML facility, a slow-moving vehicle drags down the speed of vehicles following it, much like it would on a two-lane highway or a single-lane tunnel. On the contrary, multi-lane ML facilities allow opportunities for passing, and the impact of slow-moving vehicles is expected to be lower, at least until higher flow levels are reached.

1.2.4 Access Points

The designs of termini and access points of ML facilities tie directly to ML performance, capacity, and safety (Wang *et al.*, 2012). According to the *Managed Lanes Handbook* (Kuhn *et al.*, 2005), MLs are often accessed through three types of access points: direct access ramp, slip ramp, and at-grade access (continuous or limited access). Chang *et al*. (2008) reported that the most common type of ML facility is left-concurrent (e.g. the HOV lane is on the left side of GP lanes), where at-grade access is the treatment commonly used. Of the HOV facilities identified in the compendium (Chang *et al.*, 2008), 41 (12 percent) allow continuous access, using either painted stripe or narrow buffer to separate the facilities from GP lanes. In contrast to the continuous access, limited access allows several intermediate accesses along the HOV facilities, typically by changing the pavement marking (e.g. from narrow buffer to dashed line). There are 180 HOV facilities (52 percent) with limited access nationwide. No intermediate access is allowed on 26 facilities (8 percent) located

in Arizona, Southern California, Connecticut, Hawaii, Massachusetts, New York, and Texas. The access designs for the remaining HOV facilities in Chang *et al*. (2008) are unknown. For limited access, the opening area length and access point density are expected to affect the ML lane performance.

This limited access configuration is illustrated in Figure 1.2. For a facility with limited access, vehicles are allowed to enter or exit the MLs in certain designated locations only. This type of access is often preferred by agencies as a cost-effective design when compared with direct grade-separated access. However, it requires GP on-ramp traffic that desires to enter the MLs to weave across multiple GP lanes. It is hypothesized that these "cross-weave" actions may cause significant frictions on GP lane traffic depending on cross-weave demand, the distance available to complete the cross-weave maneuvers, and the GP lane density (Liu *et al.*, 2012).

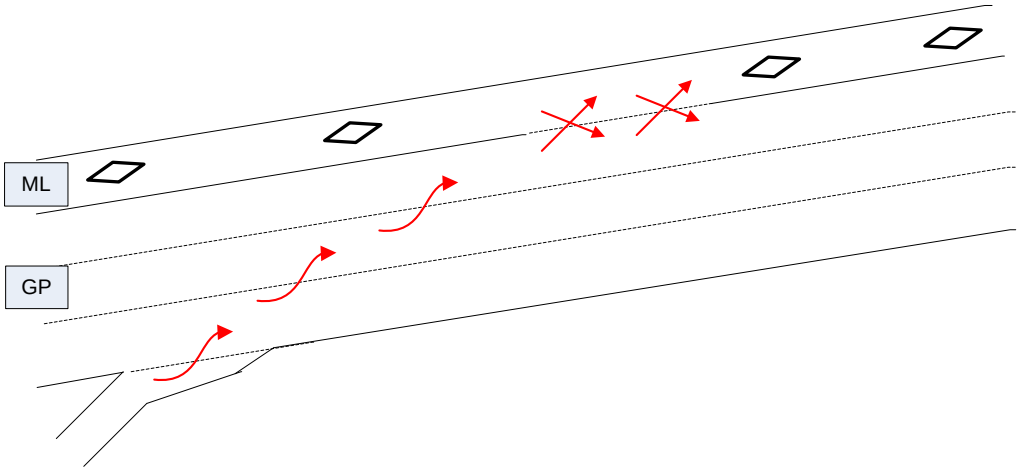

FIGURE 1.2 Schematic of At-Grade Access with Limited Access Point

1.3 Research Objectives and Originality

The ultimate objective of this study is to develop a methodological framework for performance assessment of ML facilities from the supply-side of roadway infrastructure. This study also aims to bring insights for modeling the parallel facilities to provide theoretical basis for traffic flow dynamics on those facilities. From the demand management perspective, this research strives to use a case study to illustrate the HOT lanes' demand control capability and to reveal the heterogeneity amongst SOVs lane choice preferences under various circumstances.

Specific objectives of this study are as follows:

- Identify unique characteristics of ML facilities;
- Develop a methodological framework for analyzing ML facilities;
- Determine performance measures for quantitatively evaluating the effectiveness of different designs of ML facilities;
- Develop a computational engine to test the ML analytical methodology;
- Build a traffic flow model (simulation model) on the basis of Cell Transmission Model (CTM) to capture the traffic flow dynamics for ML facilities; and
- Analyze detailed vehicle trajectory data (transponder tag) to reveal SOVs' lane choice preferences.

There are both data and methodology challenges in developing a methodological framework for modeling and analysis. Although more and more traffic data are available nowadays facilitating the evaluation of roadway performance, issues remain existed on how to effectively extract valuable information from the massive amount of data, and what type of data is really needed to

perform specific analyses. When updating the speed-flow relationship for the basic ML segments, sensor data might be needed to support such development. It would be important to appropriately identify sites whose traffic characteristics (e.g. geometric configurations, traffic composition, separation types, etc.) are representative and good quality sensor data are available. When developing weaving models to quantify the weaving behavior of ML facilities, video data might as well be needed to capture the vehicle interaction and the weaving impact on the Level of Service (LOS). It would be crucial to collect such data where weaving behavior is intense and that the video data could support the methodology development.

Methodology wise, this research aims at developing a framework and a computational engine that is capable of analyzing the ML performance based on user inputs. The user is required to enter variables such as geometric characteristics (e.g. number of lanes), behavioral attributes (e.g. free-flow speed, capacity), and traffic demands separately for each lane group (ML vs. GP lanes). The performance assessment method will be consistent with the segmentation of a GP freeway facility in HCM 2010, except that the implementation would be represented as having either one or two lane groups, depending on whether parallel MLs are present. The methodology would then assess the operational performance of each lane group, under consideration of empirically-derived interaction effect between the two lane groups. From the demand perspective, a behavioral model is developed to analyze SOVs' lane choice using SR 167 as a case study. The detailed vehicle trajectory data facilitate the modeling of people's preferences under various traffic conditions, as well as the proper inferences on people's Value of Time (VOT).

Originality of this study can be explained in twofold. It is the first methodology framework developed so far for the purpose of investigating the unique characteristics of ML facilities and providing a guideline for the practitioners in evaluation of ML performance. The *lane group* concept is introduced in this study for the freeway facilities with MLs. The lane group concept is well-established in the signalized intersection methodology of HCM 2010. By adopting it in this study, the analyst will be able to ascribe separate attributes to parallel ML and GP lane facilities, while retaining the ability to model certain degrees of interaction between the two. Second, the traffic flow model developed on the basis of CTM is capable of incorporating the findings of this framework development for effectively modeling the ML facilities in terms of traffic flow dynamics. Because the developed model incorporates both the lane group concept and the cell-based approach, it is termed as "twin-cell modeling approach". This method could be further extended in analyzing other parallel facilities and the weaving method developed in this study can bring the original cell-based link modeling to the grid-level network analysis.

1.4 Research Scope

This research focuses on the development of framework, from the supply-side, to analyze the ML performance. The framework should be transferrable as a guidance to be used by analysts and engineers for better estimating the operational performance of ML facilities. The results of this research are expected to be incorporated into the subsequent edition of the HCM. Therefore, the methodology should adhere to the developed standards being used for the HCM 2010. From the demand-side, this research aims at using case study to provide rudimentary implications about how users respond to tolling and corresponding traffic conditions, to facilitate the better implementation

of Active Traffic Management (ATM).

1.5 Dissertation Organization

To fulfill the research objectives, a four-step work flow is proposed: literature review, analysis methodology (supply and demand), operational concepts and data acquisition, empirical and modeling results. The remainder of this dissertation is organized in the order of this work flow. Chapter 2 summarizes relevant research on ML performance analysis, behavioral analysis of how drivers respond to tolling, ML traffic flow characteristics, and methodologies for modeling traffic flow dynamics. Chapter 3 focuses on analysis methodology and elaborates on the modeling techniques for both supply and demand sides of the ML facilities performance assessment. It also presents the theoretical derivation of the twin-cell modeling approach. Chapter 4 describes the operational concepts, by putting the ML analysis into the context of parallel freeway facilities. It identifies certain interactions observed between ML and GP lane groups, along with the data collected to support the proposed theoretical framework. Chapter 5 details the empirical and modeling results based on methodology proposed. Finally, Chapter 6 concludes the dissertation.

CHAPTER 2 LITERATURE REVIEW

This chapter comprehensively summarized the state-of-the-art in analysis methods for ML performance. It is recognized that the efforts are based on review of the following four aspects: ***methodology***, ***ML characteristics***, ***weaving analysis*** and ***models***. ***Methodology*** gives a review of the analytical methods developed in the previous studies for ML facilities, from both supply and demand perspectives. ***ML Characteristics*** identifies the traffic flow features unique to the ML facilities. ***Weaving analysis*** describes the methods used for quantifying the weaving performance on freeway that may potentially be adoptable for ML facilities. ***Models*** introduces the traffic flow models widely used in practice for describing the traffic evolutions on freeway.

2.1 Methodology for ML Performance Analysis

2.1.1 *Methodological Framework for Analyzing ML Facilities - Supply-side of roadway infrastructure*

Figure 2.1 shows the current methodology for analyzing a GP-only freeway facility in HCM 2010. The current methodology first establishes the input data requirements, then adjusts demands (if necessary), and computes the operational performance of each individual segment according to the updated methodologies for basic freeway segments, merge and diverge segments, or freeway weaving segments. Capacities can then be adjusted to emulate the effects of adverse weather or work-zones, before computing segment demand-to-capacity ratios (d/c). If no segment is at d/c>1.0, the methodology then aggregates the facility performance from individual segment operations. If any segment operates at d/c>1.0, an entirely different procedure applies to estimate

the effects of congestion based on shockwave theory.

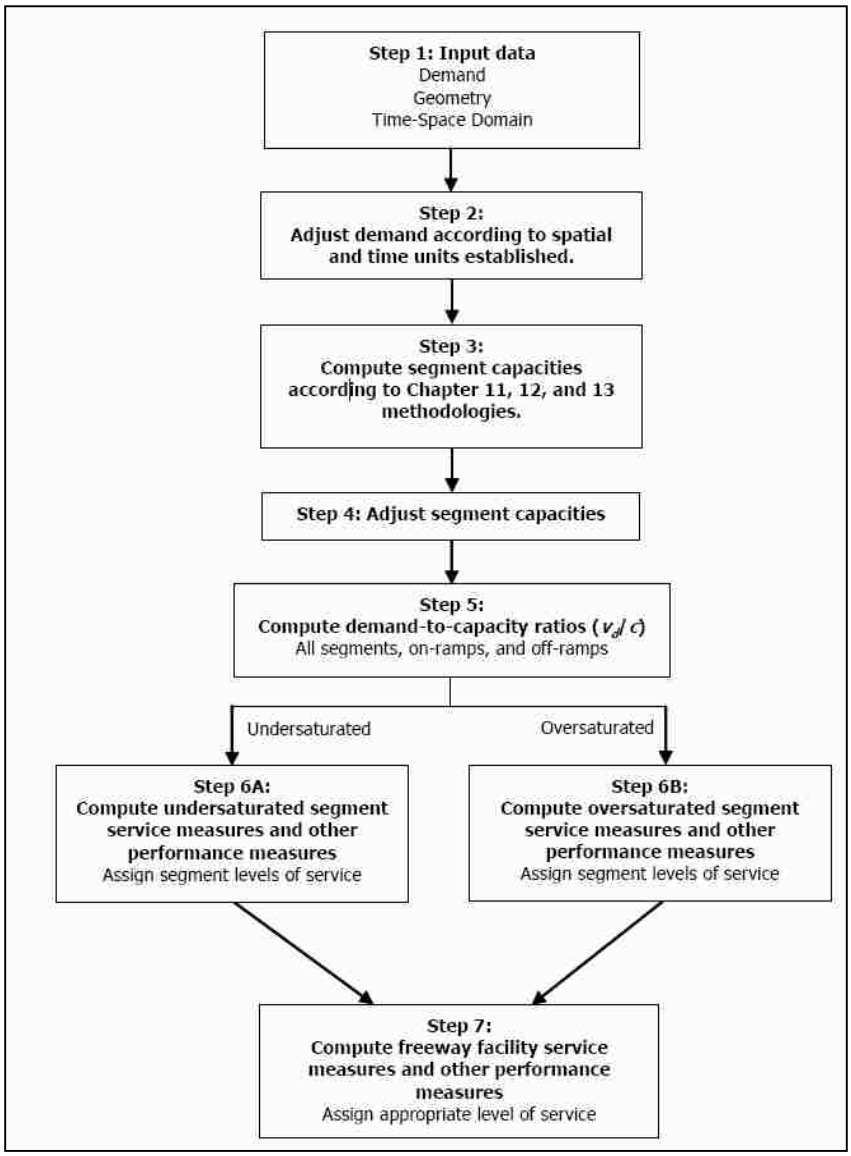

FIGURE 2.1 Existing Methodology Flow Chart based on Chapter 10 in HCM 2010

In practice, most ML facility analyses are performed in a micro-simulation context (e.g. Zhang *et al.*, 2009; Gomes *et al.*, 2004; and Bloomberg and Dale, 2000). Micro-simulation tools are appealing for analyzing ML facilities because there are no standard methods for such analyses in HCM 2010 and they allow analysts to code and evaluate various design alternatives and

operational strategies for the facility in question. Simulation tools are also capable of dealing with oversaturated or congested operations, as queuing patterns are being tracked over time and space. However, micro-simulation-based analyses are limited due to the fact that the build-in driver behavior models have severe constraints and intensive resources are needed to code and configure a network and calibrate the model to fit local conditions (Park and Qi, 2005). One of the most challenging aspects of a simulation analysis is the calibration of the actual maximum throughput or capacity of a road segment, which has been found to vary significantly with changes in calibration parameters (Tian *et al.*, 2002). Simulation tools therefore must be used with caution and require significant time and monetary investments that may exceed the available resources for an agency.

In addition to the modeling challenges associated with simulation, there is presently limited guidance on performance evaluation of ML facilities, which is confirmed by a recent report entitled *Monitoring and Evaluating Managed Lane Facility Performance* (Carson, 2005). While several states continuously monitor the performance of their ML systems (e.g. OCTA, 2011), comprehensive guidance is missing. Among the electronic tools developed specifically for assisting agencies for analyzing MLs, majority are geared at analyzing policies (not traffic operations) related to HOV lanes or HOV lane conversion to HOT lanes. For example, POET-ML is a tool for demand modeling and evaluation of HOV policies (POET-ML, 2008).

One deterministic freeway analysis tool that does include a feature to evaluate HOV lanes is FREQ (Rodrigues *et al.*, 2008). FREQ was originally developed at the University of California at Berkeley's Institute of Transportation Studies in 1970. One of the weaknesses of the FREQ tool is

its analytical approach for weaving sections, which is still based on the method in HCM 1965 (Rodrigues *et al.*, 2008). Also, a new version of FREQ may not be expected as the software is no longer supported. Other than FREQ, no analytical analysis methodologies for ML facilities could be identified by the literature review.

2.1.2 Demand Analysis for HOT Lane Facilities

Quite a few studies have been done to investigate how drivers respond to tolling using price elasticity analysis (Han and Li, 2009). For example, Dahlgren examined the circumstances in which HOT lanes could provide a more desirable alternative to HOV lanes (Dahlgren, 1999). The question of how sensitive users are to the toll level was investigated using data from SR 91 in Orange County, California. It was found that eastbound toll lane traffic showed a very low elasticity with respect to tolls— between −0.02 and −0.16. This means that if tolls are reduced by 50%, toll lane volumes will increase by 1% to 8%. The westbound analysis found a positive relationship between tolls and toll lane traffic. This controversial result is likely due to a positive correlation between tolls and total freeway traffic volume and requires further study of the interaction between the two variables. Additionally, that analysis was, to a certain extent, biased because the data only covered 2 weeks and because only hourly data were available for toll lanes. Song and Smith (2009) conducted a price elasticity analysis and developed a utility-based mode choice model for SOV behavior using traffic and tolling data from the I-394 HOT facility in Minneapolis. The result indicated that SOV behavior was insensitive to toll level and was influenced by the speed differential between the HOT and GP lanes.

In addition to price elasticity, it is also important to understand how travelers value travel time and its reliability, which often are measured using two behavioral parameters: VOT and Value of Reliability (VOR). These parameters are crucial to the evaluation of travel behavior. VOT is considered as the marginal cost of travel time in a traveler's indirect utility function, while VOR measures willingness to pay for reductions in the day-to-day variability of travel times associated with a particular trip (Brownstone and Small, 2005). Currently, many studies have been conducted to estimate VOT through similar data metrics and model estimation procedures. For example, the most widely used approaches established a multinomial logit model to identify VOT by using revealed preference or stated preference data from surveys (Steinmetz and Brownstone, 2005; Ghosh, 2001). The University of California Transportation Center has been conducting VOT-related research using data from the SR-90 and I-15 congestion pricing project over the past several years (Brownstone and Small, 2005).

Of studies using real-time traffic measurement data to evaluate SOV usage of HOT lanes, one of the most similar to the present study was conducted by Steinmetz and Brownstone (2005). In their study, motorists' responses to the actual pricing were analyzed using data collected from I-15 HOT lanes in San Diego. They obtained transponder data and matched toll rate data with the time when the vehicles identified by the transponders were reported as reaching the facility. A panel survey was also conducted to gather the demographic information about the I-15 commuters necessary to conduct mode-choice analysis. The drawback of this study is that for most of the samples, reliable information on travel time savings was missing, so a multiple imputation approach was applied to interpolate the missing data.

Goodall and Smith (2010) modeled SOV responses to toll rate when the drivers were faced with a set of traffic conditions and toll levels. Data used for their study were collected from the dynamically tolled I-394 HOT lane facility in Minneapolis. They used data from both loop detectors and transponder readers to model actual drivers' responses to minute-to-minute changes in toll rates and traffic conditions. Two types of users in the HOT lanes were classified: (a) everyday users who employ the HOT lanes as insurance against unanticipated congestion and (b) price-sensitive users who are influenced by cost per unit travel time saved. By accounting for both types of drivers separately and then combining them together in the final model, the authors predicted traffic assignments between GP lanes and HOT lanes. This method is reasonable in nature; however, the number of everyday drivers was determined by assuming an average portion based on time of day. This lack of precision may greatly hinder the accuracy of the model and its further applications.

2.2 ML Traffic Flow Characteristics

ML traffic flows were found behaving differently from those of GP lane facilities. Nee *et al.* (1999) observed that concurrent HOV lane traffic moves slower than expected when GP lanes get congested in Washington State. The two reasons for the slowing HOV traffic were attributed to HOV motorists' lack of comfort traveling at a large speed differential to GP lanes, and to the fact that vehicles merging from the uncongested HOV lane to the congested GP lane were forced to reduce their speeds. Martin *et al.* (2002) observed a similar phenomenon on HOV lanes in Utah. HOV lanes did not operate at expected speeds relative to volume. HOV lanes adjacent to congested GP lanes operated at a speed well below the speed associated with the flow level that is

significantly under the capacity.

Varaiya (2005) investigated a drop in capacity of HOV lanes on I-880 in San Francisco. The HOV facility on I-880 is the leftmost lane and is separated by skip-stripe painting. As the HOV facility restrictions on I-880 are only in effect during peak travel periods, the difference between the same facility operating as an HOV lane and a GP lane was observed. Operating as a GP lane, the capacity and speed of the lane were higher than during the times it was operating as an HOV lane. Kwon and Varaiya (2008) also observed this phenomenon as HOV's observed capacity was around 1600 vphpl. This indicated a reduction in lane capacity of at least 20% on California HOV lanes. It was also noted that the operating speed at capacity was lower than the expected speed of 45 mph. Since the studied HOV site was a single lane facility, the HOV speed reduction was contributed to a "snail" effect, where the speed on the HOV lane was governed by the slowest moving vehicle as passing was constrained. With the increase of the traffic flow, so did the number of slow drivers.

Guin *et al.* (2008) then took an in-depth look into the traffic behavior associated with the interaction of parallel, buffer-separated HOV and GP lanes along I-85 in Atlanta, Georgia. Their results indicated that the speed differential between the HOV lane and the adjacent GP lane is affected by the level of congestion in each lane. When the GP lane is uncongested, there is no speed differential between the two systems. When the GP lane is congested, the HOV lane's speed is higher than the GP lane's speed. The maximum speed differential between the facilities was between 20-30 mph. The speed differential gradually decreased until both facilities reached a state of equal congestion. The capacity of the HOV lane in the study was 1,600 vphpl, similar to the results from other studies mentioned earlier. In the meantime, research also has showed that HOV

lanes might have a smoothing effect on the adjacent GP lanes. Both theoretical work (Menendez and Daganzo, 2007) and natural experiments (Cassidy *et al.*, 2010) indicate that the capacities of GP lane bottlenecks can be significantly increased by discouraging, but not necessarily prohibiting, vehicle lane-changing maneuvers (between GP and HOV lanes) in bottleneck vicinities.

Liu *et al*. (2011) confirmed Guin *et al.*'s (2008) breakdown process of HOV facilities and described the GP facility as stochastically dominant over the HOV facility. They observed HOV speed reductions due to HOV lane's own breakdown, in addition to those caused by the slow moving traffic on the adjacent GP lane. They termed the ML speed reduction caused by adjacent GP lane congestion "frictional effect" and investigated the frictional effect between GP lanes and MLs across different separation types. The frictional effect of buffer-separated facilities appeared to be the biggest, followed in turn by soft barrier (plastic pylon) and concrete barrier separations. Concrete barrier separation appeared to have no statistically significant frictional effect.

On the basis of Liu *et al.* (2011)'s study, a series of research has identified similar phenomenon on the parallel ML facilities. Jang and Cassidy (2012) analyzed what happened on a four-mile length of I-880 in the San Francisco Bay Area when a new rule went into effect that ended access to the HOV lanes for hybrid vehicles. They predicted that shifting hybrid users into the GP lanes would worsen congestion in those lanes, in the meantime, they also predicted that speeds in the HOV lanes would decrease, despite fewer vehicles in the HOV lanes. Their explanation is a psychological one - that people driving in the HOV lane do not feel comfortable going 65 mph right next to lanes that are engulfed in stop-and-go conditions. Therefore when speeds in the GP lanes drop, so do speeds in the adjacent HOV lane. Later on, Jang *et al.* (2013) studied the vehicle

trajectory data to evaluate microscopic traffic behavior in the HOV lanes. Three hypotheses - intrinsically slow driver, disruptive lane-changing and cautious driving behavior - were individually examined to discover the reason for the induced speed reduction. And it was found that drivers in the HOV lane tend to maintain wide spacing at slow speeds when the adjacent GP lane is congested.

2.3 ML Weaving Analysis

Weaving is considered as one of the most important elements in the freeway capacity and LOS analysis in HCM. There are three key geometric characteristics that affect the weaving segment operating performance: width (number of lanes), length, and configuration. The HCM 2010 methodology utilizes a series of predictive algorithms to evaluate the weaving segment characteristics, all of which are based on theoretical or regression models (Roess, 2011). Although some research discourages the use of two-sided weave configurations (Vo, 2008), it is widely used in ML operations. The at-grade access to the ML with limited access location is just one common example that is quite similar to the two-sided weave described in HCM 2010. In the capacity model, the capacity of a weaving segment is computed using a deterministic equation related to the capacity of a basic freeway segment with the same free flow speed. It also decreases with an increase of volume ratio, and increases as the length and number of weaving lanes increases.

Several other efforts have used micro-simulation to determine the capacity of the weaving segment on a ML facility. Vo (2008) used VISSIM simulation to develop a capacity model for a two-sided Type C weaving area as a function of mainline flow, exit ramp flow and ramp-to-ramp flow. The

simulation model was calibrated based on detailed field-collected data in San Antonio (SB IH 35/410 between the Rittiman on-ramp and the SB IH 410 left exit). Williams *et al.* (2010) investigated the spacing requirements for at-grade access points to ML with respect to the location of entrance and exit ramps on the GP lanes. Again using well-calibrated VISSIM simulation model, capacity was estimated by changing the GP input flows, ramp flows, length of weave, etc. It was found that under the 4-lane GP lane scenario, the principal determinant for spacing was the weaving flow (ramp to ML flow), with a minimum weaving distance of 2,000 to 3,500 ft for flows from 200 to 400 vph. However, none of the research has established quantitative relationship between the cross-weave impact and roadway geometric and traffic conditions.

2.4 Traffic Simulation Models and Traffic Flow Theory

In comparison with analytical solutions, traffic simulation platform offers more flexible and user friendly approach to ML system performance analysis. More importantly, simulation tools can be used to assess the performance of real-time traffic control and traffic management under the Intelligent Transportation System (ITS) context. Simulation models have been evolved to fit different research needs and project scopes and are distinguished by the desired level of details for the representation of the real-world scenario. Simulation models are often classified into three different categories: microscopic, mesoscopic and macroscopic based on the level of details one requires. Microscopic traffic simulation models assume that the behavior of an individual vehicle is a function of the traffic condition in its environment (Daganzo, 1993). While macroscopic simulation assumes that the aggregate behavior of a set of vehicles, which is easier to observe and validate, depends on the traffic conditions in their environment. It utilizes the fundamental

relationship among speed, flow and density, and also requires less computational resources than microscopic simulation. Mesoscopic model is a mixture of both, which often times incorporates the movement of platoons of vehicles and their interaction (Alecsandru, 2006).

The CTM is a discrete version of hydrodynamic theory of traffic flow and has been widely recognized to simulate traffic flow evolvement under various conditions due to its analytical simplicity and ability to reproduce congestion wave propagation dynamics. It was developed by Carlos Daganzo in 1993 as a solution to the differential equations of the Lighthill, Whiteman, and Richards (LWR) hydrodynamic model for the representation of traffic flow (Lighthill and Whiteman, 1955). The basic CTM assumes a piecewise two-wave flow-density relationship. Because of its macroscopic features, it offers calibration and computation advantages over microscopic simulation models. The original CTM developed by Daganzo was used to examine the evolution of traffic over a one-way road without any intermediate access points. So vehicles enter at one end and leave at the other. In CTM, freeway is divided into homogeneous cells and the length of each cell is determined such that all vehicles in one cell will flow into the downstream cell in one time step under free-flow conditions. However, when queue is formed, the simulation will be based on a recursion where the number of vehicles (cell occupancy) in each cell at time *t+1* equals its occupancy at time *t*, plus the inflow and minus the outflow. The following expression therefore stands:

$$n_i(t+1) = n_i(t) + y_i(t) - y_{i+1}(t) \tag{2.1}$$

where $n_i(t+1)$ is the number of vehicles in cell *i* at time *t+1*. $y_i(t)$ is the inflow of cell *i* at time t. $y_{i+1}(t)$ is the outflow of cell *i*, which is also the inflow of downstream cell *i+1*.

In each cell, CTM assumes a piecewise linear relationship between flow and density. It is depicted in Figure 2.2 and expressed as:

$$q = \min\{vk, Q, w(K-k)\} \qquad 0 \le k \le K \tag{2.2}$$

where v=free-flow speed of the freeway segment
k=density of the freeway segment
K=the jam density
Q=the maximum flow rate (capacity), and
w= the backward wave moving speed

If Equation (2.2) is replaced into the flow conservation equation, differential equation that would define the evolution of traffic under the LWR model can be obtained:

$$\frac{\partial \min\{vk,Q,w(K-k)\}}{\partial x} = -\frac{\partial k}{\partial t} \tag{2.3}$$

The flow advancing equation can be correspondingly derived as (Daganzo, 1993):

$$y_i(t) = \min\{n_{i-1}(t), Q_i(t), \delta \cdot [N_i(t) - n_i(t)]\} \tag{2.4}$$

where $n_{i-1}(t)$ is the number of vehicles in cell i-1 at time t; $Q_i(t)$ is the maximum number of vehicles that can flow into cell *i* in one time step (capacity); $N_i(t)$ is the maximum occupancy of cell *i*. $\delta = w/v$.

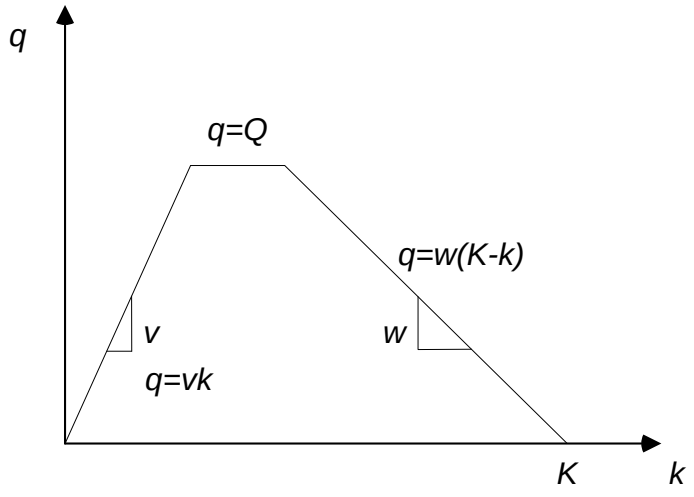

FIGURE 2.2 Flow-Density Relationship for the Basic CTM

Besides the ordinary links (one way in, one way out), CTM further evolved to model the merge and diverge junctions on the roadway (Daganzo, 1995). Using the merging scenario as an example, the two cells are denoted as a beginning cell and a complimentary cell, separately. And they are merging into an ending cell (see the network topology in Figure 2.3). The constraints on the flow advancing logic are given by Equations (2.5) through (2.7).

$$y_k(t) \leq S_{Bk} \tag{2.5}$$

$$y_{ck}(t) \leq S_{Ck} \tag{2.6}$$

$$y_k(t) + y_{ck}(t) \leq R_{Ek} \tag{2.7}$$

where $S_I(t)$ is the minimum of (Q_I, n_I), and $R_I(t)$ is the minimum of $(Q_I, \delta_I[N_I - n_I])$. Note *I* can be substituted by *BK, CK, or EK*.

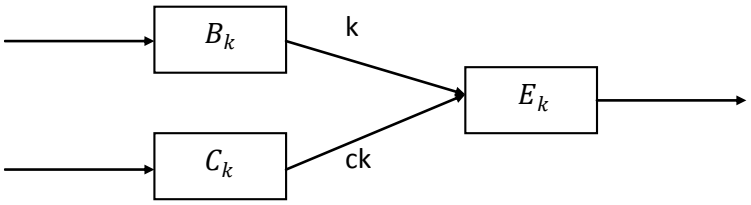

FIGURE 2.3 Representation of a Merge Area

The basic modeling block of CTM thus can only be so complicated as up to be a three-legged junction and each link in the block can only belong to no more than one junction (e.g. one link cannot be a part of both a diverge and a merge). Figure 2.4 gives examples of both valid and invalid representations of the modeling blocks.

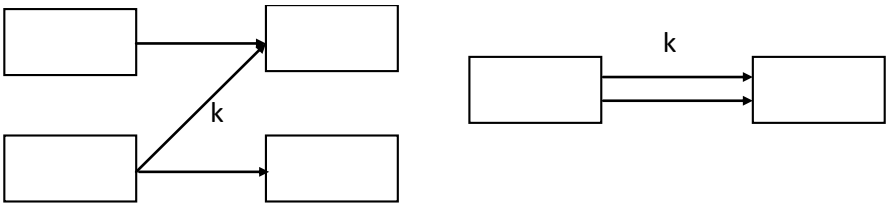

(a) Invalid Representation

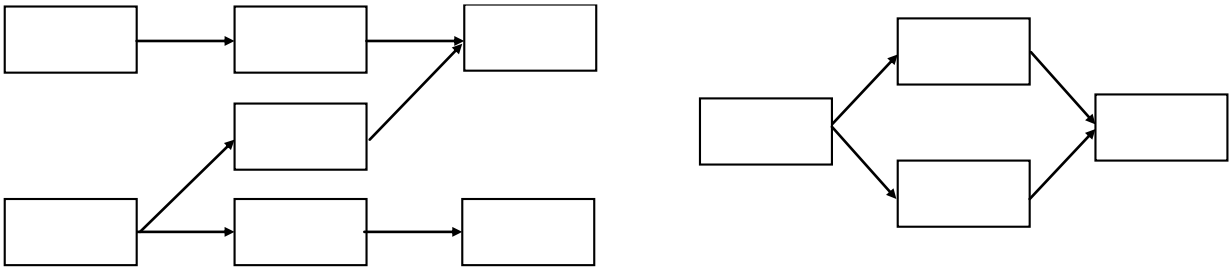

(b) Valid Representation

FIGURE 2.4 Network Topology Representation

However, due to its macroscopic nature, CTM model is not capable in analyzing the weaving or lane-changing behavior between lanes. To effectively develop simulation model of ML facilities, interaction between GP lanes and MLs makes it necessary to bring the scope of CTM to the mesoscopic grid level, where the weaving between the two lane groups and the frictional effect imposed onto the MLs from the GP lanes can be appropriately modeled.

CHAPTER 3 ML ANALYSIS METHODOLOGY FOR PERFORMANCE ASSESSMENT

3.1 Brief Introduction

In order to evaluate the ML facilities, the methods undertaken in this study can be split into four major components: HOT lane demand modeling, analysis methodology for facility performance (supply-side), operational concepts and data acquisition, and mesoscopic approach of twin-cell modeling for parallel freeway facilities.

As mentioned in Section 1.1.4, MLs, especially HOT lane systems, have a variety of tolling strategies for demand control. This study is not attempting to develop a generalize model for determining the relationship between demand and pricing, as the function indeed varies depending on the heterogeneity of roadway users. Instead, it is trying to reveal, using case study, the SOVs' response to tolling under a variety of traffic circumstances and the hidden parameters that make some travelers pay more than others.

The *analysis methodology* piece is to propose a methodological framework for analyzing the ML performance from the supply-side of roadway infrastructure. It aims at providing a guideline for engineers and designers to evaluate the operational and design specifications of their studied ML facilities. Within the framework, different computational modules were developed based on sensor-measured or simulation-generated data throughout the study, including the characterization of ML speed-flow relationship, the frictional effect of adjacent lane traffic speed, the adjustment for cross-weave effects, and the development of side-by-side facility-wide ML and GP

performance measures. Thus, the proposed methodology is sensitive to different GP and ML segment types (basic, weaving, etc.) and separation styles (none, buffer, barrier), and is capable of analyzing extended facilities across multiple time periods. In *Chapter 4 operational concepts and data acquisition*, the detailed development of the computational modules is introduced. For example, the lane group concept, which is adopted from the signalized intersection analysis in HCM 2010, enables the simultaneous evaluation of MLs and GP lanes. It allows us to ascribe separate attributes to parallel ML and GP facilities, while retaining the ability to model a certain degree of interaction between the two.

The development of the methodological framework for ML facilities analysis inspires the extension of the research for developing a twin-cell modeling approach of parallel freeway facilities. This mesoscopic approach is able to extend the existing macroscopic CTM for modeling the weaving interaction between lane groups, especially at ML access points.

3.2 HOT Lane Demand Modeling

3.2.1 Case Study Site Description

The SR 167 HOT lane system is the first and only HOT lane project in Washington State. It was opened to public in May 2008. By converting the preexisting HOV lanes into HOT lanes, SR-167 now allows solo drivers to pay for using the ML previously reserved for carpools and buses.

The single-lane HOT facility runs concurrently with two parallel GP lanes for 10.76 mi northbound and 7.69 mi southbound between Auburn and Renton, Washington. Carpools, buses, and

motorcycles continue to use the HOT lane free of charge. HOT lanes operate daily from 5 a.m. to 7 p.m. Toll rates are adjusted with the level of congestion to maintain a free-flow condition in the HOT lane (WSDOT, 2012). The SR 167 HOT lane pilot project divides the whole corridor into six segments northbound and four segments southbound with a weaving area between two consecutive segments called an access point (See Figure 3.1). A thick double white line separates the HOT lane from the GP lanes. It is illegal to cross the double line. At the weaving area, the double white line becomes dashed lines indicating that drivers can freely enter or exit the HOT lane. At each access point, an overhead sign is installed to display the current toll rate. The toll rate can change at any time, but an SOV pays only the rate at the time it entered the HOT lane.

3.2.2 Field Data Collection for Modeling HOT Lane Demand

There are a total of 26 loop detector stations deployed along the SR 167 HOT lane corridor. These loop stations measure traffic volume and lane occupancy data periodically every 20 seconds. The Traffic System Management Center of the Washington State Department of Transportation (WSDOT) archives traffic speeds calculated using Athol's approach (Athol, 1965) and the original loop detector measurements was aggregated at 1-min intervals. Therefore, in this study, 1-min speed and volume data were used for the analysis.

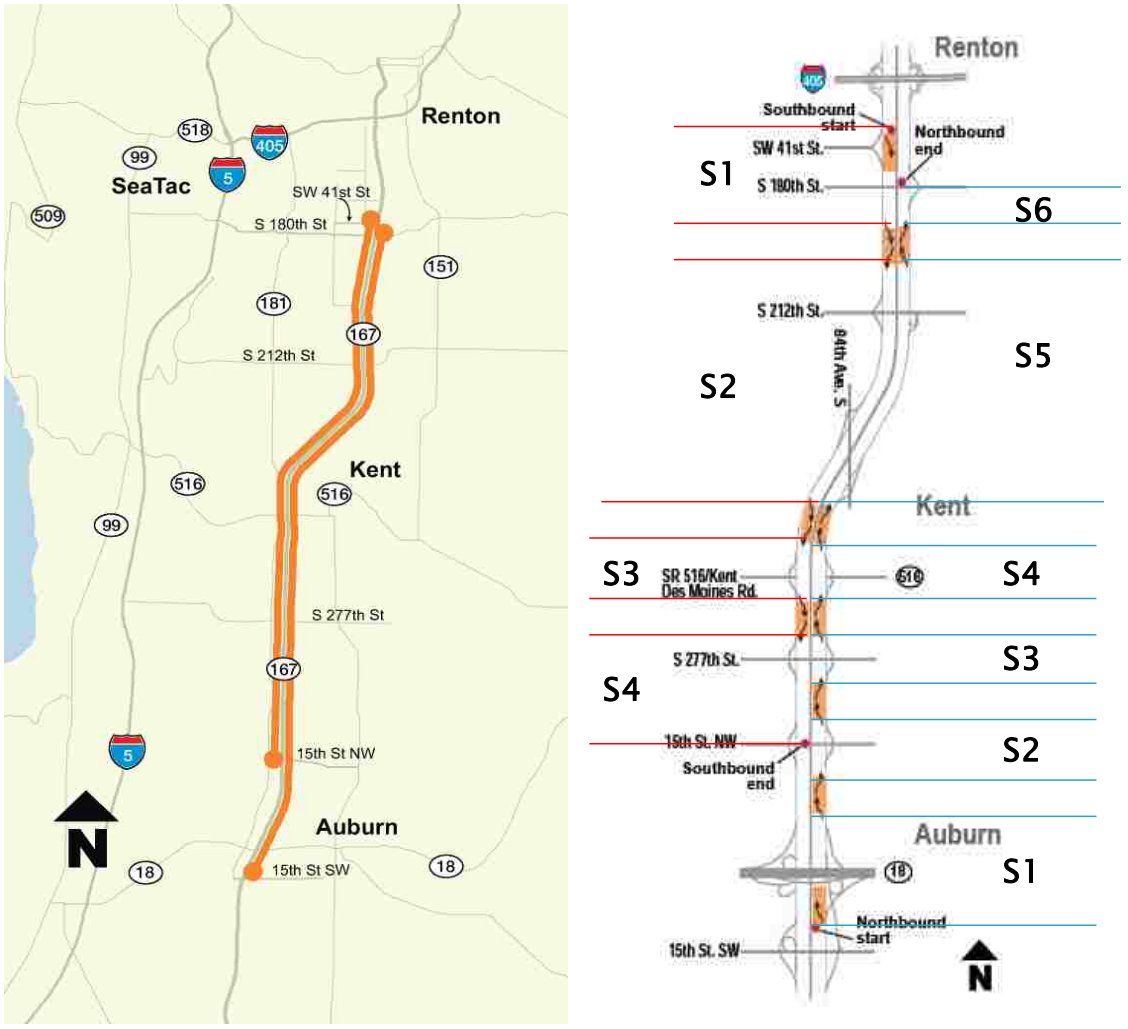

FIGURE 3.1 Location of SR 167 HOT Lane and Segmentation Information (S:segment)

Solo drivers who wish to use the HOT lane must create "*Good To Go!*" transponder accounts. A transponder serves as an electronic identification (ID) that maps toll transactions to a specific *Good to Go!* account. A transponder reader detects transponders at the entrances to the HOT lane system and charges the mapped accounts based on the toll rate at the time of entrance. By matching the transponder IDs at the HOT lane access points, the origin and destination of each SOV traveling on the HOT lane and its travel time can be collected. Then the total travel time savings of vehicles choosing the HOT lane over the GP lanes can be calculated. Loop detector data and transponder

data were collected from northbound SR 167 during the morning peak period from 5:00 a.m. to 10:00 a.m. The data were reviewed in detail and the erroneous detector readings were screened out. In total, 21 days' worth of data were obtained from the site during February and March 2009.

3.2.3 Modeling Approach for Quantifying SOVs Response to Tolling

Previous research indicates that the distribution of the value of time savings would be different for frequent users and infrequent users of HOT lanes (Goodall and Smith, 2010). The assumption is that the incentives to use HOT lanes are believed to be different for these two user types. That is, frequent users are more likely to use HOT lanes even when there is no apparent benefit in travel time savings. They would rather buy in to use the lanes as insurance for reliability of travel time, regardless of any indication of congestion downstream. Infrequent users, on the other hand, value the immediate visible travel time savings more than trip reliability, making their choices more sensitive to the relative difference in traffic conditions between the HOT and GP lanes.

To examine whether such a difference exists between these two groups of users, this study classified SOVs as frequent users and infrequent users on the basis of the frequency of transponder IDs shown in the database. A usage frequency threshold (14 days) was chosen to separate the two user groups. To calculate the VOT distribution at an individual level, the volume, speed, and travel time data at the time when an individual SOV entered the HOT lane were extracted and used for calculation. The VOT was then determined by the toll the SOV paid divided by the travel time difference between its HOT lane travel time and the corresponding GP lane travel time, which is expressed as follows:

$$VOT = \frac{Toll}{\frac{D}{S_{GP}} - \frac{D}{S_{HOT}}} \tag{3.1}$$

where D is the distance each SOV traveled in the HOT lane and S_{GP} and S_{HOT} are the traffic speeds in the GP lanes and HOT lane, respectively, when that particular SOV was traveling.

Because the loop sensors deployed along the SR 167 HOT lane corridor are single-loop detectors, traffic speed must be calculated from single-loop measurements, that is, volume and occupancy. WSDOT uses Athol's algorithm for speed calculations; however, other speed estimation algorithms exist as well (Wang and Nihan, 2000; Wang and Nihan, 2003; Yu *et al.*, 2009). Athol's algorithm is expressed as:

$$v = \frac{q}{o \times g} \tag{3.2}$$

where

v = estimated space mean speed (miles per hour),

q = vehicle volume (vehicles per hour per lane),

o = lane occupancy per lane (percent), and

g = speed estimation parameter.

The speed estimation parameter g is determined by the mean effective vehicle length for each calculation interval. However, because vehicle length data are not available from single loops, g is often assumed to be constant in practice. WSDOT assumes $g = 2.4$ in speed calculations. Because of segmentation errors in loop measurements (Yu *et al.*, 2009), traffic speed calculated from Athol's algorithm can be unbelievably high or low. Therefore, the calculated speed is capped

at 60 mph and 5 mph because the margin of error becomes too great for the speed calculation algorithm to be accurate outside this range. That is, speed is modified to 60 mph or 5 mph if the calculated result is greater than 60 mph or less than 5 mph, respectively (Liu *et al.*, 2010).

By examining the VOT distribution of the two user groups, it is easy to identify whether heterogeneous users have different responses to the tolling policy. This study further investigates, at a macroscopic level, how SOV demand for HOT lanes varies with changing traffic conditions. It is assumed that under different traffic conditions, SOVs will react differently to tolling and the indicating factors that their lane choices are based on will be varied as well. Therefore, the traffic condition was classified into three different phases: pre-congestion, congestion, and post-congestion.

It is assumed that an SOV faces an actual lane choice at time *t* among alternatives *j*. The lane choice decision is modeled between two alternatives for SOVs in an actual market setting: (*a*) solo travel in the GP lane parallel to the HOT lane, and (*b*) solo travel in the HOT lane. To quantify the attractiveness of these two alternatives, the utility functions for choosing each alternative are defined to represent SOV preferences and reasons indirectly to the preferences. The utility functions of the lane choice model to be used in this study are:

$$U_{HOT} = \alpha * TT_{HOT} + \omega * R_{HOT} + \beta * TR \tag{3.3}$$

$$U_{GP} = \alpha * TT_{GP} + \omega * R_{GP} + C \tag{3.4}$$

where TT and R stand for travel time and trip reliability, respectively. They are generic attributes which will impact the utilities of different lane types in the same way. TR is the HOT-specific attribute (toll rate) and C is the constant.

The percentage of SOVs choosing the HOT lane is modeled in a logit model format, which is the lane choice model format used for survey data. In this logit-like model, the probability of an SOV choosing to travel in an HOT lane is replaced by the percentage of SOVs choosing the HOT lane in the approaching SOV traffic. The model is written as:

$$P_{HOT} = \frac{e^{U_{HOT}}}{e^{U_{HOT}} + e^{U_{GP}}} = \frac{1}{1 + e^{U_{GP} - U_{HOT}}} \tag{3.5}$$

where

P_{HOT} = percentage of SOVs in the approaching SOV traffic choosing the HOT lane,

U_{HOT} = utility function of the HOT lane, and

U_{GP} = utility function of the GP lanes.

Among all the independent variables in the model, system reliability is relatively hard to measure and quantify. This study uses a probability-based approach to measure the travel time reliability in both the HOT lane and the GP lanes. Several studies have been done to express travel time reliability in terms of probabilistic measures (Chen *et al.*, 2002; Asakura and Kashiwadani, 1999). In this study, travel time reliability is defined as the probability that a trip can be made successfully within a specified interval of time. This probability *Pr* is a function of time of day. Assume that for a study period, the travel time at a specific time of day follows a normal distribution, with mean and standard deviation of the distribution determined by historical data at each time of day. The travel time reliability is expressed as

$$Reliability = \Pr(t < t_{r_i}) = 1 - \Pr(t > t_{r_i}) \tag{3.6}$$

where t is the actual travel time for a given time of day; and t_{ri} is the required travel time for a

given time of day.

This reliability measure converts reliability to a 0 to 1 scale, where 1 indicates most reliable and 0 least reliable. Note that all travel times used in this study are estimated with the piecewise linear speed–based model (Van Lint and Van Der Zijpp, 2003). This method reconstructs mean travel times based on time series of speed measurement at consecutive detector locations along a route. This method is almost unbiased given dense enough detector spacing (Tu *et al.*, 2005).

3.3 Analysis Methodology for ML Facility Performance (Supply-Side)

3.3.1 Methodological Framework for ML Facility

A revised methodological flowchart that incorporates ML facilities is depicted in Figure 3.2. While both undersaturated and oversaturated scenarios are shown, the proposed enhancements to the method are limited to the undersaturated conditions. By design, majority of ML facilities operate below capacity, especially when they include a pricing component (HOT lanes). It is therefore difficult to obtain ML performance data at or above its critical density, making the development of an empirical relationship impractical. It will then be assumed in this method that the operations of congested ML facilities are beyond the scope of the current HCM method, and will be reserved for a simulation-based analysis if necessary (Schroeder *et al.*, 2012). This approach is consistent with the reference to alternative tools that is a theme throughout the HCM 2010.

A significant difference between the existing and the proposed methodologies is the introduction

of the new lane group concept, which affects the definition of facility geometry in Step 1. With the introduction of MLs, the time-varying demand volumes needed in Step 1 will require additional analysis to estimate. In Step 3, capacity estimation for the GP segments is computed without considering the impact from the introduction of MLs. Several new ML-specific segment types and associated segment capacities need to be defined and calibrated in this step. Then segment capacities are adjusted for work zones and weather effects in Step 4a as in the current HCM. Adjustment to GP lane capacity is needed for those segments affected by cross-weave maneuvers in Step 4b. As this research did not see a need to specifically explore the impacts of work zones and weather on ML facilities, and the existing methods in the HCM 2010 are adopted.

Depending on the prevailing congestion levels, either undersaturated or oversaturated performance modules are invoked. It is assumed that the oversaturated methodology for GP lanes (Step 6b) will remain unchanged. For undersaturated operations (Step 6a), performance measures are estimated for each segment, under the consideration of traffic demands and appropriate adjustments to segment capacity. GP lane groups are handled through existing methodologies, and some new methods will be needed for specific ML configurations. Current HCM 2010 assigns a segment LOS at the end of Step 6 (a or b), but that the LOS assignment with MLs is now moved after the completion of assignment of adjacent friction effects (Step 7). Finally, facility MOEs are estimated as before, with the caveat that additional MOEs specific to MLs or the relative comparison between the two are needed.

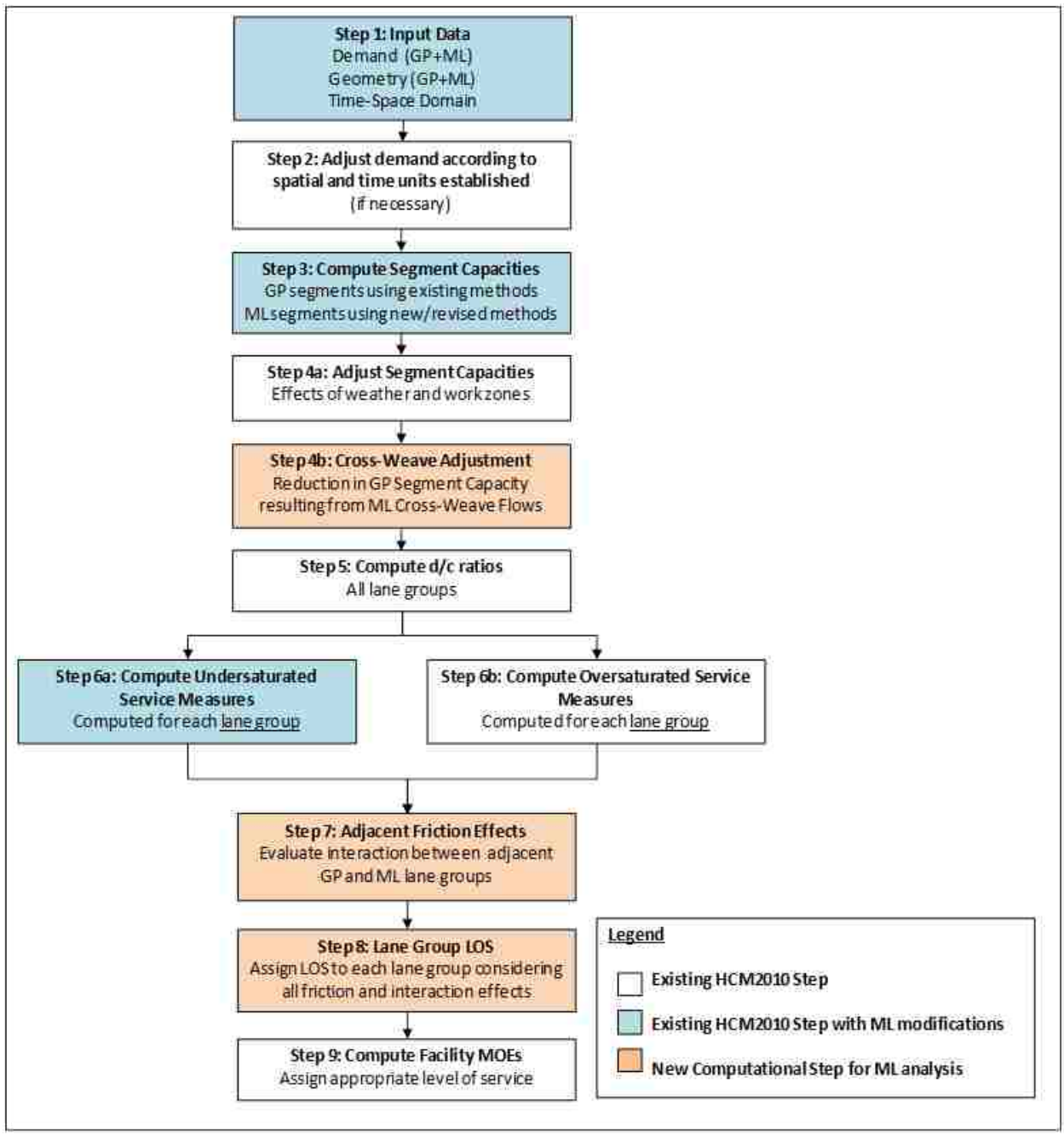

FIGURE 3.2 Revised Methodological Flow Chart Incorporating MLs

3.3.2 Defining ML Analysis Segment

The framework introduced in Section 3.3.1 assumes that all GP freeway facilities are defined in consistence with HCM 2010, including the segment type classification (basic freeway segment,

merge segment, diverge segment, and freeway weaving segment). In addition to these GP segments, five new ML segment types need to be defined.

The proposed five new ML segment types are presented in Figure 3.3. These five new ML segments are described as follows:

- ML Basic: This is analogous to the general basic freeway segment, but serves for ML traffic demands. Five different ML Basic segment types are identified and the traffic flow characteristics for these five ML segment types are analyzed in Section 3.3.3 considering separation types and number of lanes. For barrier-separated ML-Basic segments, the existing GP lane procedure is applicable because frictional effect is insignificant. For stripe or buffer-separated ML-Basic segments, as well as segments with a single ML, new speed-flow models are developed and calibrated. Note that Continuous Access ML segment type, where access between the ML and GP lanes is allowed at any point, is classified into the ML Basic type. It should be distinguished from the ML Access Segment (ML-AcS) which is introduced later in this section.
- ML On-Ramp and ML Off-Ramp: These are analogous to GP Lane On-Ramp and Off-Ramp segments, but with ML traffic demands. The ML On-Ramp and Off-Ramp segments are suitable for using the existing GP lane procedures for ramps.
- ML Weave: This is analogous to the GP Weave segment, but with ML traffic demands. The operational characteristics of an ML Weave segment are reasonably close to those of a GP Weave segment and hence the existing GP lane procedure for weaving segments can be applied.
- ML Access Segment (ML-AcS): This is a new segment type and unique to the ML facilities with intermittent access. Lane changing between the GP lane group and the ML group can occur throughout the segment. Different from the Continuous Access ML Basic type, this segment type

exists as the intermittent access segment where access between the ML and GP lanes is prohibited in the segments connect to it. It is treated as a weaving segment and the HCM 2010 weaving methodology is applied to compute its impact. By definition, an ML-AcS segment is always parallel to a GP Access Segment (GP-AcS) which is also shown in Figure 3.3. In the methodology, it is assumed that the operational performance of the ML/GP Access Segment is only estimated once, and results are applied to both ML and GP lane groups.

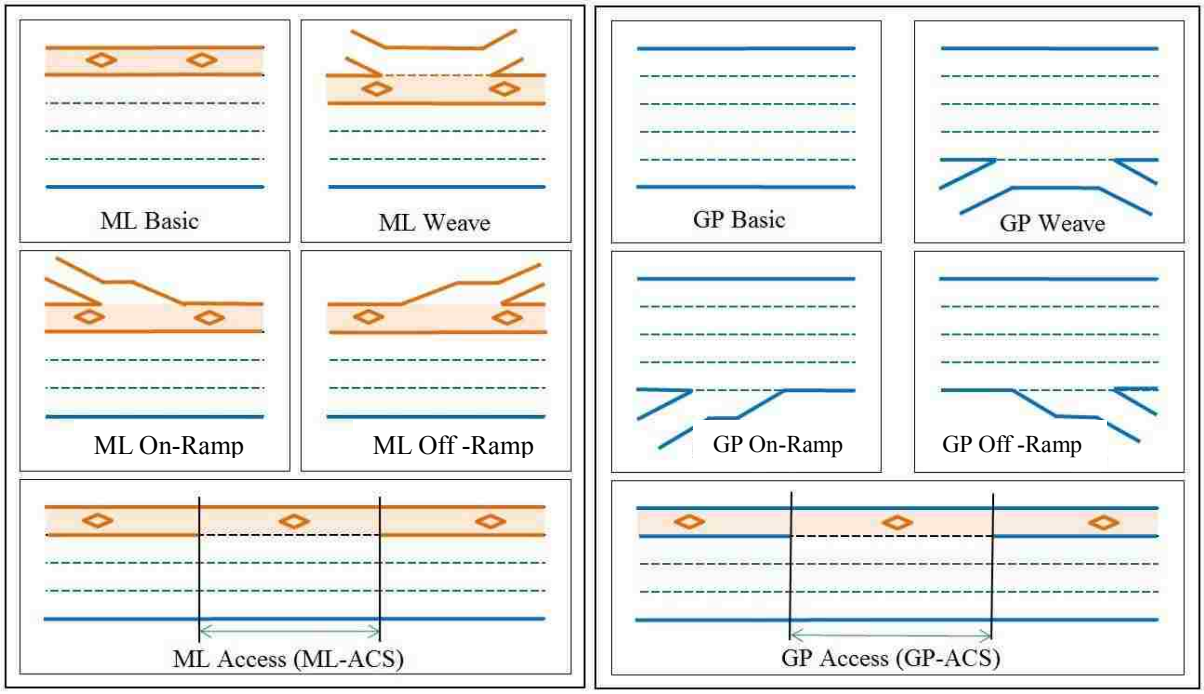

FIGURE 3.3 Different Segment Types for ML and GP Lanes

3.3.3 Speed-Flow Models Developed for ML Basic Segments

As a major component of the ML performance evaluation methods, speed-flow models for the basic ML segments were developed based on empirical data collected through this study. To this end, traffic behavior characteristics of various ML strategies were carefully identified and studied. Data from the ML and the adjacent GP lanes were gathered from each ML site to allow for the

interaction of parallel facilities to be investigated. An extensive database was created to house the large amount of data. Fifteen-minute speed and volume data were archived at each location to be consistent with the HCM 2010 procedure requirements. Heavy vehicle volumes were collected to convert vehicle volumes to units of Passenger Car Equivalents (PCE). Heavy vehicle adjustments and PCE conversions were made in accordance with the coefficient values used in HCM 2010.

For MLs that impose restrictions only during certain hours of the day or days of the week, only data from the periods of time where restrictions were in place were used. Data from each location were then grouped into one of the following five configuration types based on separation type and number of MLs:

1) **Continuous Access** – Skip-stripe or solid single line separated, single lane, continuous access
2) **Buffer 1** – Buffer-separated, single lane
3) **Buffer 2** – Buffer-separated, multiple lane
4) **Barrier 1** – Barrier-separated, single lane
5) **Barrier 2** – Barrier-separated, multiple lane

More details of the five configuration types are discussed in Chapter 4.

3.3.3.1 Form of the Speed-Flow Curve

Each ML Basic segment type does not follow the same speed flow characteristics as determined from empirical observations. Therefore, each of the five ML Basic segment types will have a

unique form of the speed-flow curve. The formation procedure will follow the HCM 2010 speed-flow methodology for basic highway segments to ensure consistency and compatibility. The methodology used in this study is similar to that described by Roess (2011).

Each speed-flow curve comprises of two parts: 1) a linear segment starting from the Free Flow Speed (FFS) at a volume of zero and ending at the breakpoint, and 2) a curvilinear segment from the breakpoint to the capacity of the ML system. Breakpoint, as defined in HCM 2010, is the point separating the linear-speed portion of the curve from the rest of it.

Linear Portion

For ML types Continuous Access, Buffer 2, and Barrier 2, where passing is allowed and the slow car following effect is not significant, the linear portion is basically flat, indicating that traffic travels constantly at the FFS. For types Buffer 1 and Barrier 1, the two ML types where vehicles are unable to perform passing maneuvers, the linear portion of the curve is sloped slightly downward.

The linear coefficient is estimated by anchoring the curve to the FFS at zero flow and determining the slope from zero flow to the breakpoint. Linear regression was used to determine the linear coefficient describing the slope of the curve. The linear portion takes the form:

$$S = FFS - C_1 v \tag{3.7}$$

where S=Speed (mph)

FFS = Free flow speed (mph)

C_1= Linear coefficient (or slope)

v=Flow rate (pcphpl)

Curvilinear Portion

This curvilinear portion takes the form:

$$S = SBP - \frac{(SBP-CS)(v-BP)^{C_2}}{(c-BP)^{C_2}} \quad (3.8)$$

where:

S = Speed (mph)

c = Capacity (pcphpl) – This value was obtained from field observations or estimation of traffic flow models calibrated using the collected data. The FFS for each facility type was assigned a maximum observed speed based on the empirical data.

SBP = Speed at breakpoint (mph) – For ML types Continuous Access, Buffer 2, and Barrier 2, this value is equal to the FFS. For ML types Buffer 1 and Barrier 1, this value should be the speed at breakpoint determined by the linear portion of the curve.

CS = Speed at capacity (mph) – For ML types that do not experience a frictional effect (Buffer 2, Barrier 1, and Barrier 2), the speed at capacity is determined by dividing the capacity by a density of 45 pcpmpl. A density of 45 pcpmpl was chosen as the end point of the speed flow relationship to conform to HCM 2010's current breakdown point for freeway facilities. For ML Basic segment types Continuous Access and Buffer 1, where a frictional effect can be observed, the speed at capacity was determined by dividing the maximum observed flow by a density of 30 pcpmpl.

v= Flow rate (pcphpl) – This is the input value to determine speed.

BP = Flow at the breakpoint (pcphpl) – Breakpoints were estimated by calculating the standard deviation of speed for each volume range of 100 pcphpl. The breakpoints are

determined at the volume where the speed standard deviation begins to increase abruptly. The breakpoint signifies the point in the speed flow relationship where the linear portion ends and the curvilinear portion begins, separating the two parts of the curve.

C_2 = Calibration constant – The calibration constant is the variable used to fit the curve to the data.

Frictional Curve

The performance of the Continuous Access and Buffer 1 facilities is dependent not only on the characteristics of the ML, but also the performance of the adjacent GP lanes. For these two ML types, a second frictional curve has been produced showing the speed-flow relationship for periods of time when GP lanes are congested.

The frictional curve is a function of both the non-friction curve and the flow rate. During the periods of low flow where a frictional effect is not observed, the frictional curve takes the value of the non-frictional curve from zero flow to the breakpoint (BP). Based on regression work using the filed-collected data, after the break point, the friction curve takes the form:

$$S_f = S_{nf} - C_f(v - BP)^2 \quad (3.9)$$

where:

S_f =ML speed during GP congestion (adjacent GP lane has density > 35 pcpmpl)

S_{nf} =Speed of the corresponding non-friction curve for the same flow rate

C_f = Frictional curve constant – While this constant was originally intended to be formed from regression, it was ultimately determined from anchoring the right end of the friction curve along the density line of 45 pcpmpl and the capacity. This method was chosen so that

the speed flow curves are consistent not only among the five basic types of MLs but also with the freeway speed-flow curves.

3.3.4 Access Point Analysis

It is determined from this study that ML On-Ramp, ML Off-Ramp, as well as ML Weave segments have similar operational models that generally match the ones developed for the GP lanes in HCM 2010. Therefore, no duplicate effort would be performed in this project.

For the ML Access Segment (ML-AcS), the vehicles entering the freeway from GP lane on-ramps need to *cross weave* over multiple GP lanes to access the ML. These weaving vehicles will have a negative impact on the operating performance of the parallel GP lanes. This cross-weave effect is found to be a function of different roadway geometric configurations as well as traffic conditions. A microscopic simulation model was built and calibrated using empirically-collected video data to explore this effect. The cross-weave intensity is consequently quantified using Capacity Adjustment Factor (CAF) to account for its impact on the parallel GP facility. This concept is discussed in greater detail in Chapter 4. Beyond the effect of cross-weaves, the ML-AcS is analyzed as regular weaving segments using the HCM 2010 procedures.

3.4 Mesoscopic Approach of Twin-Cell Modeling for Parallel Freeway Facilities

The ML facilities studied consist of MLs and parallel GP lanes. The two lane groups have distinct features in terms of traffic composition, capacity, demand, and free-flow speeds, but also interact with each other (e.g. the friction effect introduced in previous sections). In this section, a twin-cell

modeling approach is developed to improve our understanding of ML traffic flow evaluation and interactions. The approach is particularly useful and applicable for modeling the basic ML segments, and access points where weaving between the two lane groups (ML vs. GP lane) is present. On the basis of CTM, cell-based mesoscopic simulation model allows vehicle-crossing and exchanging based on the weaving demand and traffic conditions of the cells. The frictional effect is also appropriately incorporated into the traffic flow model formulation via different data mining methods to accurately reproduce the traffic dynamics on parallel freeway facilities.

This section is divided into two subsections: basic ML segment modeling and access point weaving modeling. For basic ML segment, the buffer-separated single lane ML facilities, where frictional effect exists, is of particular interests. Two analytical methods, HCM-based and unsupervised learning approaches are both implemented to model the friction on the basis of the level of sophistication one would like to simulate the facility. For the weaving analysis, the proposed model is able to extend the macroscopic CTM into a grid-level lane-based mesoscopic simulation. It thus provides guidance to the analysts and researchers for modeling the parallel freeway facilities at a finer resolution with satisfying accuracy.

3.4.1 Basic ML Segment Modeling

3.4.1.1 HCM-based Approach

The in-depth analyses indicate that the frictional effect is critical for realistically replicating the real-world parallel facilities and facilitating our understanding of traffic dynamics modeling. On the basis of NCHRP 03-96 research project, the formulation of the set of speed-flow curves for the

buffer-separated single ML facility is developed and shown in Figure 3.4. The formulation methodology for the two sets of curves for each FFS is introduced in Section 3.3.3. The friction curves terminate at a density of 45 pcpmpl, consistent with the methodology used in HCM 2010. The range of observed data for the non-friction curves never reached such high density levels, probably attributable to a low likelihood of observing non-friction cases in combination with high flow rates. As a result, the terminal density of the non-friction curves is 30 pcpmpl.

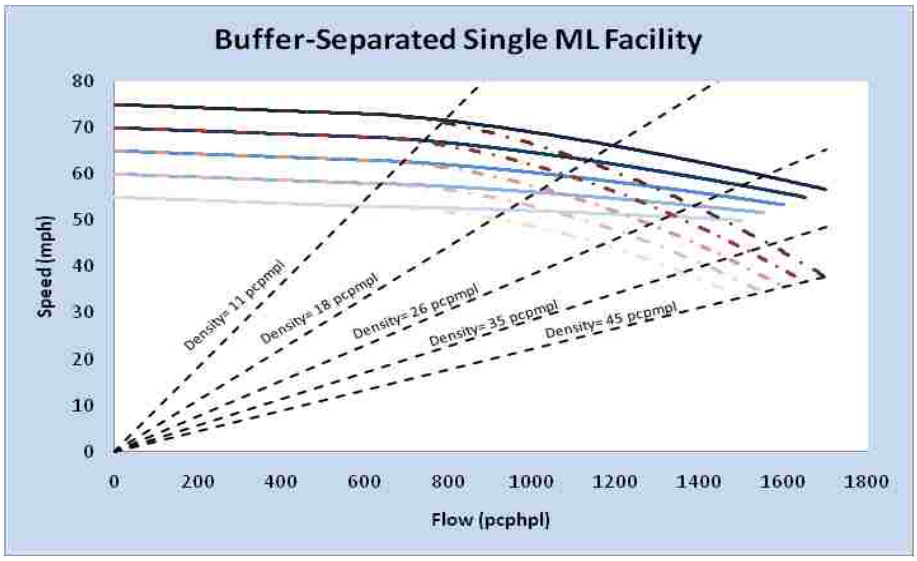

FIGURE 3.4 The Speed-flow Curve Family for Buffer-separated Single ML Facility

The developed speed-flow curves for ML facility combining with the GP speed-flow relationship published in HCM 2010 function as the basis for the proposed traffic flow model utilizing CTM. The CTM is applied here to model the one-way traffic on the ML freeway segment. A cell representation of the freeway segment of interest is shown in Figure 3.5. The freeway segment, exploited as a single unidirectional link in this study, is homogeneous. This segment is simulating the SR 167 HOT lane system in Seattle, Washington, where a single ML is separated from two GPLs by a double white line buffer. For the basic ML segment, travelers are not allowed to switch lanes between ML and GP lanes. The FFS on this segment is 65 mph from the empirical data.

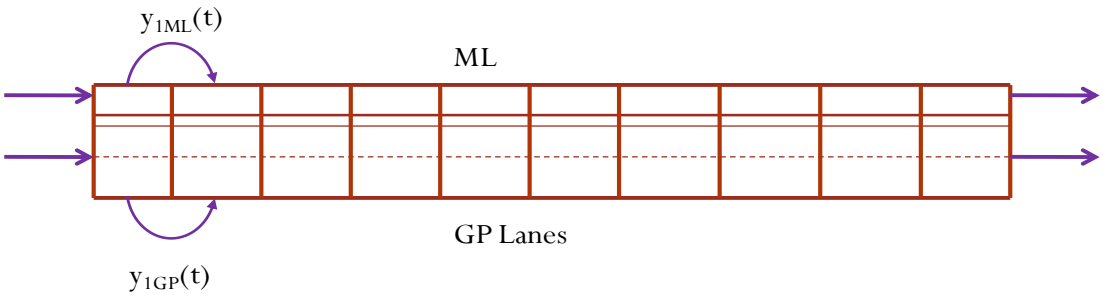

FIGURE 3.5 Cell Representation of Buffer-separated ML Facility ($y_{1ML}(t)$ and $y_{1GP}(t)$ represent cell inflow for ML and GP lanes, separately)

Under the HCM context, the parameters for the flow-density relationship characterizing the link can be calibrated. The determination of the capacity and jam density for the GP lanes and buffer-separated ML is based on the calibrated curves provided in HCM 2010 and NCHRP 03-96 research project. The lower portion of the curves is regressed using Van Aerde's steady-state car-following model (Van Aerde and Rakha, 1995). Figure 3.6 shows the flow-density curves for both the ML and GP lanes. At the SR 167 HOT lane corridor, the FFS is determined to be 65 mph for the freeway link. On the GP lanes, the capacity is chosen to be 2300 vphpl, and the jam density is approximately 165 vpmpl. Based on the assumed triangular shape of flow-density relationship, the backward wave speed is 17 mph. For the ML, when no frictional effect is present, the capacity can reach up to 2000 vphpl, and the jam density is about 160 vpmpl. The backward wave speed is therefore about 15 mph. However, when frictional effect exists, the capacity reduces to 1600 vphpl, and the jam density is only around 125 vpmpl. The corresponding backward wave speed is 16 mph.

The total length of the freeway segment analyzed in this study is 6.5 mile. The free-flow travel time is then 0.1 hour. The parameters of the CTM are set as shown in Table 3.1. The traffic advancing logic is demonstrated in Figure 3.7. For both ML and GP cells, upon the update of the inflow for each cell at each time step, the occupancy of the current cell (number of vehicles in each

cell) would be updated as well following Equation (2.1). While for ML, the flow advancing to next cell will also be determined by its neighboring GP cell condition. If the neighboring GP cell is under congested condition (>35 vpmpl), then the inflow to the next ML cell will use the set of parameters for the "friction" state. Accordingly, if the neighboring GP cell is in the uncongested scenario, then the flow advancing to the next cell will adopt the parameters of the "non-friction" state.

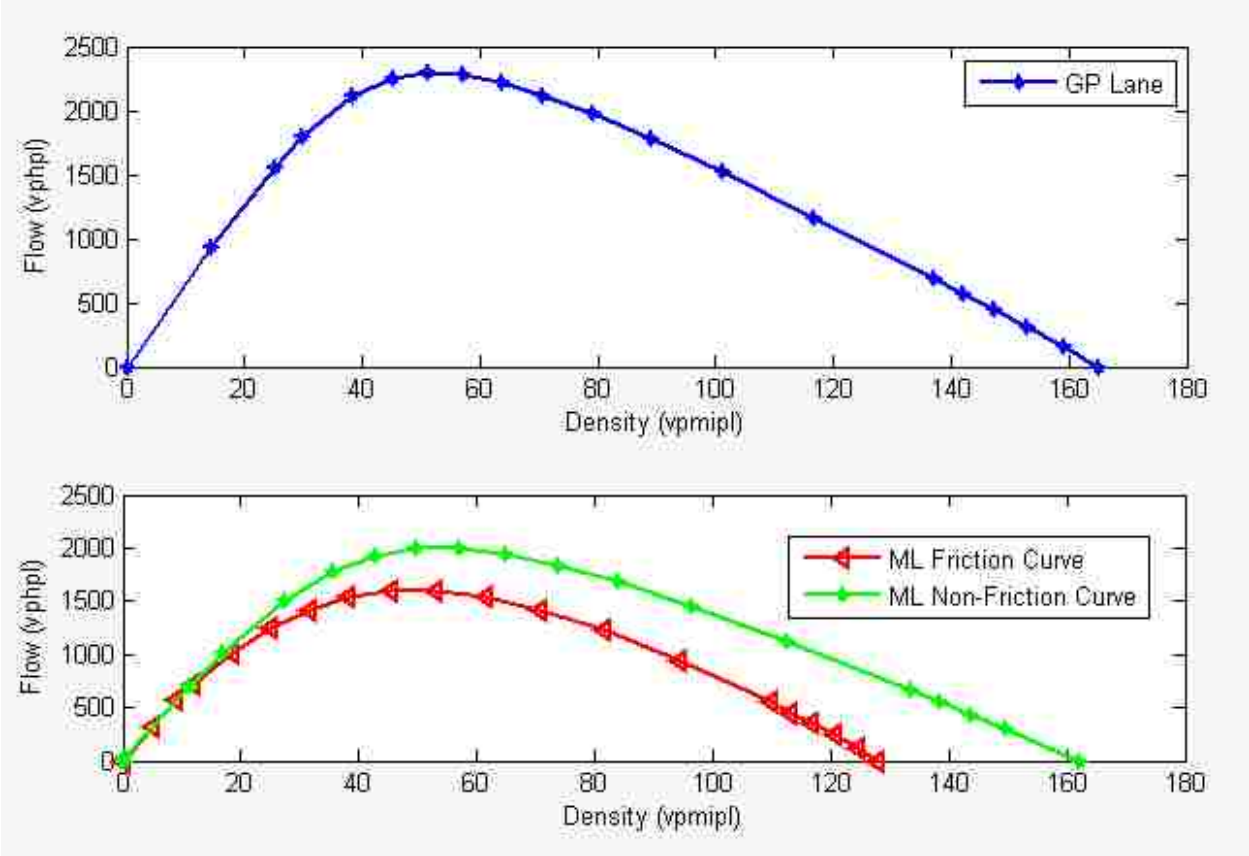

FIGURE 3.6 Flow-density Curves Calibrated for GP Lanes and Buffer-separated ML

TABLE 3.1 CTM Parameters for the Freeway Segment

Time Step	0.01 hour		
Cell Length	0.65 mile		
	GP Lanes	ML	
		Non-Friction	Friction
Jam Density	165 vpmpl	160 vpmpl	125 vpmpl
Backward Wave Speed	17 mph	15 mph	16 mph
δ	0.26	0.23	0.25
Maximum Inflow for Each Cell	23 veh	20 veh	16 veh
Maximum Occupancy for Each Cell	107 veh/lane	104 veh	81 veh

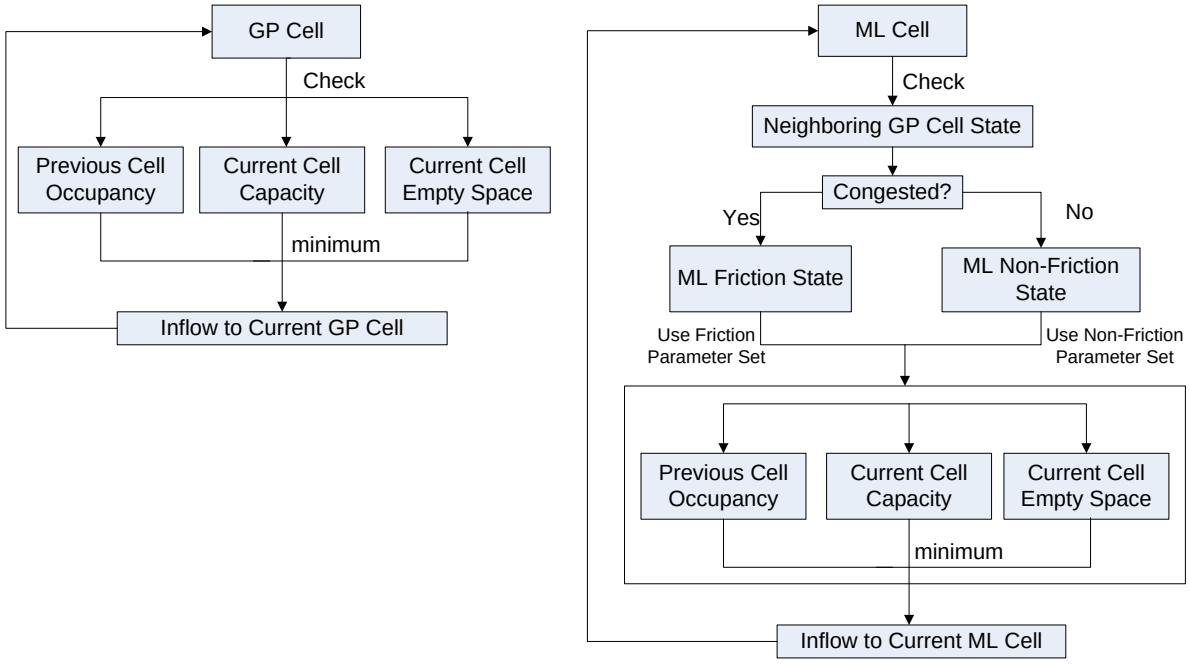

FIGURE 3.7 Framework of the Traffic Flow Model

3.4.1.2 Unsupervised Learning Approach

One disadvantage of the piecewise functions developed in Section 3.4.1.1 is that it is unable to capture the features of gradient changes of frictional effect. Particularly, the adjacent GP cell density serves as the single threshold to alternate between ML frictional vs. non-frictional modules.

This makes the concept of "GP congestion" as a sudden switch using density as criteria, while in reality, the friction might exist even when GP lanes' condition is outside the previously defined "congested" regime. Therefore, another model on the basis of unsupervised learning is developed for better capturing this effect. By adopting the viscosity concept expressed in Equation (3.10), the frictional effect imposed onto the ML cell is determined to be a function of speed differential between the adjacent GP and ML cells, as well as the density of the adjacent GP cell and flow of the ML cell (Equation (3.11)). The constant η (viscosity) can be carefully calibrated based on field collected data and classified under a variety of traffic conditions, very much resembles the fact that different fluids would have different viscosity.

$$F_{viscous} = \eta A \frac{\Delta v_x}{\Delta y} \tag{3.10}$$

where η is viscosity; A is area; and $\frac{\Delta v_x}{\Delta y}$ represents velocity gradient.

$$F_{friction} = \eta k_{GP} \frac{\Delta v_{GP,ML}}{\mathrm{q_{ML}}} \tag{3.11}$$

where k_{GP} is the density of adjacent GP cell; $\Delta v_{GP,ML}$ is the speed differential between the twin cells; and $\mathrm{q_{ML}}$ is the flow of the ML cell.

It is therefore postulated that the friction factor is correlated with several variables: GP Speed, volume, density, ML volume and speed. Using the HCM curve as a benchmark, the friction is considered as a speed reduction rate for a specific ML volume. The empirical data collected to calibrate the friction model are shown in Table 3.2. They are collected from sensors on the basic ML/GP segment with buffer-separated facilities. Based on Equation (3.11), the frictional effect can be modeled under various traffic conditions categorized by multiple variables. To determine the proper categorization, cluster analysis is applied to discover the hidden structure within the

empirical data. Clustering gives analysts an opportunity to group sample dataset in a generally unguided fashion based on the similarity amongst data. This is achieved by measuring the distance between data samples. In this study, k-means clustering algorithm is applied to identify *k* collection of clusters using a heuristic search technique.

TABLE 3.2 Sensor Data for Calibrating the Friction Model

Facility Name	Number of Sites	Span of Data Collected
I-405 Los Angeles, CA	4	1 month, TWTH, all hours
SR 167, Seattle, WA	4	1 month, all days, 5am – 7 pm
I-394, Minneapolis, MN	3	1 month, TWTH, 6 am – 10 am

At the initial state of the clustering, the entire datasets are partitioned into k clusters and all the samples are associated with their closest mean, which is the average value of the variable over the samples. The search heuristic begins with a random collection of k clusters. The distance between a sample and each of the k vectors of mean values will be measured (Williams, 2011). The distance measure that is commonly used is known as Minkowski distance, formulated as:

$$d(a,b) = \sqrt[q]{(|a_1 - b_1|^q + |a_2 - b_2|^q + \cdots + |a_n - b_n|^q)} \tag{3.12}$$

where a_1 is the value of Variable 1 for sample data a, etc. In this study, q is set to *2*, which makes the distance measure the Euclidean distance.

The sample is then associated with its closest cluster. And the mean value for the k vectors updated. The iterative process continues until no more samples move from one cluster to another. The quality of the cluster model is measured by sum of *within cluster sum of squares*, which is expressed as:

$$\arg\min_{S} \sum_{i=1}^{k} \sum_{xj \in Si} \left\| x_j - \mu_i \right\|^2 \tag{3.13}$$

where μ_i is the mean of samples in cluster Si.

In order to determine the optimal number of clusters for the sensor dataset, iterative clusters were run in this study. Figure 3.8 shows the sum of *within cluster sum of squares* for different number of clusters. The graph also shows the change in the sum of squares. A heuristic is to choose the number of clusters where we see the largest drop in the sum of the within cluster sum of square. For each categorization, ten random seeds were run and the average value is derived. It is determined from Figure 3.8 that 6 clusters is a tradeoff between computational efficiency and accuracy.

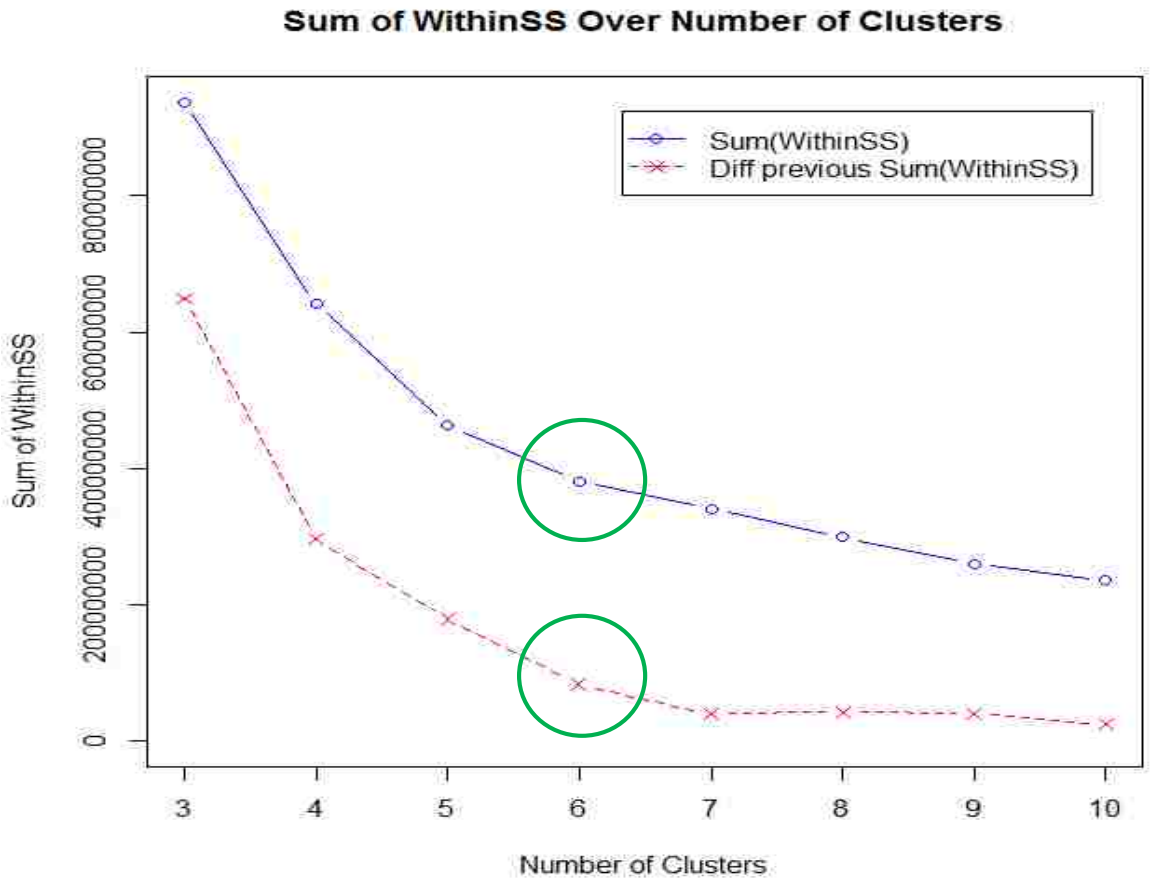

FIGURE 3.8 Sum of *Within Cluster Sum of Squares* for Different Number of Clusters

The final clustering results are shown in Table 3.3. The table illustrates the means of the variables for each cluster. Based on the clustering results, the variables, particularly *GP Density* and *Friction*, are plotted in Figure 3.9 to demonstrate the differences between clusters. The Friction is defined as the speed reduction rate of the actual ML speed comparing with the HCM benchmark, and is expressed as:

$$Friction = \frac{ML\ Actual\ Speed}{Speed_{HCM}} \tag{3.14}$$

TABLE 3.3 Means of Variables for Each Cluster

Cluster	ML Speed	ML Volume	GP Speed	GP Volume	GP Density
1	66.9	57	67.5	268	4
2	66.5	241	66.5	782	12
3	65.3	412	64.1	1220	20
4	64.3	550	62.9	1613	26
5	62.6	768	64.2	2015	32
6	48.4	1370	42.3	1680	47

*Speed in mph; Volume in passenger car/hour/lane; and Density in passenger car/mile/lane

Meanwhile, natural log function is applied to the two variables in Figure 3.9. This is due to the fact that logarithm transform can map broad range of numeric values into a narrower range, which effectively reduce the spread of the values. It is particularly useful when outliers with extremely large values are present (Williams, 2011). The general trend shown in Figure 3.9 is that, with a higher GP density level, the frictional effect becomes more pronounced. To model the friction, robust regression is applied, which is effective in eliminating the impact of outliers in the data. Table 3.4 shows the results for friction modeling. This serves as the foundation for updating the CTM cell progression logic under different regimes of traffic conditions.

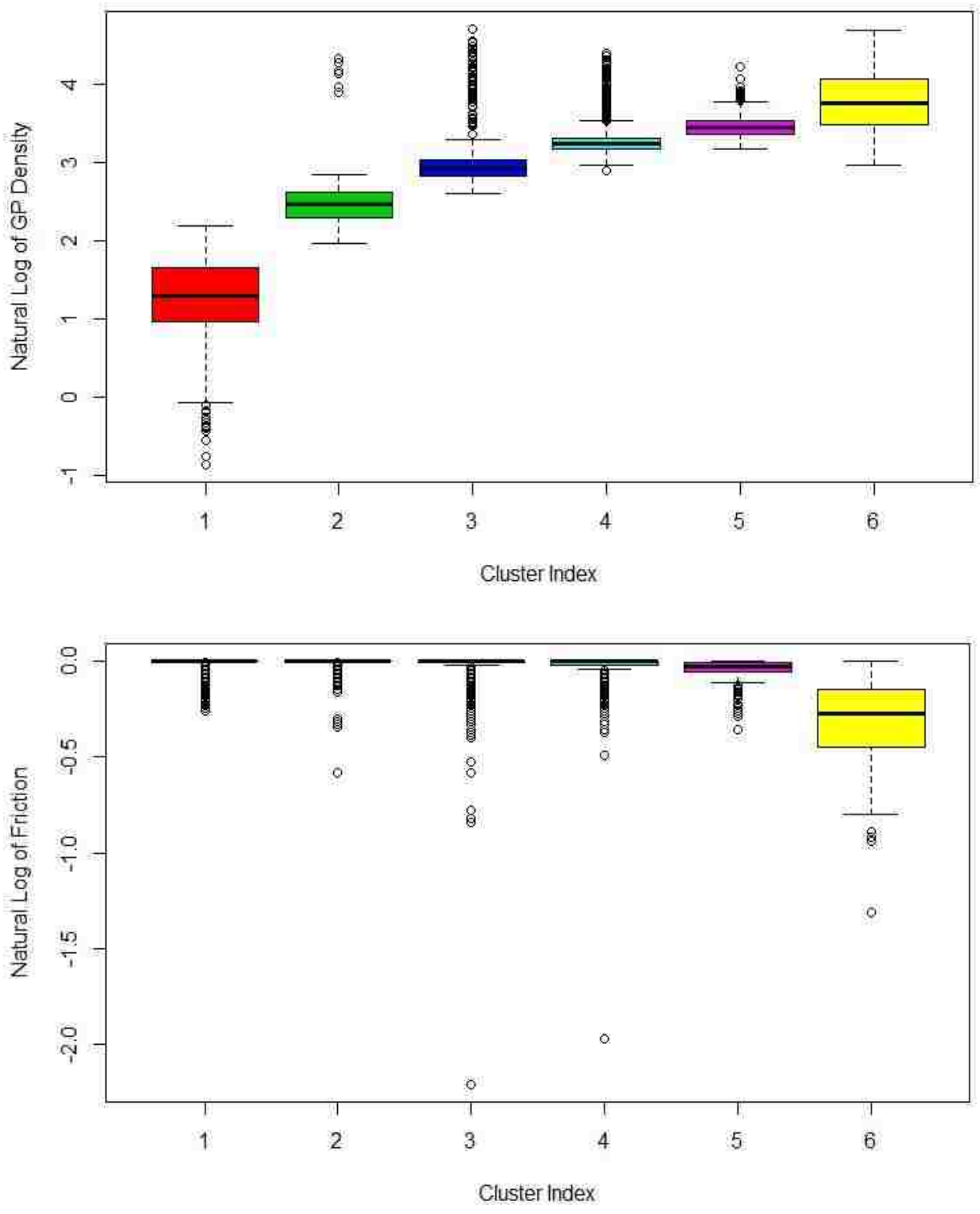

FIGURE 3.9 Box Plot of Variables *GP Density* and *Friction* for the Six Clusters

TABLE 3.4 Robust Regression Result for Friction

ML Volume Cluster	Friction
1: 0-200	1
2: 200-500	$1.02 \times D^{-0.01}$
3: 500-800	$1.17 \times D^{-0.05}$
4: 800-1100	$1.47 \times D^{-0.13}$
5:1100-1400	$2.43 \times D^{-0.30}$
6: 1400-higher	$1.64 \times D^{-0.23}$

3.4.2 Weaving Segment Modeling

The original CTM does not allow a highway network with more than three-legged junctions due to the potential complication and confusion that may result onto the link flow equations. Figure 3.10 shows such a weaving representation that is considered invalid for the original CTM.

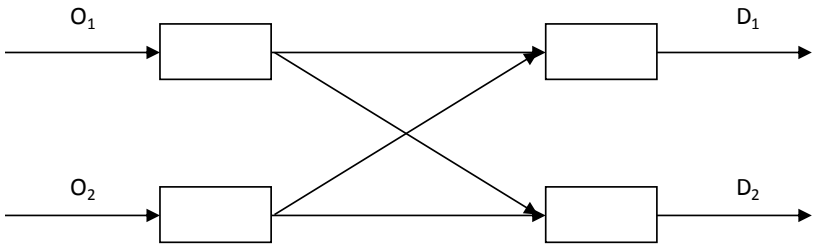

FIGURE 3.10 A Weaving Representation

Assume that the Origin-Destination (OD) volume of such a building block shown in Figure 3.10 is known. The OD matrix can be thus expressed as:

$$\begin{bmatrix} O_1D_1 & O_1D_2 \\ O_2D_1 & O_2D_2 \end{bmatrix} \tag{3.15}$$

Let x_i denotes the actual through volume, and y_i denotes the actual weave volume, with i being the lane index. R_i represents the maximum occupancy for the receiving cell, r_i represents the existing number of vehicles in the receiving cell. The receiving cell's maximum occupancy can be decomposed into two components: R_i^{TH} and R_i^{LC}, representing the maximum allowing occupancy for through traffic and lane change traffic, separately. Therefore, the following relationships stand:

$$x_1 + y_2 = \min(Q, R_1 - r_1, O_1D_1 + O_2D_1) \tag{3.16}$$

$$x_2 + y_1 = \min(Q, R_2 - r_2, O_2D_2 + O_1D_2) \tag{3.17}$$

The above two equations are not sufficient for solving the four variables, as more questions are generated from the relationship. For example, is there a priority given to either through or weave traffic when the downstream cell/block is dominating the progress? Or since the relationships presented above only give range constraints, are the variables $x_i$and y_i stochastic or deterministic?

3.4.2.1 Causality Regime Discussion

With these questions raised, three causality regimes are discussed in this section.

1. ***Forward***: the traffic condition is dictated by the upstream traffic (e.g. waves moving forward). This situation implies that no congestion is potentially formed at the current tick of clock. Then

$$x_1 + y_2 = O_1D_1 + O_2D_1 \tag{3.18}$$

$$x_1 = O_1D_1 \tag{3.19}$$

$$y_2 = O_2D_1 \tag{3.20}$$

2. ***Backward a***: the traffic condition is dictated by the downstream traffic, due to the lack of available downstream cell capacity. Then

$$x_1 + y_2 = Q \tag{3.21}$$

Here we define a parameter p as the ratio between the actual through volume and lane change volume, where $p = \frac{TH}{LC}$. This parameter can be served as the calibration parameter for adjusting the progression volume when the receiving cell has limited capacity (or occupancy as for the causality regime 3). It can also serve as a gauge for measuring people's driving aggressiveness, suggesting

the priority given to the through traffic. If p=1, it indicates that through and lane change demand are treated with equal weight. If p<1, then the downstream cell is giving more priority to the lane change traffic, such that lane changers are more aggressive in getting into the target lane position. If p>1, then the downstream cell is giving more priority to the through lane traffic, such that the through traffic is less willing to give gaps for the lane change traffic.

$$x_1 = Q \times \frac{p \times O_1 D_1}{p \times O_1 D_1 + O_2 D_1} \tag{3.22}$$

$$y_2 = Q \times \frac{O_2 D_1}{p \times O_1 D_1 + O_2 D_1} \tag{3.23}$$

3. ***Backward b***: the traffic condition is dictated by the downstream traffic, due to the lack of available downstream storage. Then

$$x_1 + y_2 = R_1 - r_1 \tag{3.24}$$

$$x_1 = (R_1 - r_1) \times \frac{p \times O_1 D_1}{p \times O_1 D_1 + O_2 D_1} \tag{3.25}$$

$$y_2 = (R_1 - r_1) \times \frac{O_2 D_1}{p \times O_1 D_1 + O_2 D_1} \tag{3.26}$$

CHAPTER 4 OPERATIONAL CONCEPTS AND TRAFFIC FLOW PRINCIPLES IN MANAGED LANES

4.1 Segment Type

In practice, some ML facilities are physically separated from GP lanes (e.g. with a barrier), while others are constructed concurrent with GP lanes with only narrowly painted lane markers or buffers in separation. In all cases, the composition and behavior of the ML traffic stream is expected to be very different from traffic in the GP lanes. Most notably, traffic volumes, FFS, driver type (commuter vs. casual), and potential per-lane capacity, are expected to differ between ML and GP lanes. This dichotomy of geometric and behavioral attributes of parallel ML and GP facilities poses a major challenge for a deterministic analysis framework. Further, despite this difference in attributes, it is postulated that there is at least some degree of interaction between traffic operations in the ML and GP lanes. This is especially true for concurrent ML facilities, as ML and GP traffic is oftentimes only separated by narrow unobtrusive striping as documented by Liu *et al.* (2011). Interaction may even apply to barrier-separated facilities, where congestion in the GP lanes may have a "rubbernecking" effect on the parallel MLs.

4.1.1 The Lane Group Concept

To capture interaction effects between ML and GP lanes, while allowing varying demand, capacity, and speed inputs, it is proposed to introduce the concept of *lane groups* into the analytical framework for freeway MLs. The lane group concept is well-established in the signalized intersection methodology of the HCM 2010 (TRB, 2010), where it is recognized that exclusive left

turn lanes have different geometric and/or behavioral characteristics from the adjacent through lanes, or from shared lanes. By adopting the lane group concept in the ML context, the analyst will be able to ascribe separate attributes to parallel ML and GP facilities, while retaining the ability to model some degree of interaction between the two.

Each segment of a freeway facility in the proposed implementation would therefore be represented as having either one or two lane groups, depending on whether parallel MLs are present. The analyst codes input variables such as geometric characteristic (e.g. number of lanes), behavioral attributes (e.g. free-flow speed, capacity), and traffic demands separately for each lane group, but still within the same computational engine environment. The methodology would then assess the operational performance of each lane group, under consideration of empirically-derived interaction effects between the two lane groups. Any portion of the facility where no ML is present would simply be coded as a single lane-group that serves all traffic demand.

The following assumptions apply to the proposed framework:

- A freeway GP segment with a parallel ML segment is coded as two adjacent lane groups in the methodology.
- Adjacent lane groups (one GP and one ML segment) must share the same segment lengths.
- Adjacent lane groups can be of different segment types for example, a basic ML segment may be concurrent with a GP segment with an on-ramp.
- Each lane group may have different geometric characteristics, including number of lanes, lane widths, shoulder clearance, etc.

- Each lane group can have unique behavioral attributes, including free flow speed, segment capacity, or various capacity- or speed-reducing friction factors. The attributes are represented by GP speed-flow relationships available in HCM 2010, as well as ML-specific relationships presented in this report.
- Each lane group can have unique traffic demand parameters, which are input by the user, and which are obtained through an external process. As an operational methodology, the HCM is not intended to make predictions about traffic demands.
- The operational performance of adjacent ML and GP lane groups is interdependent in that congestion in one lane group may have a frictional effect on operations in the adjacent lane group depending on the type of separation. This friction effect was empirically-derived in this project, can be user-calibrated, and is sensitive to the type of physical separation between lane groups (i.e. striping vs. buffer vs. barrier).

The method assumes that all ML segments should have a demand-to-capacity ratio less than 1 ($d/c<1$), which means that no congestion would occur on ML segments. Congested ML facilities are relatively rare in practice, as one of the underlying principles for ML operations (especially for HOT lanes) is to assure that ML traffic density is below the critical density level even in peak periods, which in turn guarantees satisfactory service to ML customers. Congestion on GP lanes can and should be considered by the method, as systems of congested GP lanes with below-capacity ML conditions are very common.

4.2 Speed-Flow Model Development for Basic ML Segments

This section presents the operational performance and speed-flow relationships for the basic

segments of ML facilities. Data collection sites selected for this study were located at least 1,500 ft from merging and diverging segments to minimize possible weaving impacts. That distance threshold was selected because it corresponds to the length of the ramp influence area in HCM 2010 (TRB, 2010).

For the development of the speed-flow relationship for basic segments of ML facilities, HOV, HOT, and express toll lane facilities were combined. While it is recognized that differences in operations between facilities affect the demand, it was assumed that traffic behavior on basic segments was independent of the management practice on the facilities. Only the separation type and number of lanes were hypothesized to affect the traffic flow behavior of the ML facility (Thomson *et al.*, 2012).

4.2.1 Different Separation Type Characteristics

4.2.1.1 Continuous Access

Continuous Access separation type refers to single lane, concurrent ML facilities in which access between the ML and GP lanes is allowed at any point. Entrances and exits to the ML lane are unrestricted. These facilities are typically located on the leftmost lane on freeways parallel to the GP lanes. Figure 4.1 shows the schematic of this configuration. The solid single line separating the ML from the GP lanes can also be skip-striped. Either way, vehicles can cross between the ML and GP lanes at any time. A section of I-5 in Seattle, Washington, provides an example of the solid-line separated Continuous Access facility, and a section of I-95 in Broward County, Florida, provides an another example for skip-strip separated Continuous Access facility, as shown in Figure 4.1. Although these types of facilities are very common, they are not favorable for HOT

lane operations as continuous access is more difficult to manage for most tolling schemes.

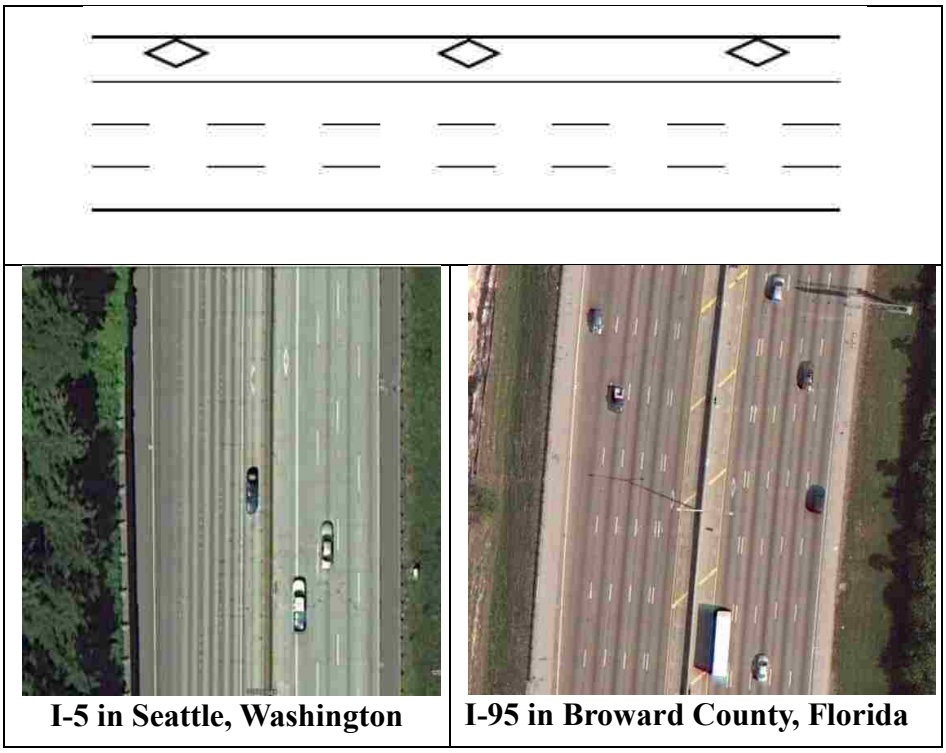

I-5 in Seattle, Washington | I-95 in Broward County, Florida

FIGURE 4.1 Schematic of Continuous Access and Examples at I-5 Seattle, Washington and I-95 in Broward County, Florida (Source: Google Earth)

4.2.1.2 Buffer 1

Buffer 1 refers to the single, concurrent lane ML facilities with intermittent access. Similar to Continuous Access, these facilities are located in the leftmost lane of the freeway cross section. They are separated from the GP lane with a two- to four-foot striped buffer. The striping techniques for Buffer 1 also vary by location, and can feature a double white line, a double yellow line, or two yellow stripes and one white stripe (as is typical in California). Access to and from the ML is limited to occasional buffer opening areas designated by dashed line separation. This geometry is commonly used for both HOV and HOT facilities. Figure 4.2 shows the basic schematic of a Buffer 1 facility along with an example at I-394 in Minneapolis, Minnesota.

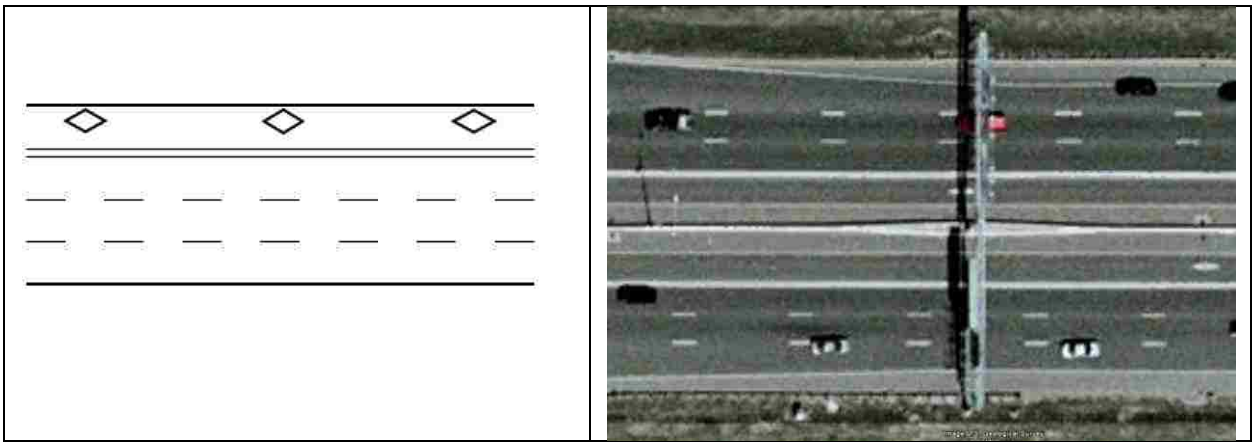

FIGURE 4.2 Schematic of Buffer 1 and Example at I-394 Minneapolis, Minnesota (Source: Google Earth)

4.2.1.3 Buffer 2

Segment type Buffer 2 is similar to type Buffer 1 but with multiple MLs. It is generally separated from the GP lanes with a two- to four-foot buffer consisting of various painting schemes. This type of facility is the rarest of the five facility types studied, although it may become more popular in future deployments. I-110 in Los Angeles, California was the only location with data available for this type of configuration. Figure 4.3 displays a schematic of the facility type and an aerial view of I-110 in Los Angeles, California.

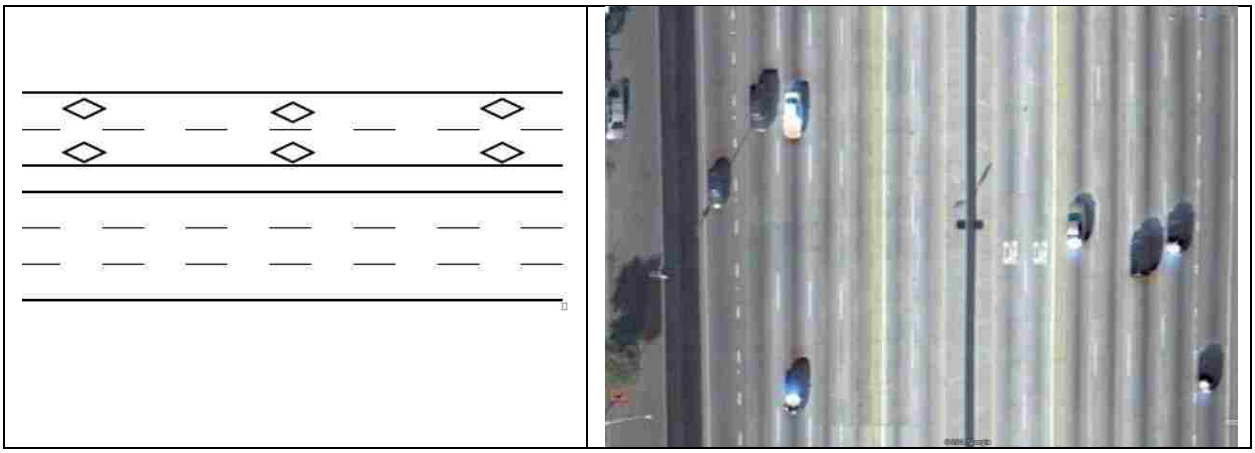

FIGURE 4.3 Schematic of Buffer 2 and Example at I-110 Los Angeles, California (Source: Google Earth)

4.2.1.4 Barrier 1

Barrier 1 refers to single lane barrier separated MLs. The barrier in all facilities used in this study was concrete barrier. Other physically separating schemes such as landscaping could also be considered barrier-separated. This facility type is suitable for HOV, HOT, and express toll lanes. Figure 4.4 shows the schematic of Barrier 1 separation and an example of Barrier 1 with an aerial view of I-5 in Orange County, California.

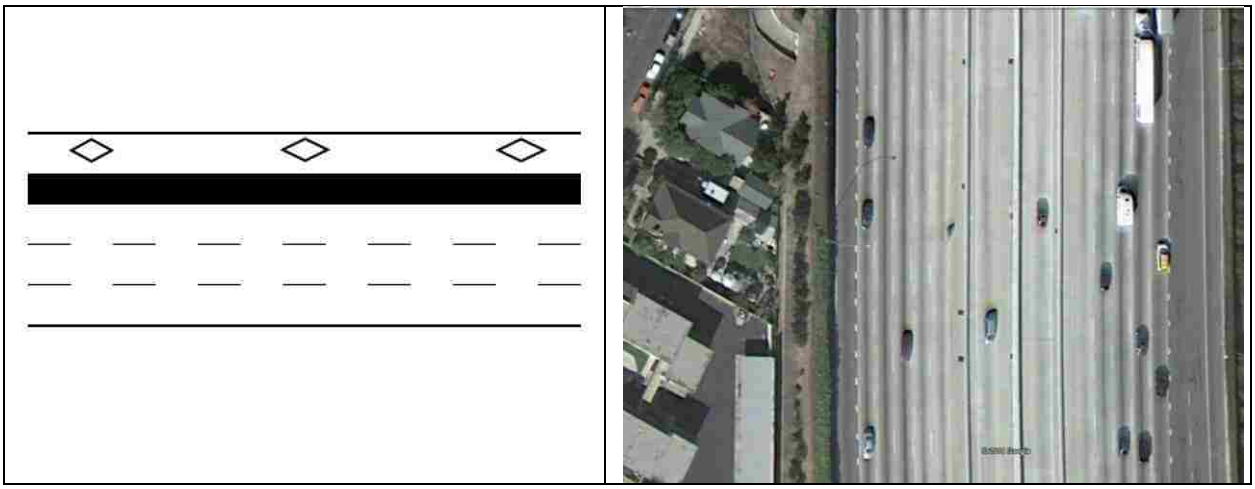

FIGURE 4.4 Schematic of Barrier 1 and Example at I-5 Orange County, California (Source: Google Earth)

4.2.1.5 Barrier 2

Barrier 2 refers to barrier-separated facilities with multiple lanes. The barrier can consist of a concrete barrier or wide landscaped separation. Access between the MLs and GP lane are limited and can be in the form of either a weave access, or direct ramp access. This type of facility is commonly used for HOV, HOT, and express toll lanes. Note that pylon separated facilities were not considered in this study and should not be compared to barrier separation. Figure 4.5 shows a sample schematic of the Barrier 2 configuration and an image of I-5 in Seattle, Washington is shown as an example of a Barrier 2 facility.

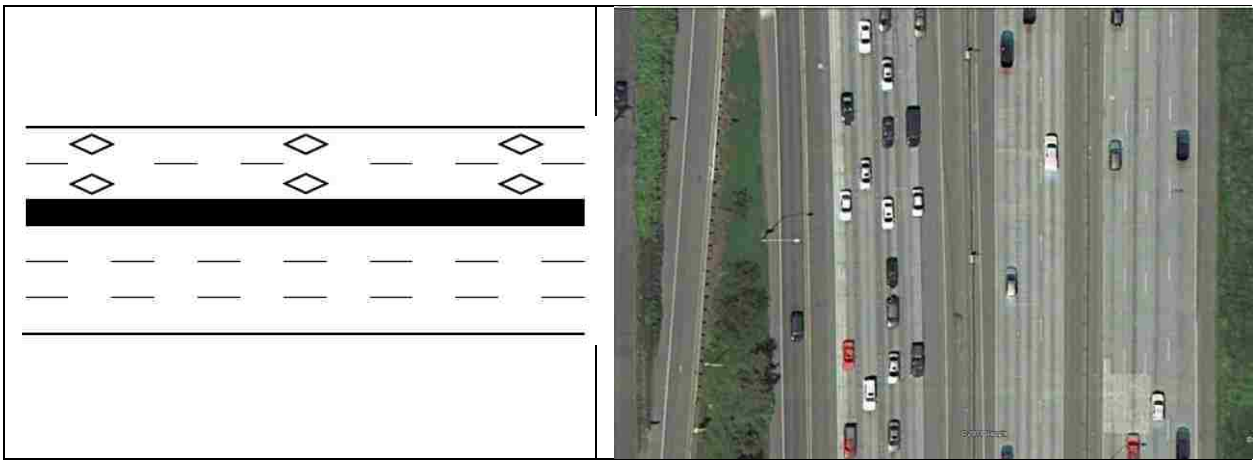

FIGURE 4.5 Schematic of Barrier 2 and Example at I-5 Seattle, Washington (Source: Google Earth)

4.2.2 Data Acquisition

Data were collected at different sites across the country for each of the five segment types.

4.2.2.1 Continuous Access Sites

I-5 Seattle, Washington, and I-405 King County, Washington

Two facilities from the Puget Sound region in Washington were used in the continuous access dataset. I-5 in Seattle, Washington and I-405 in King County, Washington contain continuous access HOV facilities located in the leftmost lane in both the northbound and southbound directions. The HOV lane is separated from the GP facility by a single solid striped line. The HOV restriction of 2+ occupants is enforced at all times on I-5, and every day from 5:00am to 7:00pm on I-405. Data from the two facilities were collected from the WSDOT Compact-disc Data Retrieval (CDR) system and for the entire month of August 2010. August was chosen for data collection because it is a dry month and the weather impacts on driver behavior can be minimized. The locations from each of the facilities are summarized in Table 4.1.

TABLE 4.1 Continuous Access Data Site, I-5 & I-405 Washington State

Facility	Direction	Milepost	Cross-Street
I-5	Northbound	172.89	NE Northgate Way
I-5	Northbound	176.74	NE 185th St
I-5	Northbound	179.76	NE 213th St
I-5	Northbound	193.03	SW 36th St
I-5	Southbound	173.75	NE 130th St
I-5	Southbound	174.60	NE 145th St
I-405	Northbound	6.08	SE 24th St
I-405	Northbound	18.07	NE 97th St
I-405	Southbound	3.59	SE 3rd St
I-405	Southbound	7.00	SE 37th St
I-405	Southbound	18.07	NE 97th St

I-95 Broward County, Florida

Two locations along I-95 in Broward County, Florida were used as part of the dataset for continuous access MLs. The HOV lanes operate both northbound and southbound parallel to the GP lanes on the leftmost side of the traffic stream for each direction. They are separated from the GP lanes by a double dashed line. The HOV lane restrictions are only active during peak travel times, limiting use to vehicles with 2+ persons during the periods of 7:00-9:00 AM and 4:00 to 6:00 PM, Monday through Friday.

Data were gathered from Florida's Statewide Transportation Engineering Warehouse for Archived Regional Data (STEWARD). It is a central database program sponsored by Florida Department of Transportation (FDOT) and maintained by University of Florida Transportation Research Center.

TABLE 4.2 Continuous Access Data Sites, I-95 Florida

Facility	Direction	Milepost	Cross-Street
I-95	Northbound	29.6	NW 19th St
I-95	Northbound	20.4	Johnson St

4.2.2.2 Buffer 1 Sites

I-405 Los Angeles, California

Four sites along I-405 in Los Angeles, California were used as part of the data set for Buffer 1 separation. These sites are listed in Table 4.3. This facility has intermittent access to the HOV lane on the leftmost side of both the northbound and southbound directions. The HOV lane is separated from the GP lanes by a double yellow line buffer. Data from each of the sites were taken from California's Performance Measurement System (PeMS).

TABLE 4.3 Buffer 1 Sites at I-405 California

Facility	Direction	Milepost	Cross-Street
I-405	Northbound	39.20	Crenshaw
I-405	Southbound	39.28	Crenshaw
I-405	Northbound	32.46	Alameda
I-405	Southbound	31.82	Santa Fe

SR 167 King County, Washington

Four sites along SR 167's HOT lane in King County, Washington were used as part of the Buffer 1 dataset. SR 167's HOT lane was introduced in May 2008, converted from an underutilized HOV lane. A single HOT lane and two GP lanes run in each direction along the corridor. The HOT lane is separated from the GP lanes by a double white line buffer. Movement into and out of the HOT lane is restricted to specific access points. Dynamic pricing is used to optimize the performance of the corridor, maintaining a speed above 45 mph. The HOT lane's restrictions are in effect from 5:00am to 7:00pm daily. Data from SR 167 was collected from the WSDOT CDR system. Data for the entire month of August 2010 was gathered. The locations from which the data were

gathered are summarized in Table 4.4.

TABLE 4.4 Buffer 1 Data Sites, SR-167 Washington State

Facility	Direction	Milepost	Cross-Street
SR-167	Northbound	24.61	SW 41st St
SR-167	Northbound	23.90	S 187th St
SR-167	Northbound	22.93	S 202nd St
SR-167	Southbound	22.93	S 202nd St

I-394 Minneapolis, Minnesota

Three sites from I-394's HOT lane in Minneapolis, Minnesota were used in the Buffer 1 dataset. The buffer-separated section on this facility stretches eight miles west from downtown Minneapolis. The HOT lane is located on the leftmost side of the traffic stream in both the eastbound and westbound directions. Access to the HOT lane is restricted to specific locations. The HOT lane is separated from the GP lanes by a double white line buffer. The toll rate along the corridor is dynamically adjusted to ensure the system operates above 50 mph at all times. Data for the corridor was obtained through the Minnesota Department of Transportation's online Data Extract Tool.

TABLE 4.5 Buffer 1 Data Sites, I-394 Minnesota

Facility	Direction	Cross-Street
I-394	Eastbound	General Mills Blvd
I-394	Eastbound	US 169
I-394	Eastbound	Co Rd 73

4.2.2.3 Buffer 2 Site

I-110 Los Angeles, California

I-110 in Los Angeles, California is the only ML facility identified in the United States with a buffer-separated multilane configuration. Both the northbound and southbound directions have two HOV lanes located on the inside lanes. The HOV lanes are separated from the GP lanes by a

double yellow line buffer for part of the freeway (other sections have barrier-separation). While this facility is over ten miles in length, data from only two locations can be used. This is due to the fact that the high density of ingress and egress points' deployment caused many of the sensor locations to fall outside of the required 1,500 ft for basic segment consideration. Data was gathered from Caltrans' PeMS database.

TABLE 4.6 Buffer 2 Data Sites, I-110, Los Angeles, California

Facility	Direction	Cross-Street
I-110	Northbound	N/o Florence Ave
I-110	Southbound	S/o Florence Ave

4.2.2.4 Barrier 1 Site

I-5 Orange County, California

Barrier 1 sites were located all along I-5 in Orange County, California. The location information is shown in Table 4.7.

TABLE 4.7 Barrier 1 Data Site, I-5 Orange County, California

Facility	Direction	Cross-Street
I-5	Northbound	W Santa Clara Ave
I-5	Southbound	N/o 17th Ave
I-5	Southbound	S/o 17th Ave
I-5	Southbound	W Santa Clara Ave

4.2.2.5 Barrier 2 Sites

I-5 Seattle, Washington

I-5 in Seattle, Washington has reversible express lanes that run through the center of the facility. These lanes serve traffic heading inbound to the City during the morning commute and outbound during the evening commute. Data from only one site could be used as part of the Barrier 2 dataset. The site is located at the cross of 63rd Street. Both northbound and southbound traffic was gathered.

I-394 Minneapolis, Minnesota

A three-mile portion of I-394's HOT lane system is a two lane, concrete barrier-separated facility. SOV users pay an electronic toll upon entering the facility. Data were gathered from the Minnesota Department of Transportation's online Data Extract Tool from the locations shown in Table 4.8.

TABLE 4.8 Barrier 2 Sites, I-394 Minneaplois, Minnesota

Facility	Direction	Cross-Street
I-394	Eastbound	W/o Wirth Pkwy
I-394	Eastbound	E/o Wirth Pkwy
I-394	Eastbound	Penn Avenue

4.2.2.6 Site Summary

Table 4.9 displays the summary of the data used for each segment type including the total number of 15-min sample points. As Continuous Access and Buffer 1 are the two most common facility types, a greater amount of data could easily be collected from these sites. Buffer 2, Barrier 1, and Barrier 2 are less common configurations. Data collection sites were therefore limited and the total number of data points was less than those for the Continuous Access and Buffer 1.

After data had been gathered, they were classified into different FFS categories. FFS categories of 55, 60, 65, 70, and 75 mph were considered. FFS was determined based on the average speed of the facility at a flow rate less than 100 pcphpl. Based on this average speed, sites were assigned to the closest FFS category. For example, any average FFS that fell between 62.5 mph and 67.5 mph belongs to the category of 65mph. The rounding to the nearest 5 mph is consistent with guidance in the HCM 2010 (TRB, 2010). Table 4.10 summarizes the number of fifteen-minute data points in each FFS category for each segment type. Although an extensive amount of data were collected, not every FFS could be covered for each segment type.

As data were collected from a variety of sources, filtering of erroneous data was imperative. Data

points outside of the normal distribution pattern, or outliers, were removed from the dataset. This included many data points with unreasonably high speeds, such as over 100 mph. Data points with very low speeds under low flow conditions were also removed as these were likely attributed to queue spillback from downstream congestion, or may be associated with detector error.

TABLE 4.9 Data Site Summary

Segment Type	Facility	No. of Sites	Span of Data Collected	No. of Points
Continuous Access	I-405, King County, Washington	5	1 month, All days, 5:00am to 7:00pm	30,617
	I-5, Seattle, Washington	6	1 month, All days, all hours	
	I-95, Broward County, Florida	2	1 month, TWTh, 7:00 am-9:00am and 4:00pm-6:00pm	
Buffer 1	I-405, Los Angeles, California	4	1 month, Wednesdays only, all hours	17,683
	SR-167, King County, Washington	4	1 month, all days, 5:00am-7:00pm	
	I-394, Minneapolis, Minnesota	3	1 month, TWTh, 6:00am - 10:00am	
Buffer 2	I-110, Los Angeles, California	2	2 months, TWTh, all hours	4,981
Barrier 1	I-5, Orange County, California	4	1 month, TWTh, all hours	5,263
Barrier 2	I-5, Seattle, Washington	1	1 month, Mon-Fri, 5:00am-11:15am, noon-11:00pm (Reversible lanes in operation)	5,112
	I-394, Minneapolis, Minnesota	3	1 month, TWTh, 6:00am - 1:00pm	

TABLE 4.10 Number of Sample Points for FFSs by Separation Type

	Number of Points				
FFS (mph)	**Continuous Access**	**Buffer 1**	**Buffer 2**	**Barrier 1**	**Barrier 2**
55	-	-	-	-	-
60	2,794	-	-	1,321	2,170
65	16,267	13,154	2,485	3,942	1,646
70	1,118	4,529	2,496	-	1,296
75	438	-	-	-	-

Note: "-" denotes not available

4.2.3 Observed Traffic Flow Characteristics of Basic ML Segments

As mentioned in Chapter 2, previous efforts have indicated that traffic behavior on ML facilities differs from that on GP lanes. The differences established in previous research can be summarized into four categories:

1) Lower Capacity –The capacity of ML is lower than it would be expected on GP lanes under the same demand.
2) Sensitive to congestion in GP lanes – Vehicles in the ML will slow down to reduce the discomfort of traveling at high speed differentials.
3) Affected by the inability to pass slow moving vehicles (single-lane facilities only) – The inability for passing slow moving vehicles in the single ML can result in slower than expected facility speeds.
4) Breakdown stochastically dominated by GP lanes – GP lane capacity exhibits a dominant effect on the ML's, particularly, HOV's capacity, resulting in the phenomena that HOV lanes are more readily experiencing breakdown concurrent with the GP lanes.

4.2.3.1 Examining ML Capacity

Although previous studies have indicated that the capacity of MLs is less than that of GP lanes,

researchers have not explored the differences between capacities of various ML facility types. We investigated the approximate capacities of each facility type for an FFS of 65 mph. Rather than showing individual sites, all sites with an FFS of 65 mph were combined for each facility type. All data points with a density of over 45 pcpmpl were removed from the database to avoid including periods of time where the facility had already reached a congested state (TRB, 2010). The 99.5th percentile flow from each of the five data sets was calculated to provide an approximate value for capacity for each separation type. Because it is difficult to specify a single capacity value, the 99.5th percentile flow was used as a guide for establishing the capacity value. Engineering judgment was used to ensure that the 99.5th percentile flow corresponds to the facility capacity rather than simply the maximum observed flow rate. The observed capacity was also rounded to the nearest 50 pcphpl. Figure 4.6 shows speed-flow plots for the FFS of 65 mph for each of the five facility types.

Figure 4.6 (a) clearly shows some flow values in excess of 1,800 pcphpl for the Continuous Access facilities. However, the capacity for Continuous Access segment with FFS 65 mph was determined to be 1,700 pcphpl, using the 99.5th percentile flow method, as well as adjusting based on empirical data from adjacent FFS curves of 60 mph and 70 mph. The capacity for the other types was determined using the same method. For Barrier 2, no sites with an FFS of 65 mph, or any other FFS's, appeared to reach capacity. Therefore, a capacity for Barrier 2 could not be determined. The several points that fall below 50 mph at lower flow rate can be seen as outliers as no breakdown trend appears.

The results from the capacity analysis show that there are differences in capacity between ML

facility types. The facility with the highest observed flow was the Buffer 2 facility. The Barrier 2 facility, although not reaching capacity, showed higher flow rates as well. The highest observed volume for Barrier 2 approached 1,800 pcphpl. One reason for the higher capacity in the multiple lane facilities is that there is no slow car following effect. Slower vehicles can be passed on multi-ML facilities. Also, for Barrier 2 facilities, the presence of the barrier removes the frictional effect from the congested GP lanes. Compared with the capacity of GP lane for FFS = 65 mph, all the ML types have a lower capacity than that of GP lanes, as GP lane capacity is generally observed between 2200 and 2400 pcphpl (TRB, 2010).

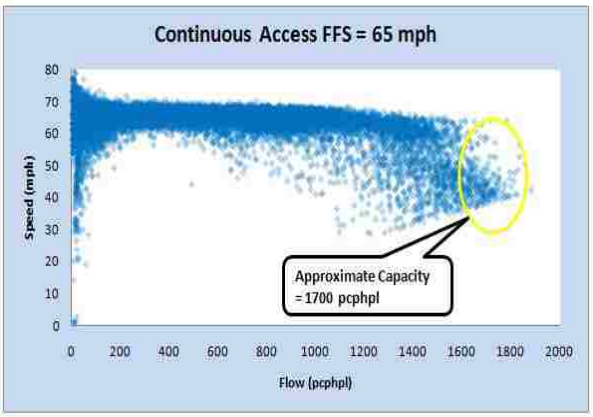

(a) Continuous Access

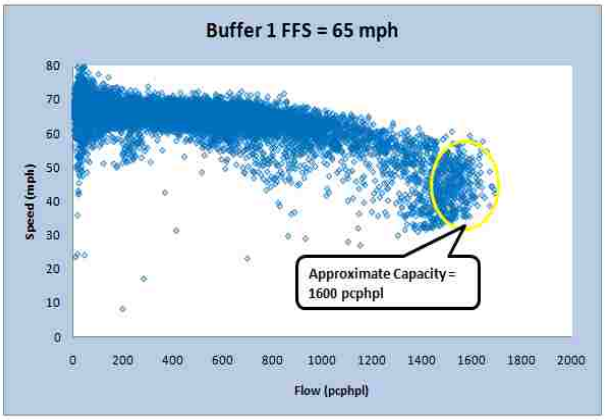

(b) Buffer 1

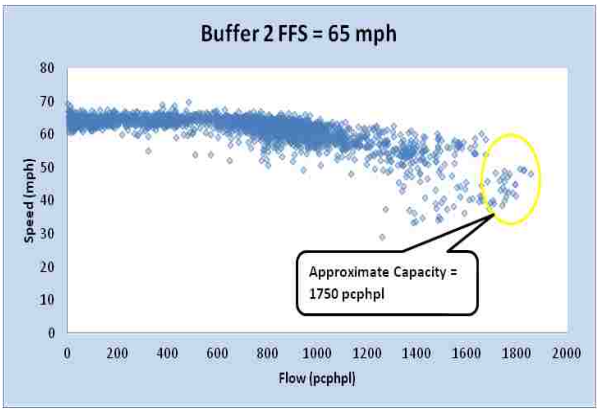

(c) Buffer 2

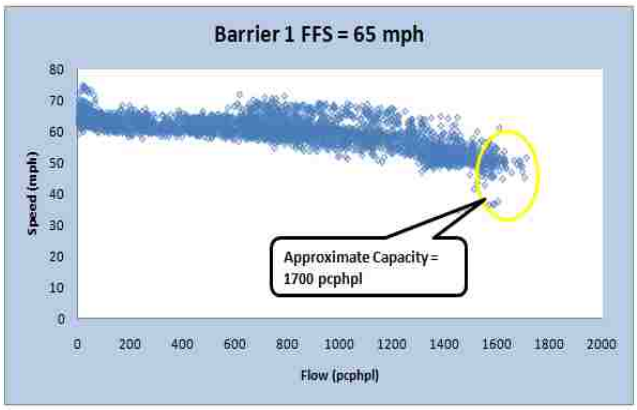

(d) Barrier 1

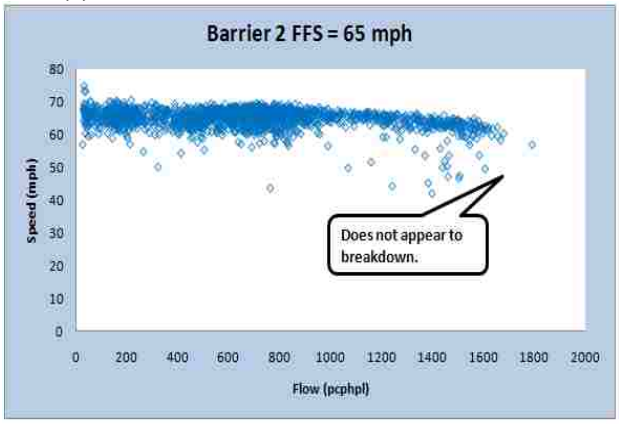

(e) Barrier 2

FIGURE 4.6 Speed Flow Plots for FFS=65 mph for the Five Facility Types

4.2.3.2 Slow Car Following Effect

The slow car following effect for ML facilities can be defined as the degradation in speed in a single lane ML facility, due to the inability for passing slower vehicles. As passing is allowed on

multiple lane facilities, they are not subject to this effect. Although previous research indicates the presence of this slow car following effect as a motivation for different traffic flow behavior on ML facilities, its effect was never quantified.

Figure 4.7 (a) provides an example of the speed-flow plot for a Buffer 1 separated facility. Figure 4.7 (b) shows an example of the speed flow plot for a Buffer 2 separated facility. The major difference between the two shapes of the curves can be seen on the left side of the data plot under low flow conditions. The Buffer 1 facility shows a negative slope for this low flow section of the curve while the Buffer 2 facility shows a flat line with no slope. Under low flow demand, the Buffer 2 separation type maintains its free flow speed while the Buffer 1 speed decreases with an increase in flow. Figure 4.7 (c) shows an example plot of speed-flow data from a facility with Continuous Access. Although the Continuous Access facility consists of only one lane, under low flow scenarios, passing can occur on the facility. As long as there is an acceptable gap in the adjacent GP lane and speeds in the GP lane are not below that of the vehicle in the HOV lane, a passing maneuver can be completed through the GP lane. Therefore, the speed-flow curve of Continuous Access facilities remains at FFS at lower flow rates.

To determine whether the slow car following effect could be observed on the facility, video data were collected at one of the single lane ML facilities in Dallas, Texas. The presence of platoons on the HOV facility was analyzed. The details of the validation results are presented in Chapter 5.

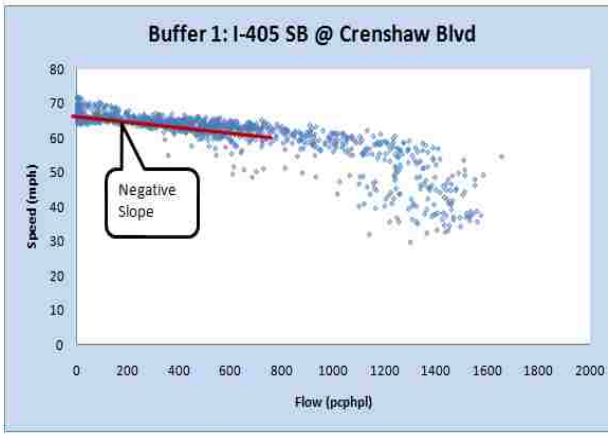

(a) Buffer 1 Facility

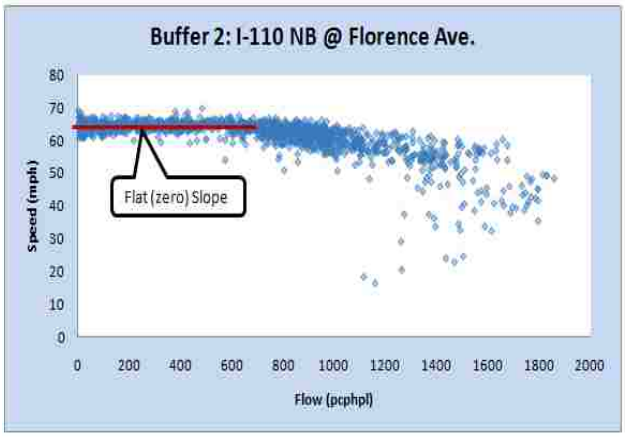

(b) Buffer 2 Facility

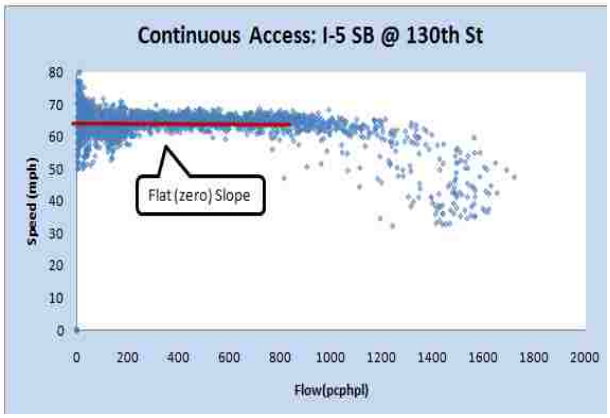

(c) Continuous Access Facility

FIGURE 4.7 Slow Car Following Effect Observations

4.2.3.3 Frictional Impact from GP Lanes

Previous research suggests that poor performance of the GP lane causes degradation in speed on the adjacent ML. Research has also indicated that this frictional effect is stronger on facilities with less physical separation such as Continuous Access and Buffer 1 (Liu *et al.*, 2011). The frictional effect can first be observed by viewing speed-flow plots for a buffer-separated single lane SR 167 HOT lane facility. As shown in Figure 4.8 (a), there is a wide dispersion of speed for flow range between 600-1200 pcphpl. This trend is atypical for what is usually seen in GP lane speed flow curves, which normally has little variance in speed between windows of equal flows, particularly

within the under-capacity region. When the data are segregated based on the operations in the GP lanes as shown in Figure 4.8 (b), the reason for the dispersion of speed becomes obvious. A density of 35 pcpmpl is used as a threshold for the drop in performance of the GP facility. This particular threshold was selected as it serves as the transition point from LOS D to LOS E in the HCM 2010. During periods of time where the GP lane has a density greater than 35 pcpmpl, lower speeds can be observed on the ML. The lack of continuity to the curve can be seen as breakdown appears to occur at different levels of flow depending on the GP lane's performance.

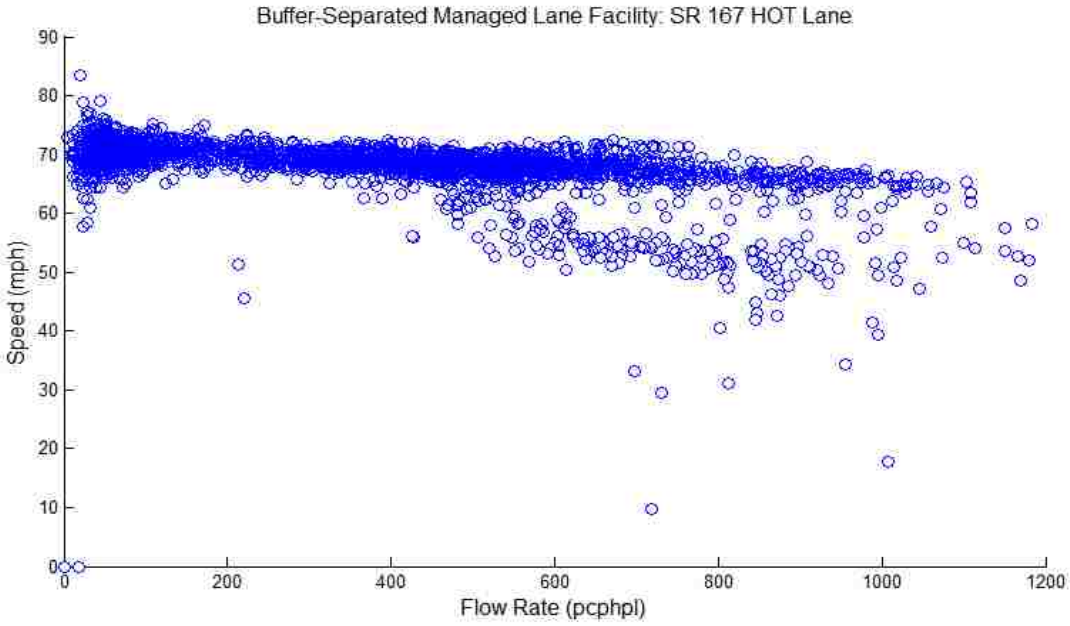

(a) All ML Speed-Flow Data

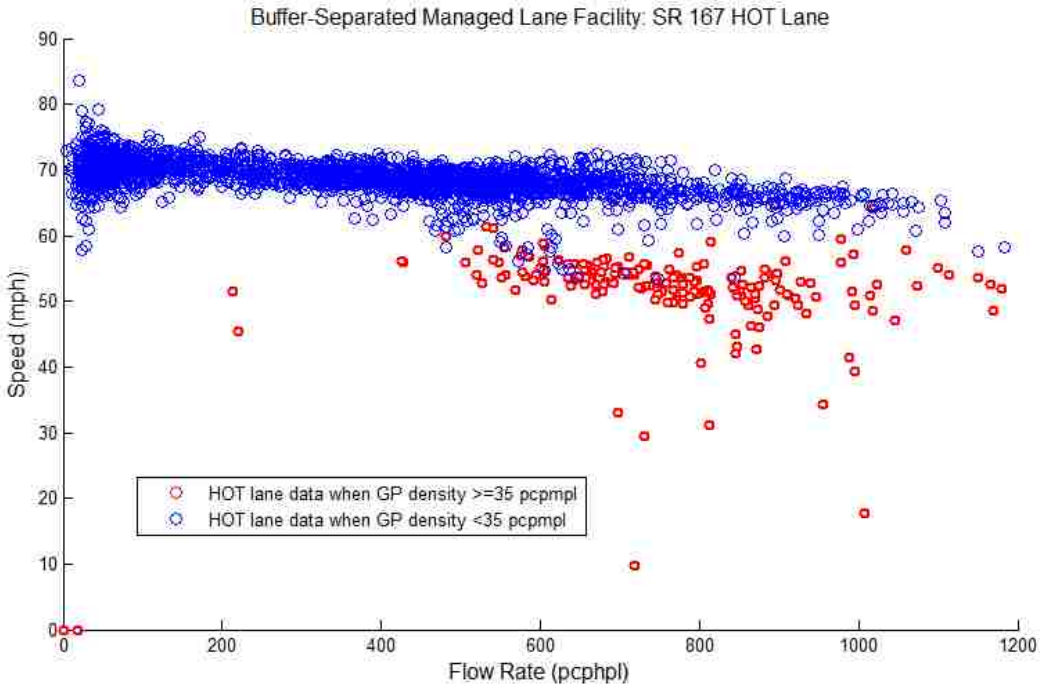

(b) Paired ML Speed-Flow Data by GP Density

FIGURE 4.8 Speed-Flow Data for Buffer-Separated Facility at SR 167 HOT Lane System in Washington

4.2.3.4 Stochastic Dominance of GP Lane Capacity

HOV facilities are expected to exhibit different traffic operational characteristics than HOT facilities, because demand is not dynamically managed by a tolling component. Consequently, HOV lanes are expected to be more readily experiencing breakdown concurrent with the GP lanes as entering demands are not controlled through pricing. The demand volume that causes the breakdown in the real traffic flow scenarios and the flow rate that a breakdown depends on, vary from day to day and from one location to another (Brilon *et al.*, 2005). Therefore, breakdown volume is considered to be a random variable and it is plausible to be estimated using a stochastic approach. It is hypothesized that GP lane capacity exhibits a dominant effect on the HOV's capacity, which explains the frictional effect between the two lane groups. A breakdown is defined as the average speed falling below a certain threshold, and the observed throughput volume dropping below the capacity to the congested portion of the speed-flow curve.

To investigate how the HOV's traffic is stochastically dominated by the GP lanes' traffic, a stochastic capacity estimation approach is applied. In this approach, the capacity distribution function is based on the analogy to the statistics of lifetime data analysis, which serves to describe the statistical properties of human life duration. This approach was first proposed to be used in capacity analysis by Minderhoud *et al.* (1997). Later, Geistefeldt (2010) further modified some basic assumptions of this method specific to application for freeway operations. The breakdown events can be detected using time series analysis containing both traffic volume and speed. Using a constant speed threshold value determined from the time series speed plot and justified by the speed flow diagram, if the speed falls below the threshold value in the next interval $i+1$, and lasts for more than 15 minutes (3 intervals), the traffic volume in interval i is regarded as causing a

breakdown. For the stochastic capacity estimation, not only the intervals that cause breakdown but also the intervals that are not followed by a breakdown deliver valuable information on the capacity. The latter type of the data is called "censored data".

The capacity estimation involves both non-parametric and parametric methods. The non-parametric approach to estimate the survival function is the Product Limit Method (PLM) (Kaplan and Meier, 1958), in which the capacity distribution function $F_c(q)$ can be estimated by:

$$F_c(q) = 1 - \prod_{i:q_i \le q} \frac{k_i - d_i}{k_i}, \qquad i \in \{B\} \tag{4.1}$$

where q = flow rate (vphpl)

q_i = flow rate in interval i (veh/h/ln)

k_i = number of intervals with a flow rate of $q \ge q_i$

d_i = number of breakdowns at a flow rate of q_i

{B} = set of breakdown intervals.

The relationship in Equation (4.1) is calculated over all observed data $q_i \le q$ that were followed by a breakdown. The distribution function will only reach 1 when the maximum observed volume is an uncensored data sample. Otherwise, it will terminate at a value of $F_c(q) < 1$. For parametric estimation, the parameters are pre-determined based on statistic techniques to find a distribution that best fits PLM curve. Typically, a Weibull distribution is chosen over other distribution functions such as Gamma and Normal distribution. The Weibull distribution function is expressed as:

$$F(x) = 1 - e^{-(\frac{x}{\beta})^{\alpha}} \qquad \text{for } x \ge 0 \tag{4.2}$$

where α = shape parameter

β = scale parameter

The maximum log-likelihood method used to calibrate the parameters of the Weibull distribution is given as:

$$LL = \sum_{i=1}^{n} \{\delta_i \cdot \ln[f_c(q_i)] + (1-\delta_i) \cdot \ln[1 - F_c(q_i)]\} \quad (4.3)$$

where $f_c(q_i)$ = statistical density function of the capacity *c*

$F_c(q_i)$ = cumulative distribution function of the capacity *c*

n = number of intervals

δ_i =1, if interval i contains an uncensored value; = 0, if interval i contains a censored value

Figure 4.9 shows the time series plot of speed and flow using a representative data sample of SR 91 HOV facility in Orange County, California on September 03, 2009. It is noted that the HOV lane speed and flow pattern appear to closely trail operations in the GP lanes. When the GP lane is experiencing a speed drop, the HOV lane is also operating at a lower speed. This finding is in contrast to the HOT lane operations as shown in Figure 1.1, where the demand management in the HOT lanes assured satisfactory operations in the MLs, despite breakdown conditions in the GP lanes.

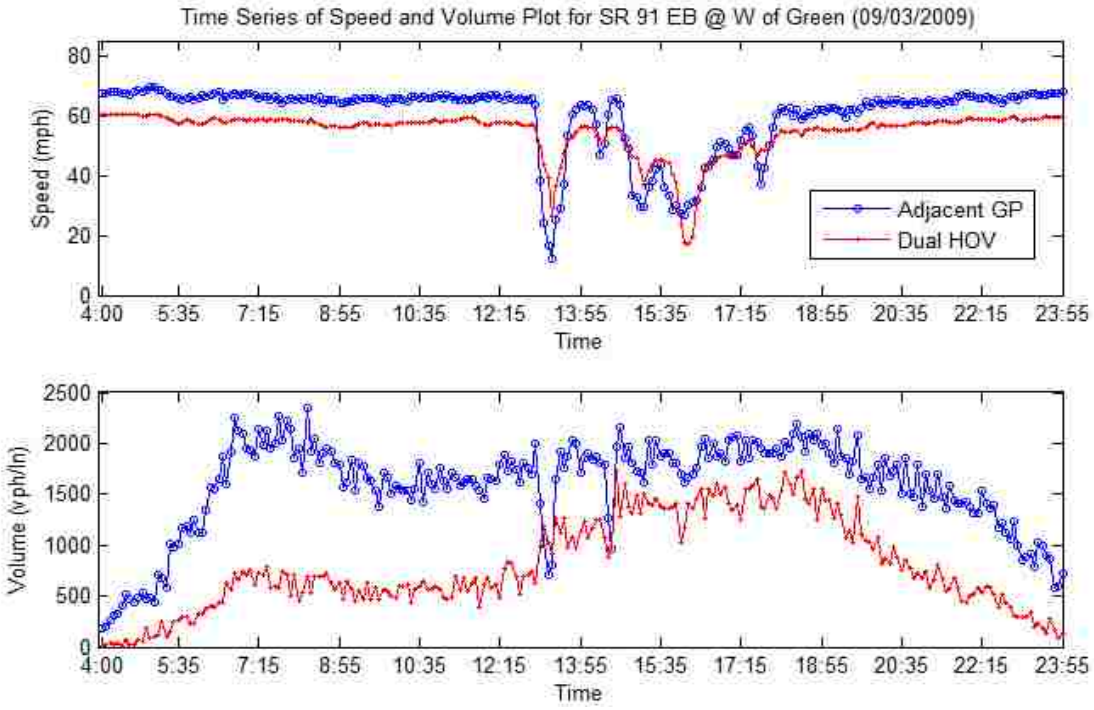

FIGURE 4.9 Time Series of Speed and Volume Plot for Buffer-Separated HOV Facility for SR 91 in Orange County, California

The apparent interaction between HOV and GP lanes in Figure 4.9 are not necessarily attributable to a frictional effect of GP on HOV lanes, in that the HOV lanes may themselves be in a breakdown state. By examining the speed-flow curve of the HOV site in Figure 4.10, it is easy to identify that HOV lane operations also exhibit periods in the unstable portion of the speed-flow curve. Therefore, the drop of speed in HOV lane cannot be classified as having a frictional effect from GP lane, rather it is due to the breakdown state it is experiencing itself.

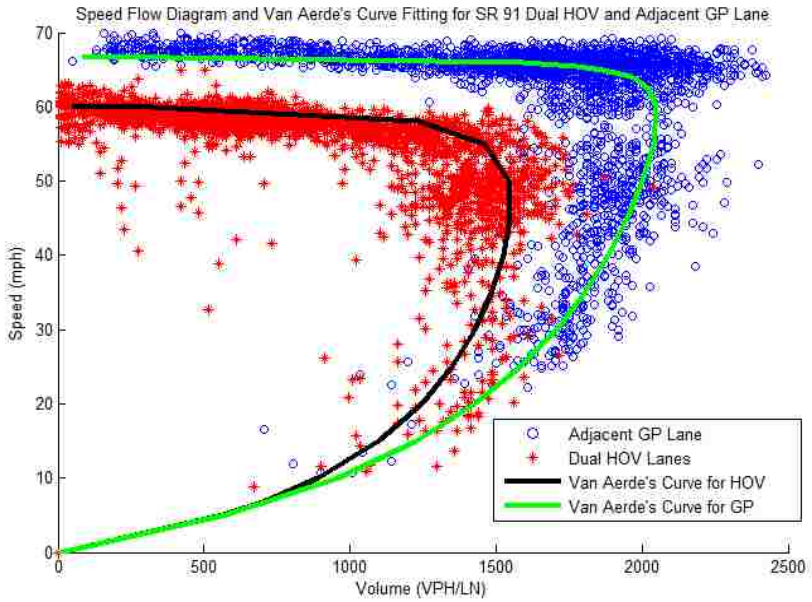

FIGURE 4.10 Speed-Flow Diagram and Van Aerde's Curve Fitting

From the time series plot of speed in Figure 4.9 and speed-flow curve in Figure 4.10, it is easy to identify the stable state and congested state for both HOV and GP lanes using 50 mph and 60 mph as speed thresholds, separately. Therefore, we use these two thresholds to identify the breakdown state for HOV and GP lanes, respectively. To further justify these speed thresholds, Van Aerde's steady-state car-following model is used for the calibration of the speed-flow diagram as shown in Figure 4.10. It is noted that 50 mph and 60 mph are the critical speed for the dual HOV and the adjacent GP lane, separately. The operational parameters derived from the Van Aerde's model are shown in Table 4.11.

TABLE 4.11 Operational Parameters Estimated Using Van Aerde's Model

Lane Type	Free Flow Speed (mph)	Critical Speed (mph)	Jam Density (veh/mile)	Capacity (vphpl)
Dual HOV	60.2	49.5	155.9	1550
Adjacent GP	66.8	59.6	145.6	2051

Using the stochastic capacity analysis approach introduced above, the capacity distribution of both HOV and GP lanes can be determined. The capacity distribution curve (shown in Figure 4.11) can provide information about the probability of a freeway location being in breakdown state at the observed flow for both HOV and GP lanes. Table 4.12 shows the fitted Weibull distribution result. It is noted that when the observed volume reaches 1540 vphpl for HOV and 2310 vphpl for adjacent GP lane, then there is a 15% probability that the location would breakdown, separately. The capacity distribution estimation for both HOV and GP also indicates that GP lane's capacity is always stochastically dominating over the HOV's capacity. For comparison, the theoretical capacity of a GP basic freeway segment with a free-flow speed of 65mph is 2350 vphpl.

TABLE 4.12 Stochastic Capacity Estimation using Weibull Distribution Function

Lane Type	α	β	Capacity (vphpl)@ 15% Breakdown Probability
Dual HOV	7.55	1950	1540
Adjacent GP	17.68	2565	2310

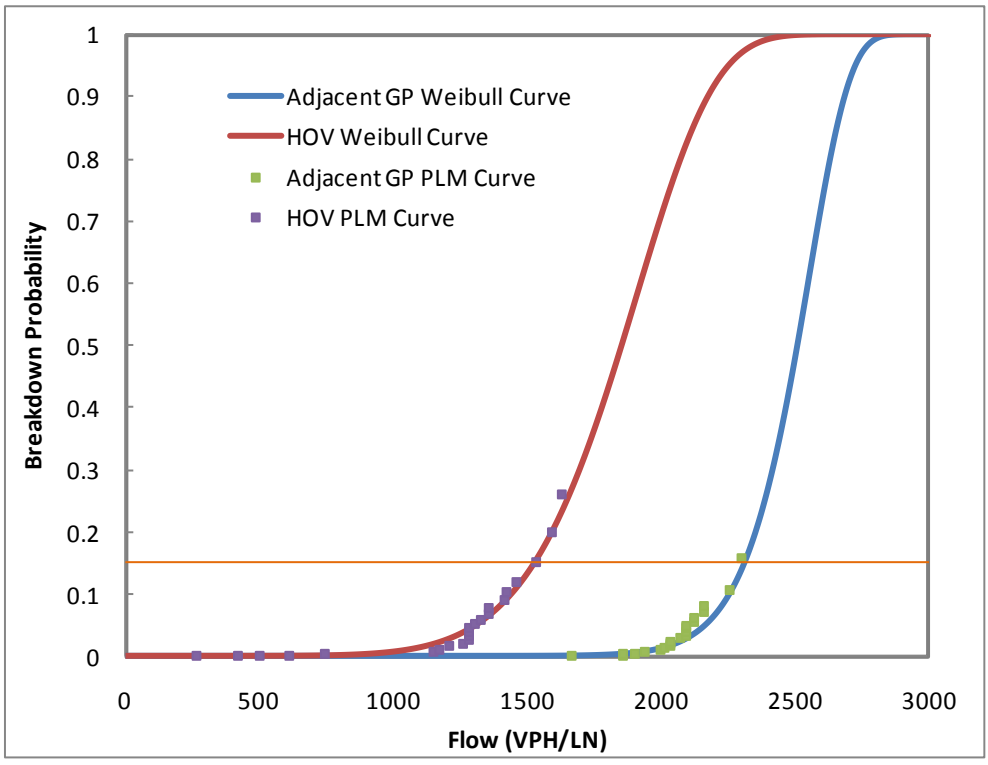

FIGURE 4.11 Estimated Capacity Distribution Functions using PLM and Weibull Method

4.3 ML Access Points

4.3.1 Access Point Configurations for ML facilities

Clearly, one of the significant sources of potential congestion for an ML facility is the treatment at the access points to the ML lanes, in addition to any direct cross-flows between the ML and GP lanes. The three ML principal types of access configurations are described below and illustrated in Figure 4.12.

A. **At-Grade Lane-Change Access (Type A)** occurs where ML traffic enters the GP lanes through a conventional on-ramp roadway (from the right), weaves across multiple GP lanes, and then enters the ML facility. The configuration is also a form of a weaving movement. This access strategy is common for concurrent ML facilities. Access between ML and GP is sometimes constrained to specific locations or openings, which affect the weaving intensity at these access points, as well as the intensity of the two-sided weaving maneuver across the GP lanes. The Type A access configuration requires a *cross-weaving* movement across GP lanes for drivers to position themselves prior to the access point, and a *lane-change movement* to get from GP into the managed lane.

B. **At-Grade Ramp Access (Type B)** occurs where arterial traffic weaves across multiple GP lanes (similar to Case A above), but where the entrance to (or exit from) the ML facility is confined to an at-grade on-ramp (off-ramp). Operationally, the GP lanes are affected by the cross-weaving flow, as well as friction caused by the on and off-ramps. The ML lane operations are in turn impacted by the cross-weaving maneuvers from and/or to the access points at the ramps. The Type B access configuration requires a *cross-weaving* movement

across GP lanes for drivers to position themselves prior to the access point, and a *ramp movement* to get from GP into the managed lane.

C. **Grade-Separated Ramp Access (Type C)** occurs where access to the MLs occurs on a grade-separated structure (i.e. flyover, bridge, or underpass). The operational impact to the GP lanes is minimal in this case, since the cross-weaving movement is eliminated entirely. The MLs are affected by friction from the entering or exiting ramp flows in the normal fashion as GP lanes. The Type C access configuration does not require any cross-weaving across GP lanes due to a grade separated ramp, and the ML access is handled by a *ramp movement*.

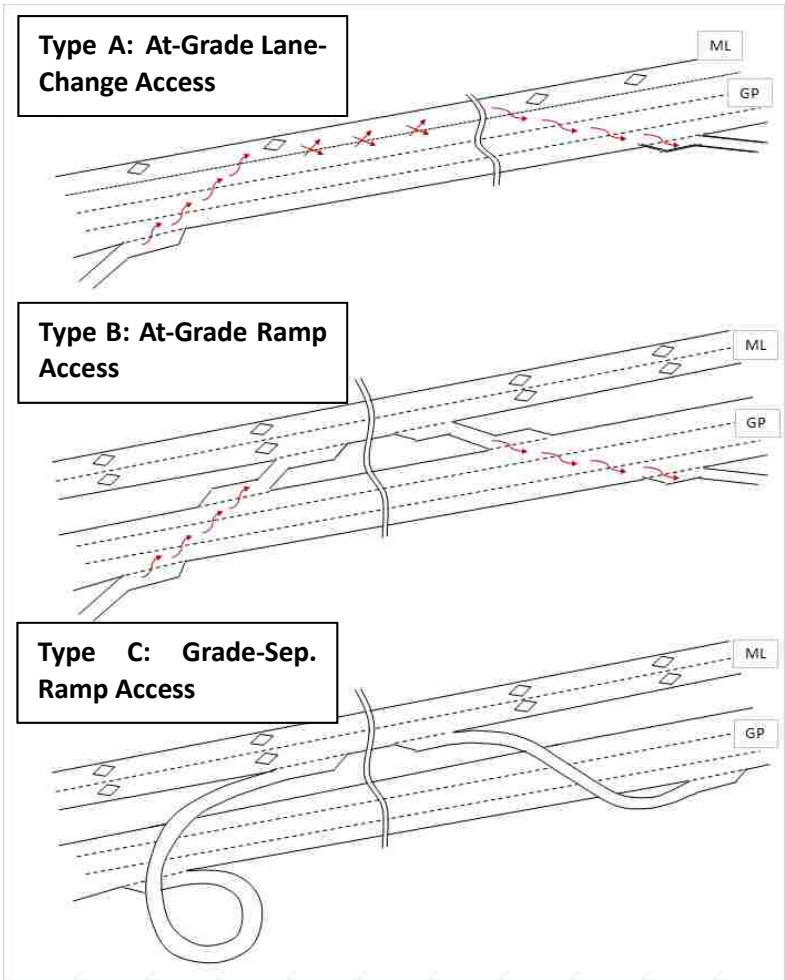

FIGURE 4.12 Illustrated of Access Point Designs

Incorporating these various access types into the lane group analysis framework is straightforward for Type C, since the spatial extent of the *Access-Point Influence Area* (APIA) is already defined in HCM 2010 ramp junction methodologies. The ramp influence area for GP facilities is defined as 1,500 feet from the ramp gore for both on-ramps (measured downstream) and off-ramps (measured upstream). The APIA for Type-C ML access points is assumed to follow the same convention.

For Types A and B access points, the challenge lies in predicting the intensity and impact of the

cross-weaving (CW) flows between a GP ramp and the access region between the GP lanes and MLs. The minimum cross-weave length ($L_{CW\text{-}Min}$) is defined as the distance between the closest upstream GP on-ramp gore point to the start of the ML access opening. The maximum cross-weave length ($L_{CW\text{-}Max}$) is defined as the distance from the ramp gore point to the end of the access opening. Figure 4.13 illustrates this concept for a concurrent single ML next to three GP lanes with stripe-separation. In this case, on-ramp vehicles desiring to enter the ML will complete all three lane-change maneuvers (not counting the merge from the acceleration lane), resulting in a cross-weave friction on the GP lanes. It is assumed that most drivers will strive towards completing the lane change maneuver as early as possible, possibly resulting in a disturbance on the GP lanes operating speed and capacity before the ML access point. The overall cross-weave intensity profile is postulated to be correlated to the number of lane change maneuvers as a function of the minimum and maximum available distances to complete all lane changes ($L_{CW\text{-}Min}$ and $L_{CW\text{-}Max}$). The Buffer Opening Area (BOA) is defined by the difference of these two distances.

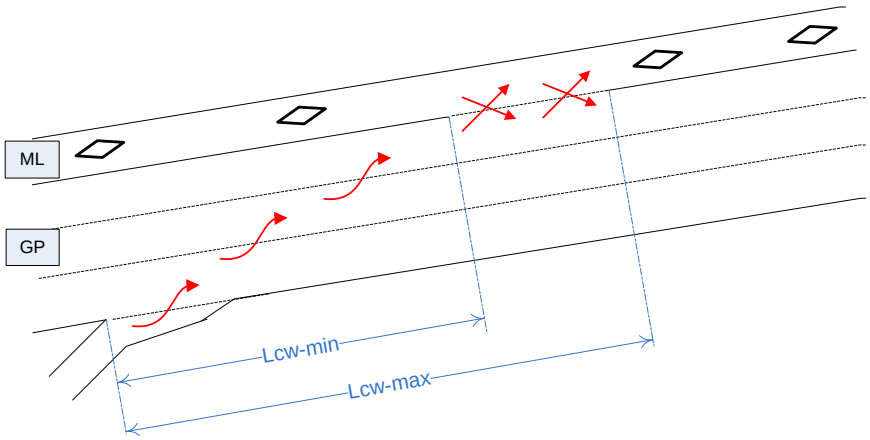

FIGURE 4.13 Defining Dimensions of APIA through Minimum and Maximum Cross-Weave Lengths

Methodologically, the cross-weave friction may result in a reduction in GP segment capacity and operating speeds, similar to the way a weaving segment with significant weaving traffic has a

lower capacity than a basic freeway segment. Due to the technical difficulties in estimating this capacity reduction effect in the field, this study relies mostly on calibrated micro-simulation models to estimate this effect. Field measurements of this effect are very challenging, because the $L_{CW\text{-}Max}$ distance can cover a length of up to one mile of freeway or more, at which point roadside (human observer) or overhead observations (surveillance cameras) are not very useful. Through a well-calibrated simulation model, various scenarios with different number of GP lanes, cross-weave demand, $L_{CW\text{-}Min}$ length can be tested. We proposed to use a Capacity Reduction Factor (CRF) and/or Capacity Adjustment Factor (CAF) feature to account for the capacity reducing impacts of cross-weave traffic on one or more GP segments. Lane change intensity information can also be collected from the simulation model to be applied to the overall estimates of cross-weave friction.

4.3.2 Simulation Test Scenario

A calibrated simulation model was used to simulate freeway operations as entering vehicles weave across multiple GP lanes to enter the ML. Capacity estimates for a variety of scenarios encompassing different number of lanes, $L_{CW\text{-}Min}$, GP demand, and cross-weave demand were tested in the model. CRF/CAF was subsequently estimated corresponding to various configurations. The details about the simulation model configuration are presented in Chapter 5.

4.3.2.1 Capacity Estimation from Simulation Output

After each simulation run, a speed-flow diagram was developed using the simulated data collected at virtual sensor locations. Heuristic and analytic methods were considered for capacity estimation

from the diagram. In this study, an analytical approach developed by Van-Aerde is used to calibrate the speed-flow relationship from the simulated data. Van Aerde's steady-state speed-flow model is a multivariate estimation procedure that provides better fits than other single-regime models (Van Aerde and Rakha, 1995). The capacity estimated is independent of the speed or density threshold between congested and non-congested states, which is needed in two-regime traffic flow models. The functional form of Van Aerde's model is expressed as:

$$d = \frac{1}{c_1 + \frac{c_2}{s_f - s} + c_3 s} \tag{4.4}$$

where d is the density (veh/km) or the inverse of the vehicle headway, s is speed (km/h), s_f is the free flow speed (km/h), c_1 is the fixed distance headway constant (km), c_2 is the first variable distance headway constant (km^2/h) and c_3 is the second variable distance headway constant (h^{-1}).

SPD_Cal software developed by Rakha and Arafeh (2009) is used for regressing the speed-flow curves from empirical data. The software uses an iterative numerical search technique proposed in Van Aerde and Rakha (1995) to determine capacity, free-flow speed, speed at capacity, and jam-density. The parameters in Equation (4.4) can then be determined by the following equations:

$$k = \frac{2s_c - s_f}{(s_c - s_f)^2} \tag{4.5}$$

$$c_2 = \frac{1}{d_j(k + 1/s_f)} \tag{4.6}$$

$$c_1 = kc_2 \tag{4.7}$$

$$c_3 = \frac{-c_1 + \frac{s_c}{v_c} - \frac{c_2}{s_f - s_c}}{s_c} \tag{4.8}$$

where s_c is speed at capacity (km/h), v_c is capacity (vph), and d_j is jam density.

4.3.2.2 Lane Change Intensity Calculation

In the simulation model, virtual sensors were configured on each GP lane starting from the ramp gore point all the way to the end of BOA. The sensors recorded aggregated volume by vehicle type, as well as speed within the designated time interval. Each set of sensors was set 200 ft apart to collect aggregated data for the entire simulation period (one hour). Since the cross-weave flows were set as "ramp" vehicle type, sensors at each location could report the number of cross-weave vehicles present at that location. Using the algorithm described below, the number of lane changes conducted within each 200 ft segment was determined:

$$LCI_m = \sum_{i=1}^{n} i * (Vol_{m,i} - Vol_{m-1,i}) \qquad n = 2, 3 \; or \; 4 \tag{4.9}$$

where LCI_m is the cross-weave lane change intensity of the m^{th} segment. Since each set of sensors is 200 ft apart, Vol_{m-1} represents the cross weave volume collected at the upstream 200ft away. i is the lane index, labeled 1 for the right-most lane. For different lane configuration scenario (two-GP lane, three-GP lane or four-GP lane), the maximum lane index is different.

The profile of lane change intensity vs. distance can therefore describe within the specific distance, how many cross-weave lane changes have happened. The higher the *LCI*, the more disturbance will be generated to the GP segment.

CHAPTER 5 EMPIRICAL AND MODELING RESULTS

This chapter presents the empirical and modeling results for ML operational data gathered. From the demand side, the results reveal certain important features about how SOVs' usage of HOT lanes under various scenarios, which provides implications for optimal settings of tolling policies. From the supply side, the computational modules developed (as part of the methodological framework) for quantifying performance of ML facilities provides critical guidance for the transportation practitioners to evaluate the design and operational performance of their studied facilities. The data used for developing those modules were obtained either from sensors along instrumented ML facilities of several states in the U.S., or via micro-simulation models to supplement the data needed but were scarce or impractical to gather from field. From the modeling perspective, the twin-cell modeling approach successfully modeled the traffic flow dynamics on parallel facilities, taking into account the unique interactions and weaving characteristics.

5.1 HOT Demand Modeling

5.1.1 VOT Distribution Analysis for Infrequent Users and Frequent Users

To examine whether infrequent users and frequent users have different VOT distributions, the transponder records were extracted from the database for the SR 167 northbound commute during the morning peak period between 5:00 a.m. and 10:00 a.m. The transponder data cover in total 21 days in February and March 2009, Tuesdays through Thursdays. Figure 5.1 shows the histogram of SOV usage in the HOT lane based on transponder records. The threshold for distinguishing the two groups of users was 14 days; that is, within the 21-day study period, transponders that appeared

fewer than 14 days were considered to be infrequent users, and those that appeared more than 14 days were considered frequent users. The users chosen for the VOT study were those who traveled the entire northbound corridor for the morning peak period. The reason for this criterion is that individuals may have varied sensitivities to time spent in different travel distances and time periods. They may not be willing to pay as much for saving a minute of travel time from a longer-distance trip as opposed to saving a minute from a shorter-distance trip. Therefore, restricting the data to users who travel the same distance in the same study period enables the VOT distribution to be better studied and reasonably interpreted. In total, 5,247 transponder samples were collected across the span of the sampling period.

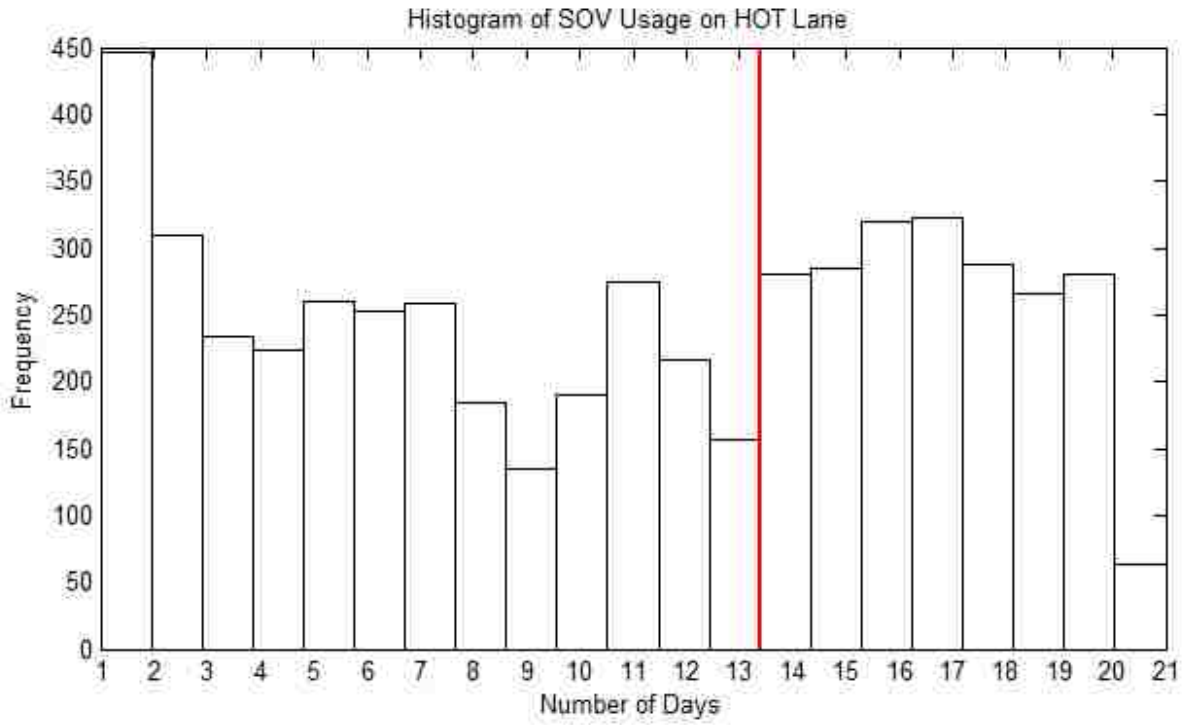

FIGURE 5.1 Histogram of SOV Usage on HOT Lane Based on Transponder Record

The VOT distributions for the two groups of users were calculated separately using the methodology proposed in Equation (3.1). The VOT distribution results and cumulative

probabilities are shown in Figure 5.2. For the two user groups, the VOT distribution follows a very similar pattern, with a close mean value ($17.9/h for infrequent users, and $18.1/h for frequent users). The t-test indicates that the VOT difference between the two datasets is statistically insignificant (t=0.37, P =0.35) at the 95% confidence interval. This implies that the VOT distribution for frequent users is not statistically different from that of infrequent users. That is to say, frequent users and infrequent users care about travel time savings in a similar way. Therefore, when modeling the SOV response to tolling, it is not necessary to separate the two user groups, as demonstrated in the following section.

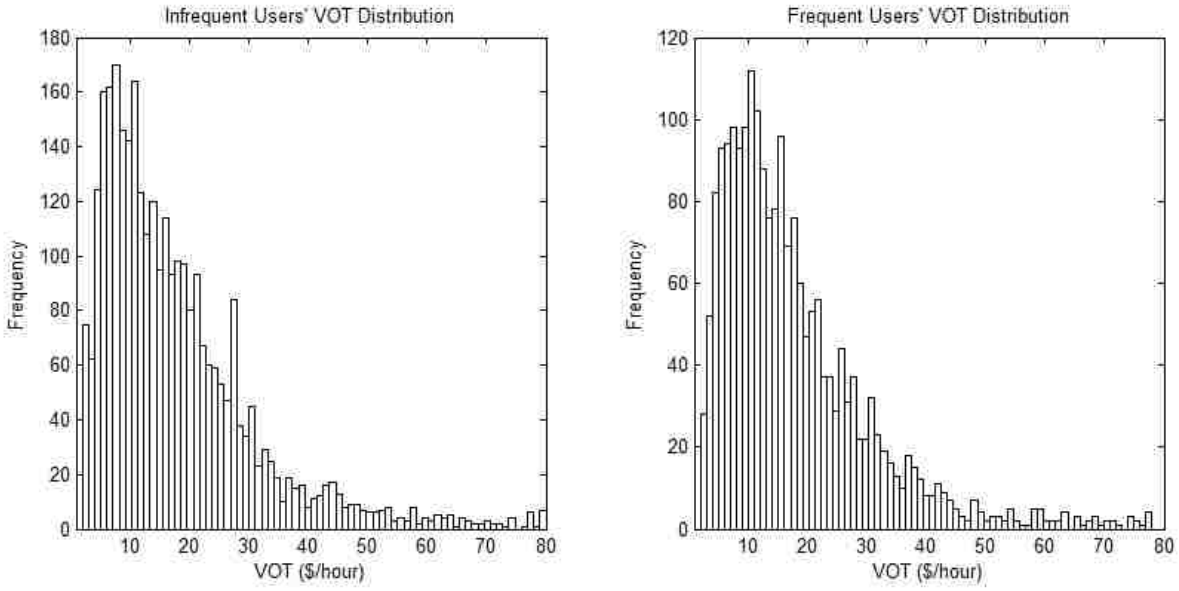

(a) **(b)**

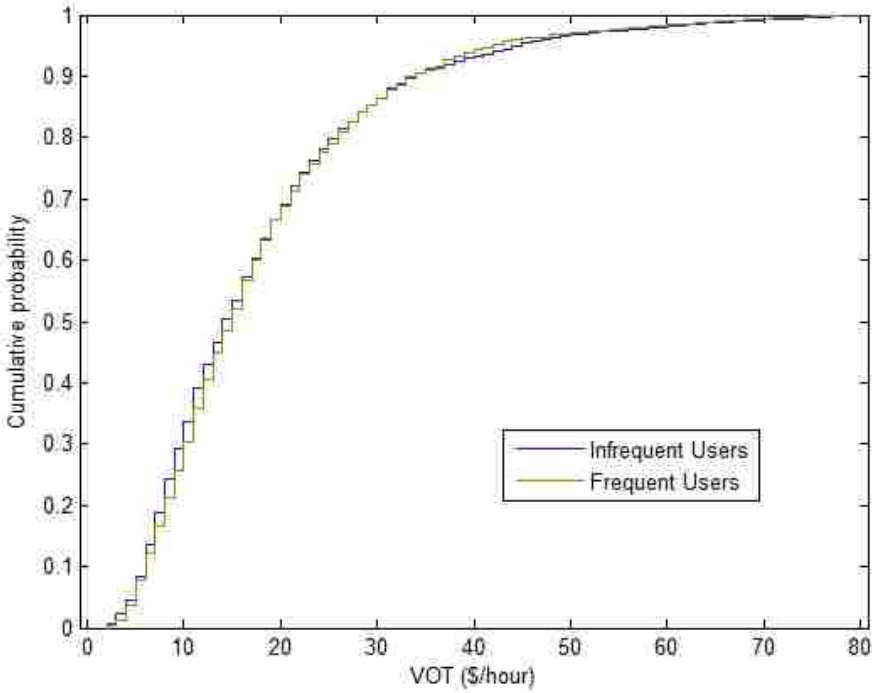

(c)

FIGURE 5.2 VOT Histogram for (a) Infrequent Users and (b) Frequent Users, and (c) VOT Cumulative Probability for Infrequent Users and Frequent Users

5.1.2 Modeling SOV Response to Tolling and Traffic Conditions

To further model the SOVs' response to changing traffic conditions, the morning peak period was categorized into different traffic phases. A time series speed plot is shown in Figure 5.3. The period of GP lane breakdown is easily identifiable in the figure, where a sudden speed drop below 40 mph is observed. Before 6:30 a.m., the average speed across the GP lane is relatively high, remaining above 40 mph. However, at 6:30 a.m., the GP lane experiences a sharp speed drop to below 40 mph and generally remains below that threshold until 8:30 a.m., where speeds recover to the pre-congestion state. During the congestion period, the speed of the HOT lane does not break down, although a slight drop in speed to around 55 mph on average is observed. Therefore, when modeling the SOV response, the entire morning period is divided into three traffic phases: pre-congestion period (5:00 a.m. to 6:25 a.m.), congestion period (6:30 a.m. to 8:30 a.m.), and post-congestion period (8:35 a.m. to 10:00 a.m.).

The SOV demand is therefore modeled following the methodology proposed in Equations (3.3) through (3.5) for the three different traffic phases. The probability that approaching SOVs would choose to use the HOT lane is modeled in a logit-like format. By substituting Equations (3.3) and (3.4) into Equation (3.5), the model can be rewritten as:

$$\ln(\frac{1-p}{p}) = \partial * TR + \beta * (TT_{GP} - TT_{HOT}) + \omega * (R_{GP} - R_{HOT}) + C \quad (5.1)$$

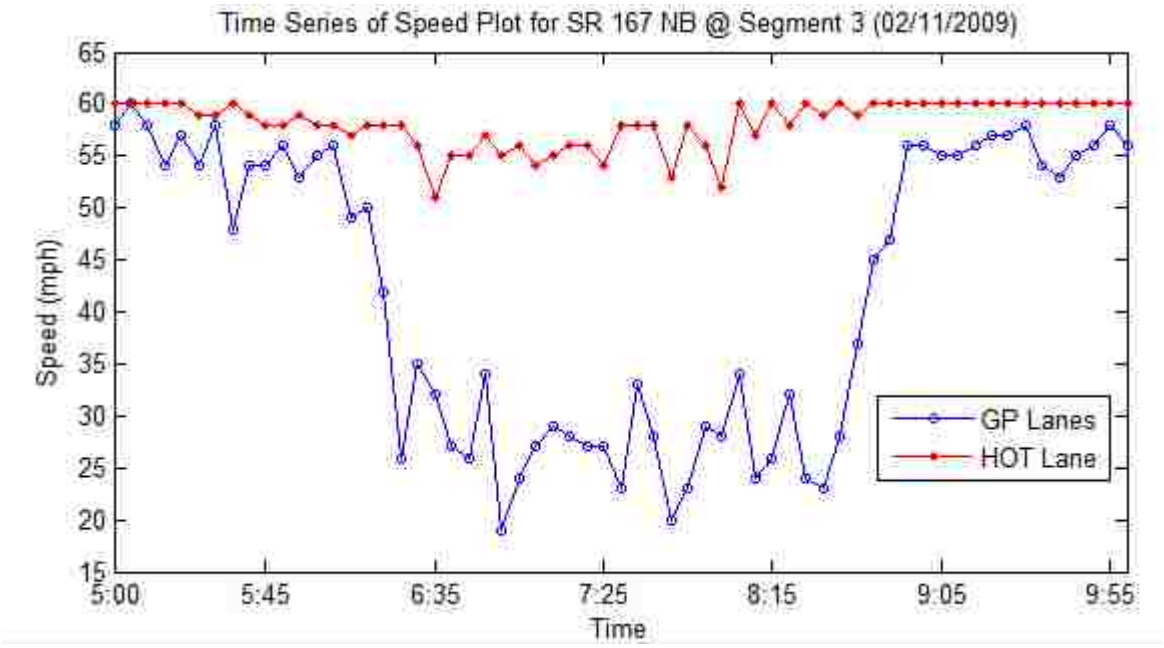

FIGURE 5.3 Time Series of Speed Plot for SR 167 NB @ Segment 3

The modeling results are shown in Table 5.1. All the models in the three phases yield reasonable estimation results, with R-squared values ranging from 0.6 to 0.8. The left side of Equation (5.1) can be interpreted as the ratio between the SOV GP lane demand and the SOV HOT lane demand. Note that the toll rate in Phases 1 and 3 and the reliability in Phase 2 are not significant at the 95% confidence level; therefore, they are eliminated from the final model. The final utility functions for the three traffic phases can therefore be written as follows:

Pre-Congestion:

$$U_{HOT} = -0.012 * TT_{HOT} + 1.042 * R_{HOT} \tag{5.2}$$

$$U_{GP} = -0.012 * TT_{GP} + 1.042 * R_{GP} + 2.511$$

Congestion Period:

$$U_{HOT} = 0.214 * TR - 0.005 * TT_{HOT} \tag{5.3}$$

$$U_{GP} = -0.005 * TT_{GP} + 2.78$$

Post-Congestion:

$$U_{HOT} = -0.003 * TT_{HOT} + 1.030 * R_{HOT} \quad (5.4)$$

$$U_{GP} = -0.003 * TT_{GP} + 1.030 * R_{HOT} + 3.338$$

TABLE 5.1 Statistic Result for Modeling SOVs Demand to Tolling and Traffic Conditions

Traffic Phase	Variables	Coefficients	t Value	p Value
1. Pre Congestion	Toll Rate	0.239	1.973	0.049
	Travel Time	-0.012	-8.070	0.000
	Reliability	1.042	6.863	0.000
	Constant	2.511	16.125	0.000
2. Congestion	Toll Rate	0.214	3.206	0.001
	Travel Time	-0.005	-5.205	0.000
	Reliability	0.017	0.182	0.855
	Constant	2.78	23.192	0.000
3. Post Congestion	Toll Rate	0.600	1.540	0.124
	Travel Time	-0.003	-10.574	0.000
	Reliability	1.030	4.429	0.000
	Constant	3.338	12.135	0.000

It is confirmed from the models above that, for different traffic phases, the SOV demand is adjusted based on different user concerns. For the pre- and post-congestion periods, SOVs care more about travel time savings and travel time reliability, which play a significant role in the models. This is reasonable, because for those two periods, the toll rate normally fluctuates between $0.5 and $1. Because of this relatively lower rate, the lane choice may not be determined by the fee but rather by travel time savings or trip reliability. During the congestion period, however, toll rate has a significant impact on SOV demand. During that period, the SOV HOT lane demand increased as the toll rate went up. This seems counterintuitive at first glance, but is easily explainable within the dynamic tolling context, because it captures the signaling effect of the congestion pricing scheme. The toll adjusts on the basis of the real-time volume and speed measurements in both the HOT lane and the GP lanes. The SR 167 HOT lane seldom experiences any congestion, the toll

rate thus (normally fluctuating between $1.00 to $2.75) functions as a signal indicating the traffic condition in both the downstream HOT lane and the GP lanes. For the majority of morning commuters who are familiar with the roadway condition, when the toll rate goes up during the congested hours, it indicates that the downstream traffic in the GP lane is fairly congested. Therefore, people would rather pay more to use the HOT lane to avoid the congestion. Also, it is noted that travel time is significant in all three phases, which indicates that the priority for people choosing the HOT lane is for an immediate benefit of travel time savings.

5.2 Slow Car Following Effect Validation

Video data were used to validate the presence of the slow car following effect on single lane ML facilities. The video data used in this process were from eastbound I-635 in Dallas, Texas. This ML facility is buffer-separated with a single HOV lane, or type Buffer 1. One hour of data were used from the hours 10:40 am to 11:40 am on March 21st, 2008. This time period represented light traffic conditions in both the GP lanes and the HOV lane. Under this situation, the assumption that no frictional effect from the GP lane was significantly degrading the speed of the HOV facility was valid.

To determine whether the slow car following effect could be observed on the facility, the presence of platoons on the HOV facility was analyzed. Platoons on the HOV facility were defined as a group of vehicles traveling closely together with car-following headways. These platoons were seen as the natural response of the traffic stream to a slow-moving vehicle. The first vehicle in the platoon would represent a slow-moving vehicle while the trailing vehicles were all vehicles that

had been traveling at higher speeds until catching up to the slower-moving platoon.

The speed and number of vehicles in the platoon were recorded throughout the study period. Figure 5.4 below shows the study location on I-635. In Figure 5.4, a platoon of four vehicles can be observed in the HOV lane. The speed of the platoon was then calculated using time measurements and distance between light posts along the facility. Google Earth was used in determining the distance between light posts. Ninety-six (96) data samples were collected throughout the hour. Each sample consisted of the number of vehicles in the platoon and the corresponding speed.

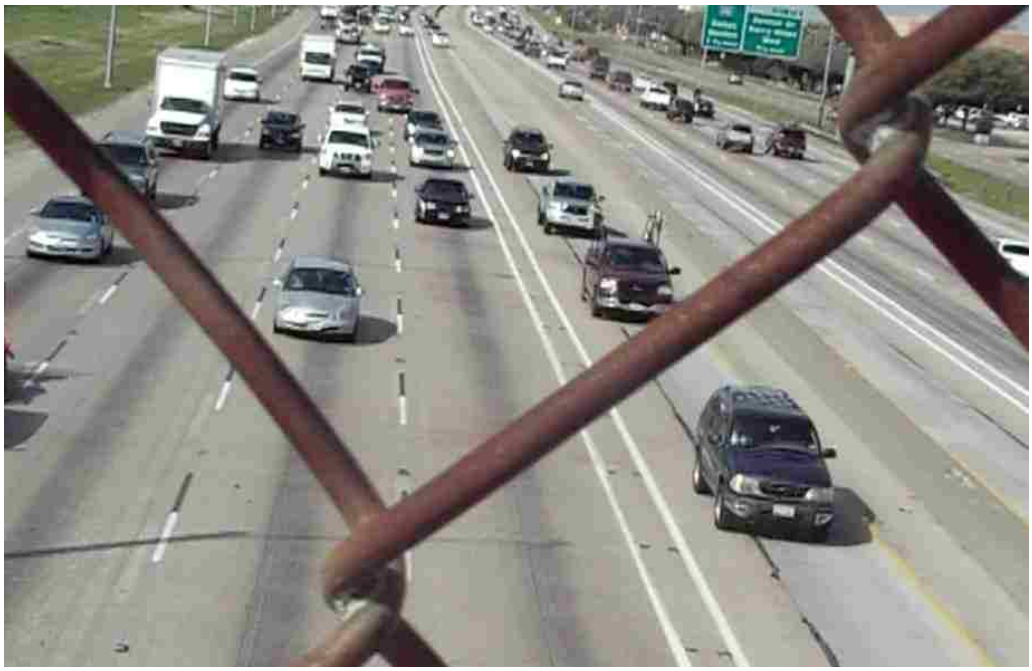

FIGURE 5.4 Snap Shot of Platoon Effect from Video Data at I-635, Dallas, Texas (Source: University of Texas at Arlington)

To determine whether there is a significant difference in speeds between vehicles traveling in the platoons and those traveling alone, a t-test was conducted (Table 5.2). The speed of the group with solo vehicles was compared to the speed of the vehicles in a platoon. The number of vehicles in the platoon was not considered for the t-test, as platoons of all sizes were grouped together. It is shown that the speed of single vehicles is significantly greater than that of the platoon vehicles at

99% confidence level. This verifies that slow-moving lead vehicles affect the speed of the platoon they inherently create. In addition to verifying that single lane facilities experience a slow car-following phenomenon, the speed for platoons of different sizes can also be examined. Figure 5.5 shows a clear relationship between platoon size and speed. The R^2 for the linear regression is 0.7203. The linear fit shows that the greater the number of vehicles in the platoon, the lower the speed of the platoon.

TABLE 5.2 t-Test Results for Slow Car Following Effect

	Single Vehicles	Platooned Vehicles
Observations	39	57
Mean (mph)	70.83	67.43
Variance	15.76	9.18
t-Statistic	4.76	
P value	0.00	

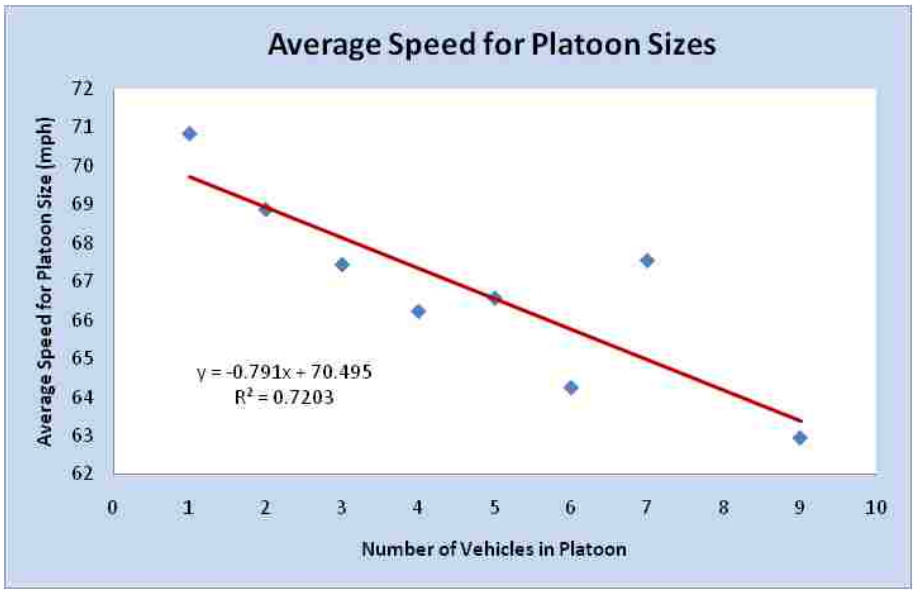

FIGURE 5.5 Relationship Between Average Speed vs. Platoon Size

Two conclusions can then be drawn from this relationship. First, the slower the leading vehicle is traveling, the greater the effect it will have on the single-lane ML system. More vehicles will

experience a reduction in speed when the platoon is traveling at lower speeds. Second, there is a greater drop in the speed of the system as volume increases. With volumes increase, the chance that more vehicles will be experiencing the effects of the slow moving vehicles increases. These observations verify that the degradation in speed on single lane ML facilities can be a direct consequence of the slow car following effect. As the flow rate of the HOV lane increases, both the number of slow-moving vehicles and the number of vehicles got affected by the slow-moving vehicle increase. This slow car-following effect needs to be implemented into the formation of the speed flow curves for MLs.

5.3 Speed-Flow Models for Basic ML Segment

5.3.1 Continuous Access

Unlike any other separation type, in Continuous Access, ML users are able to move freely between the ML and GP lanes. Although Continuous Access separation may consist of only one ML, users are not subject to the same effects of slower drivers as in other single-lane ML facilities. Continuous Access users have certain degree of freedom to change into the adjacent GP lane and pass slower vehicles. The ML user's ability to make this maneuver is, however, dependent on the performance of the adjacent GP lane. When the GP facility is congested, ML users are unable to pass slower moving vehicles. Slower speeds and fewer lane changing opportunities prevent ML vehicles from overtaking the slow moving vehicles.

During this congested period on the GP lanes, a frictional effect can be observed. ML users drive at slower speeds when adjacent GP traffic is congested. Drivers tend to drive more cautiously due

to their proximity to a dense stream of slowly moving vehicles. ML drivers are also aware that GP vehicles can enter the ML at any point at relatively low speeds, increasing their tendency to operate the vehicles at a slower speed. Figure 5.6 shows the speed-flow relationships of Continuous Access facility for each FFS. Non-friction curves are shown as solid lines, while the corresponding friction curves are shown as dashed lines.

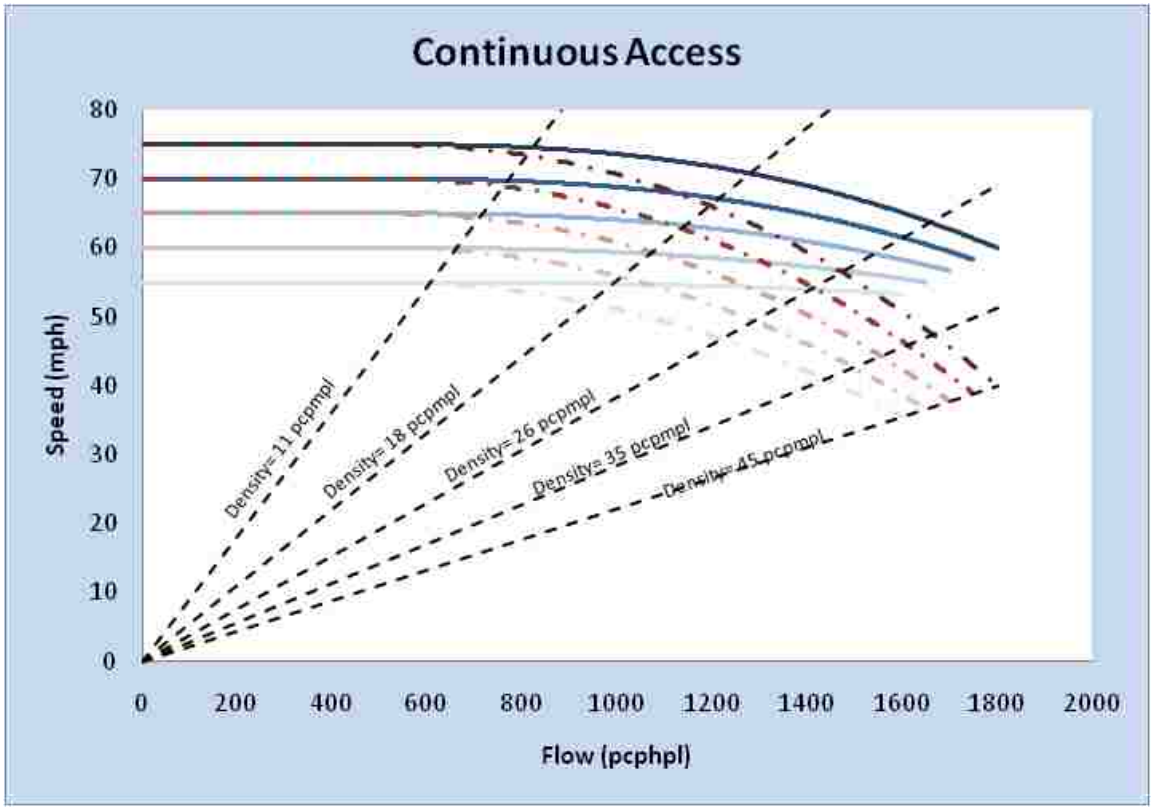

FIGURE 5.6 Continuous Access Speed-Flow Curves

Table 5.3 provides the variables used for the formation of the non-friction and friction speed-flow curves, respectively. Table 5.4 provides the speed-flow equations for the Continuous Access segments. It should be noted here that the friction curves terminate at a density of 45 pcpmpl, which is consistent with the methodology used in HCM 2010. The range of observed data for the non-friction curves never reached such high density levels, probably attributable to a low

likelihood of observing non-friction cases in combination with high flow rates. As a result, the terminal density of the non-friction curves is 30 pcpmpl. Consequently, the points corresponding to maximum observed flow rates in Table 5.3 (a) occur at a density of 30 pcpmpl, while the Table 5.3 (b) flow rates occur at the higher HCM LOS=F density of 45 pcpmpl. The common density principle was upheld also for all other speed-flow curves in accordance with HCM 2010.

TABLE 5.3 Continuous Access Speed-Flow Model Parameters

(a) Non-Friction Curve Values

FFS (mph)	Maximum Observed Flow Rate (pcphpl)	Speed @ Capacity (mph)	Breakpoint (pcphpl)	C_2
55	1600	53.33	500	2.5
60	1650	55.00	500	2.5
65	1700	56.67	500	2.5
70	1750	58.33	500	2.5
75	1800	60	500	2.5

Note: Refers to Equations (3.7) and (3.8)

(b) Friction Curve Values

FFS (mph)	Maximum Observed Flow Rate (pcphpl)	Speed @ Capacity (mph)	C_f
55	1600	35.56	1.47×10^{-5}
60	1650	36.67	1.39×10^{-5}
65	1700	37.78	1.31×10^{-5}
70	1750	38.89	1.24×10^{-5}
75	1800	40.00	1.18×10^{-5}

Note: Refers to Equation (3.9)

TABLE 5.4 Speed-Flow Equations for Continuous Access

	Flow Rate Range	
FFS (mph)	**0 - 500 pc/hr/ln**	**500 pc/hr/ln - Max. Flow***
75	75	$75 - (2.46 \times 10^{-7}(v_p\text{-}500)^{2.5}) - (0/1)(1.18 \times 10^{-5}\ (v_p\text{-}500)^2)$
70	70	$70 - (2.12 \times 10^{-7}(v_p\text{-}500)^{2.5}) - (0/1))1.24 \times 10^{-5}\ (v_p\text{-}500)^2)$
65	65	$65 - (1.67\times 10^{-7}(v_p\text{-}500)^{2.5}) - (0/1)(1.31 \times 10^{-5}\ (v_p\text{-}500)^2)$
60	60	$60 - (1.12\times 10^{-7}(v_p\text{-}500)^{2.5}) - (0/1)(1.39 \times 10^{-5}\ (v_p\text{-}500)^2)$
55	55	$55 - (4.15\times 10^{-8}(v_p\text{-}500)^{2.5}) - (0/1)(1.47 \times 10^{-5}\ (v_p\text{-}500)^2)$

*(0/1) represents values for non-friction (0) and friction (1) curves, respectively

5.3.2 Buffer 1

Users of Buffer 1 ML facilities are subject to slow vehicle following and also the frictional effect from the adjacent congested GP facility. In being subject to a slow car following effect, the flat section of the left side of the curve is replaced with a tilt line sloping down slightly.

The data sites used for the formation of Buffer 1 come from three different facilities: I-405 in Los Angeles, California, SR 167 in King County, Washington, and I-394 in Minneapolis, Minnesota. Of the eleven sites used, three held an FFS of 70 mph and eight held an FFS of 65 mph. FFS's of 55, 60, and 75 mph were not represented. The curves for the three unrepresented FFS's were determined from extrapolation. Figure 5.7 shows the set of curves for describing the speed-flow models of Buffer 1 facility.

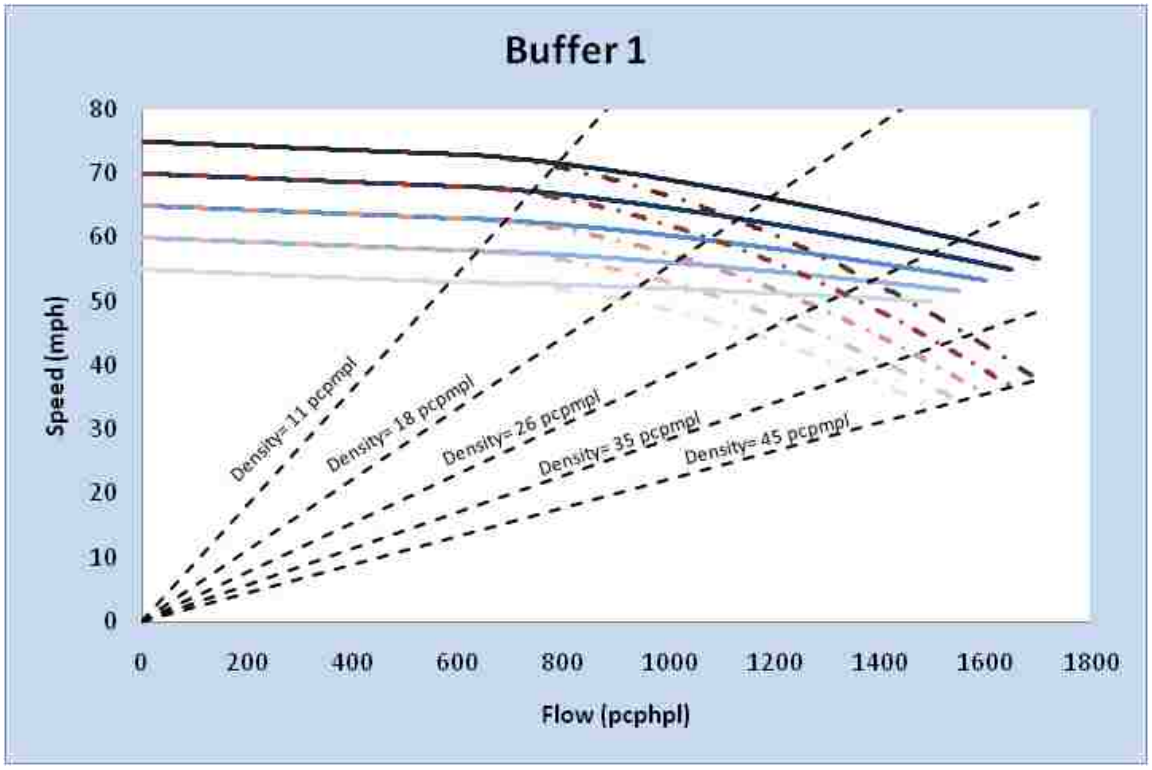

FIGURE 5.7 Buffer 1 Speed-Flow Curves

Tables 5.5 (a) and (b) provide the variables used for the forming of the non-frictional and frictional

speed-flow curves, respectively. Table 5.6 provides the speed-flow equations for the Buffer 1 segments. As with the Continuous Access curves, the non-friction curves terminate at a density of 30 pcpmpl as higher densities were not observed during periods of time where the GP lane was not congested. The set of friction curves terminates at a density of 45 pcpmpl.

TABLE 5.5 Buffer 1 Speed-Flow Model Parameters

(a) Non-Friction Speed-Flow Values

FFS (mph)	Maximum Observed Flow Rate (pcphpl)	Speed @ Capacity (mph)	C_1	Breakpoint (pcphpl)	Speed @ BP_1	C_2
55	1500	50.00	0.0033	600	53	1.4
60	1550	51.67	0.0033	600	58	1.4
65	1600	53.33	0.0033	600	63	1.4
70	1650	55.00	0.0033	600	68	1.4
75	1700	56.67	0.0033	600	73	1.4

Note: Refers to Equations (3.7) and (3.8)

(b) Friction Speed Flow Values

FFS (mph)	Maximum Observed Flow Rate (pcphpl)	Speed @ Capacity (mph)	C_f
55	1500	36.67	1.65×10^{-5}
60	1550	36.67	1.66×10^{-5}
65	1600	37.78	1.56×10^{-5}
70	1650	38.89	1.46×10^{-5}
75	1700	40.00	1.38×10^{-5}

Note: Refers to Equation (3.9)

TABLE 5.6 Buffer 1 Speed-Flow Equations

	Flow Rate Range	
FFS (mph)	**0 - 600 pc/hr/ln**	**600 pc/hr/ln – Max. Flow***
75	$75 - .00333(v_p)$	$73 - 0.00090(v_p-600)^{1.4} - (0/1)(1.38 \times 10^{-5} (v_p-600)^2)$
70	$70 - .00333(v_p)$	$68 - 0.00077(v_p-600)^{1.4} - (0/1)(1.46 \times 10^{-5} (v_p-600)^2)$
65	$65 - .00333(v_p)$	$63 - 0.00061(v_p-600)^{1.4} - (0/1)(1.56 \times 10^{-5} (v_p-600)^2)$
60	$60 - .00333(v_p)$	$58 - 0.00043(v_p-600)^{1.4} - (0/1)(1.66 \times 10^{-5} (v_p-600)^2)$
55	$55 - .00333(v_p)$	$53 - 0.00022(v_p-600)^{1.4} - (0/1)(1.65 \times 10^{-5} (v_p-600)^2)$

*(0/1) represents values for non-friction (0) and friction (1) curves, respectively

5.3.3 Buffer 2

As a slow car following effect and frictional effect were not observed in Buffer 2's small data set, only single curve is produced for each FFS. While it is somewhat intuitive to believe the buffer separated nature of the facility is susceptible to some influence from the GP lanes, none was observed in the two study sites used in this project. Figure 5.8 shows the family of speed-flow curves for Buffer 2.

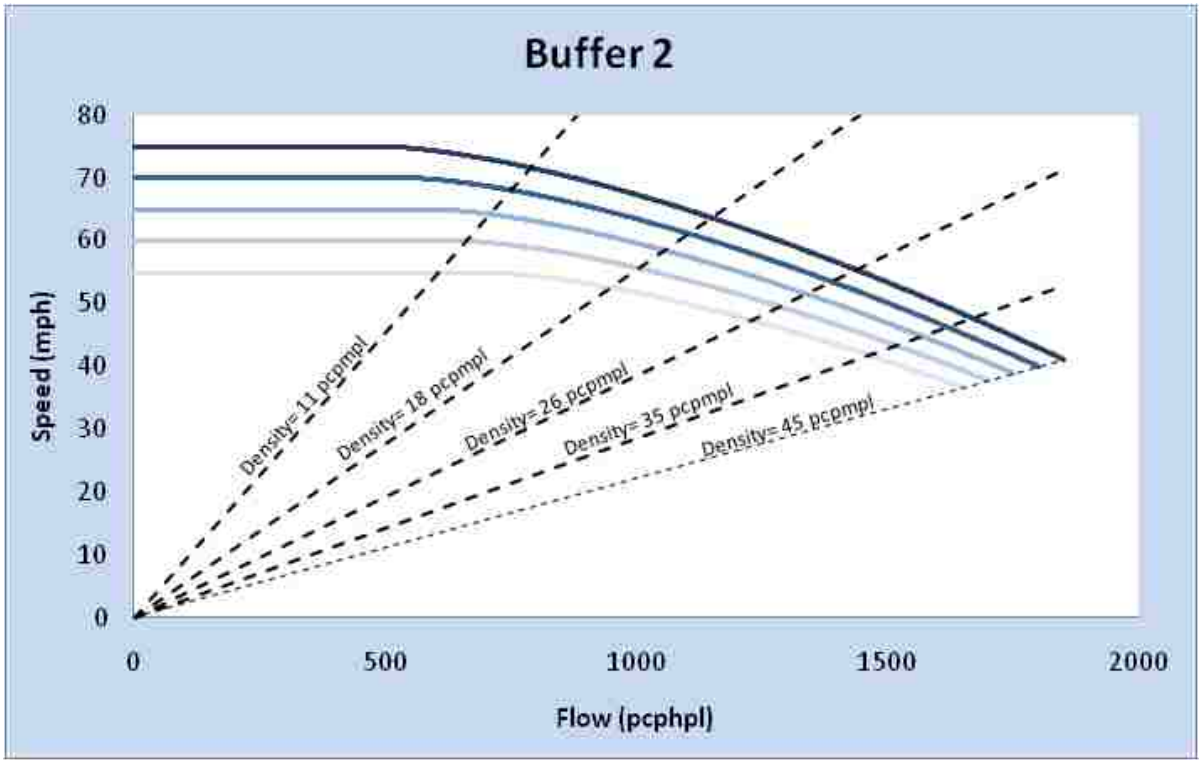

FIGURE 5.8 Buffer 2 Speed Flow Curves

Table 5.7 provides the variables used for the forming of the Buffer 2 speed-flow curves. Table 5.8 shows the speed-flow equations for the Buffer 2 segments. With only one site's worth of data for the 65 mph FFS curve and 70 mph FFS curve, these curves must be considered preliminary and used with caution. As no frictional impact was observed and the multiple lanes of the facility should prevent or minimize the effects of slow car following, the early drop in speed and lower

capacity is difficult to understand. If possible more sites with this geometry should be investigated.

TABLE 5.7 Buffer 2 Speed-Flow Curve Variable Values

FFS (mph)	Maximum Observed Flow Rate (pcphpl)	Speed @ Capacity (mph)	Breakpoint (pcphpl)	C_2
55	1650	36.67	700	1.5
60	1700	37.78	650	1.5
65	1750	38.89	600	1.5
70	1800	40.00	550	1.5
75	1850	41.11	500	1.5

Note: Refers to Equations (3.7) and (3.8)

TABLE 5.8 Buffer 2 Speed-Flow Equations

	Flow Rate Range	
FFS (mph)	**0 – Breakpoint pc/hr/ln**	**Breakpoint – Max Flow pc/hr/ln**
75	75	$75 - 0.000683(v_p-500)^{1.5}$
70	70	$70 - 0.000679(v_p-550)^{1.5}$
65	65	$65 - 0.000670(v_p-600)^{1.5}$
60	60	$60 - 0.000653(v_p-650)^{1.5}$
55	55	$55 - 0.000626(v_p-700)^{1.5}$

5.3.4 Barrier 1

The slow car following effect can be observed in Barrier 1 separation type. Therefore, the left side of the speed-flow relationship is sloped from a flow rate of 0 to that of the breakpoint. The presence of the barrier eliminates the frictional impact from the GP lanes, so only a single curve is used for each FFS.

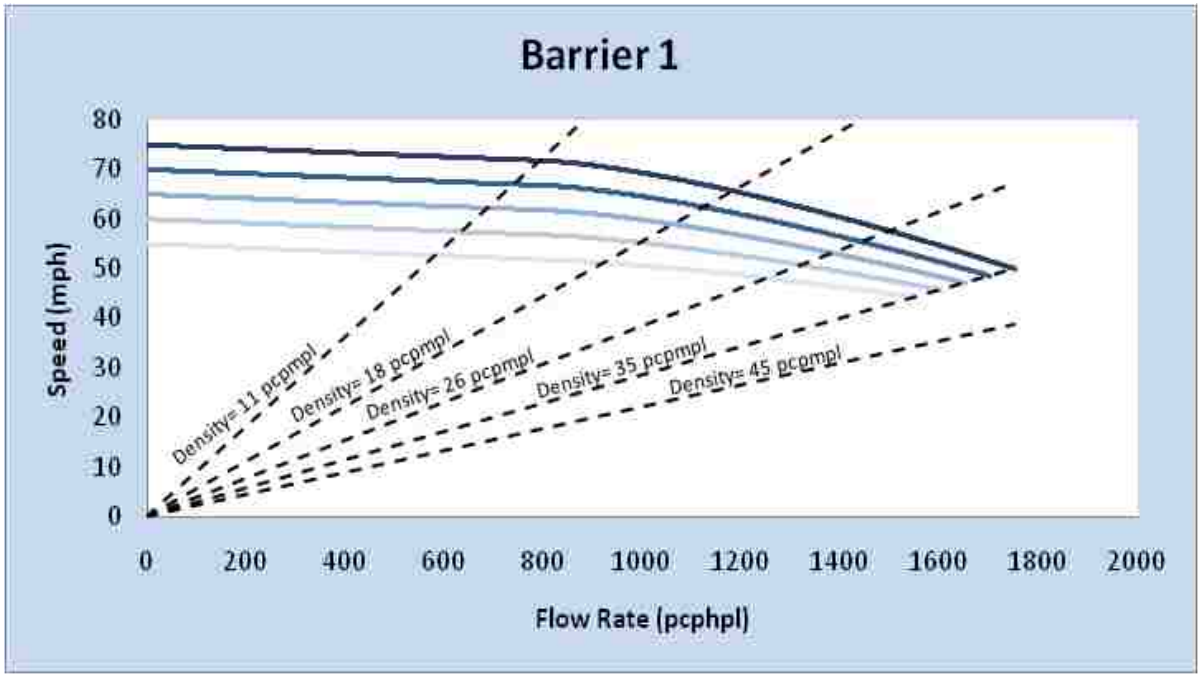

FIGURE 5.9 Barrier 1 Speed-Flow Curve

Table 5.9 provides the parameters used for the formation of Barrier 1 speed-flow curves. Table 5.10 shows the speed-flow equations for the Barrier 1 segments. While the curves for other facility types terminate at a density of 45 pcpmpl, the breakdown for Barrier 1 facilities was observed to occur at a lower density. The termination point for the Barrier 1 speed-flow curves was determined to be 35 pcpmpl. This lower density at the point of flow breakdown could be attributed to barrier impact of this type of facility. As barriers are present on one or both sides of the facility, there is little room for a trailing driver to maneuver. Should a vehicle brake, the trailing vehicle that follows the leading vehicle closely has to brake harder to avoid a possible rear-end collision because the driver does not have the option of swerving to the right or left. The reduction in headway would cause breakdown at a lower density.

TABLE 5.9 Barrier 1 Speed-Flow Curve Parameters

FFS (mph)	Maximum Observed Flow Rate (pcphpl)	Speed @ Capacity (mph)	C_1	Breakpoint (pcphpl)	Speed @ Breakpoint (mph)	C_2
55	1550	44.29	0.004	800	51.8	1.4
60	1600	45.71	0.004	800	56.8	1.4
65	1650	47.14	0.004	800	61.8	1.4
70	1700	48.57	0.004	800	66.8	1.4
75	1750	50	0.004	800	71.8	1.4

Note: Refers to Equations (3.7) and (3.8)

TABLE 5.10 Barrier 1 Speed-Flow Equations

	Flow Rate Range	
FFS (mph)	**0 - Breakpoint pc/hr/ln**	**Breakpoint – Max. Flow (pc/hr/ln)**
75	$75-(0.004v_p)$	$71.8 - 00148(v_p-800)^{1.4}$
70	$70-(0.004v_p)$	$66.8 - 0.00133(v_p-800)^{1.4}$
65	$65-(0.004v_p)$	$61.8 - 0.00116(v_p-800)^{1.4}$
60	$60-(0.004v_p)$	$56.8 - 0.00096(v_p-800)^{1.4}$
55	$55-(0.004v_p)$	$51.8 - 0.00071(v_p-800)^{1.4}$

5.3.5 Barrier 2

The Barrier 2 speed-flow curve is more similar to that of a basic freeway segment than any other ML types. It can essentially be thought of as its own independent facility as there is no slow car following or frictional effect. All Barrier 2 study sites were found operating well below capacity. The maximum observed flow was about 1,500 pcphpl. This makes it challenging to determine the capacity of this segment type. Engineering judgment was ultimately used in determining the maximum flow rate for the development of the speed-flow curves based on the experience of basic freeway segments.

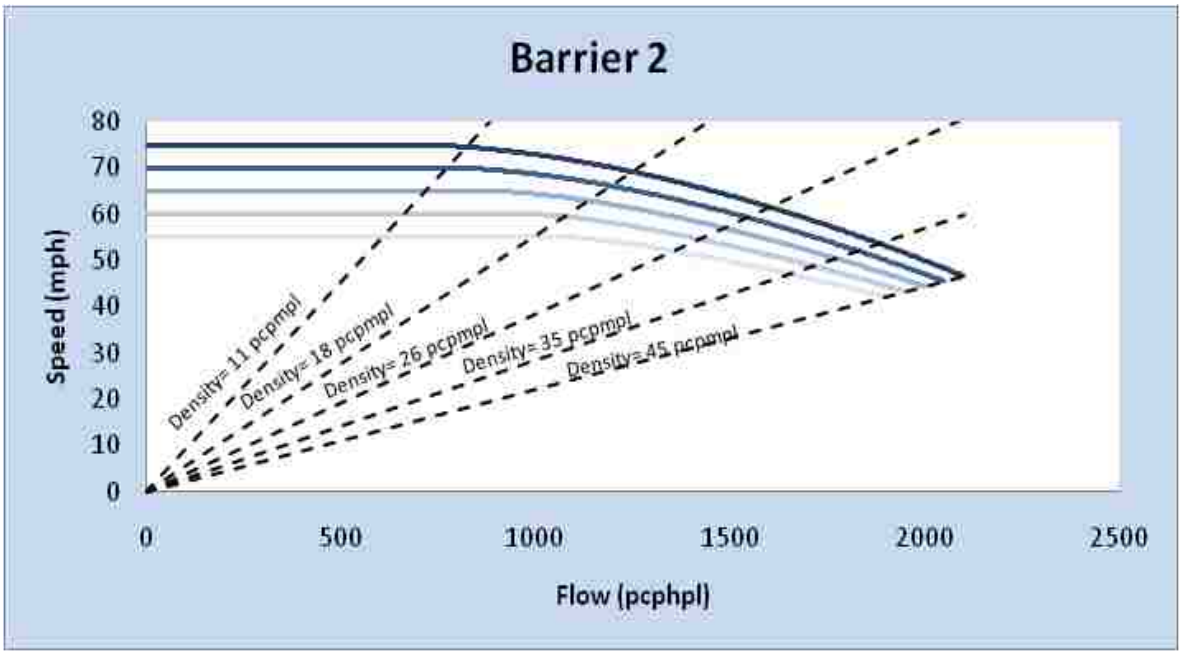

FIGURE 5.10 Barrier 2 Speed-Flow Curves

Table 5.11 lists the parameters used for the formation of Barrier 2 speed-flow curves. Table 5.12 provides the speed-flow equations for the Barrier 2 segments.

TABLE 5.11 Barrier 2 Speed-Flow Curve Parameters

FFS (mph)	Maximum Observed Flow Rate (pcphpl)	Speed @ Capacity (mph)	Breakpoint (pcphpl)	C^2
55	1900	42.22	1100	1.3
60	1950	43.33	1000	1.4
65	2000	44.44	900	1.5
70	2050	45.56	800	1.6
75	2100	46.67	700	1.7

Note: Refers to Equations (3.7) and (3.8)

TABLE 5.12 Barrier 2 Speed Flow Equations

	Flow Rate Range	
FFS (mph)	**0 - BP pc/hr/ln**	**BP pc/hr/ln - Max. Flow**
75	75	$75 - (0.000127(v_p-700)^{1.7})$
70	70	$70 - (0.000271(v_p-800)^{1.6})$
65	65	$65 - (0.000563(v_p-900)^{1.5})$
60	60	$60 - (0.00113(v_p-1000)^{1.4})$
55	55	$55 - (0.00215(v_p-1100)^{1.3})$

5.3.6 Comparison of Speed-Flow Models amongst Different Basic ML Types

Figure 5.11 uses FFS =60 mph as an example across the five segment types. For those segment types where frictional effect would be present, two sets of curves were developed for each FFS under friction and non-friction scenarios. Each curve consisted of two parts: a linear portion stretching from zero flow to the breakpoint, and a curvilinear portion from the breakpoint to the maximum observed flow. For single lane facilities where passing is prohibited, the linear portion was sloped downward due to the slow moving vehicle effect. For other segment types, the linear portion had a slope of zero remaining at the FFS until the breakpoint. Breakpoints were estimated by calculating the standard deviation of speed for each volume range of 100 pcphpl. The breakpoints were then determined at the volume where the speed standard deviation begins to increase abruptly.

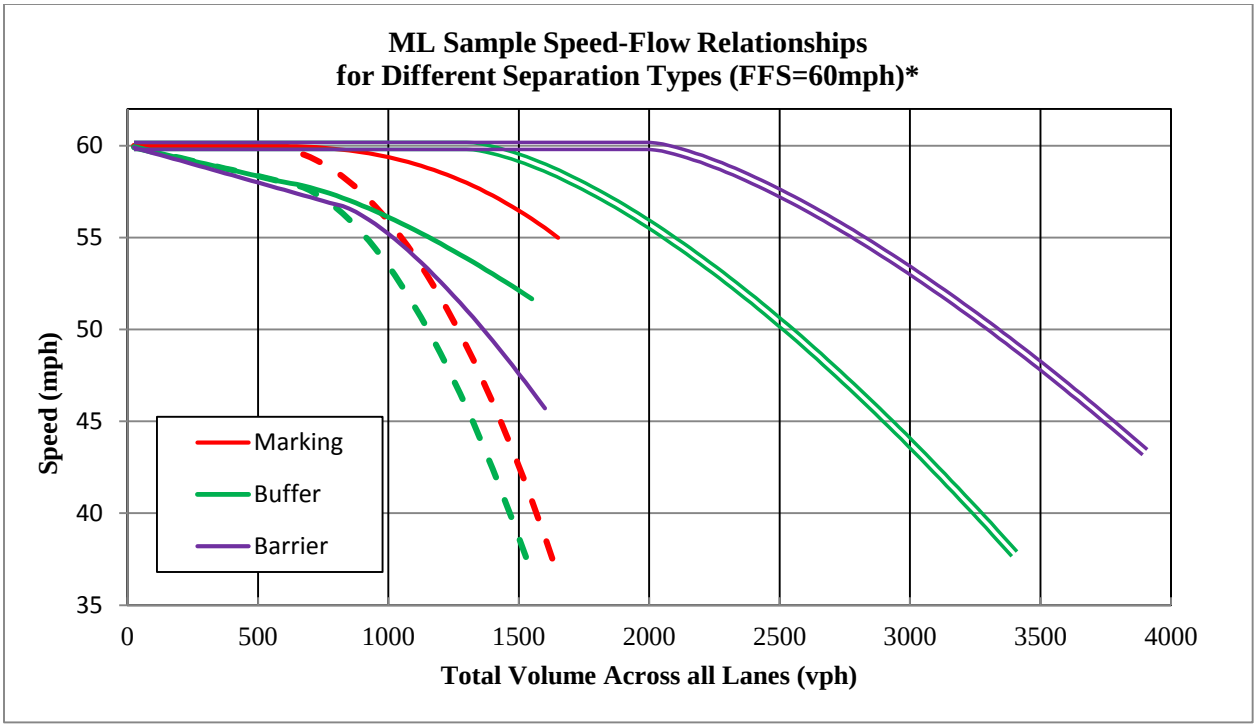

* Single lines refer to one-lane ML facilities, double lines to two-lane ML facilities; dashed lines correspond to the speed-flow relationship under *friction effect* conditions

FIGURE 5.11 Sample ML Speed-Flow Relationships for FFS=60mph

For single lane ML facilities separated by buffer or barrier, vehicles are unable to perform passing maneuvers. As a result, the linear portion of the curve has a negative slope even at a low volume. This initial slope of the curve can be attributed to the fact that slow-moving vehicles cannot be passed as they would have been able to in facilities with multiple lanes. The overall speed of a platoon on such a facility is then dictated by the speed of the slower vehicle.

As described earlier, the performance of the Continuous Access and Buffer 1 facilities is dependent not only on the characteristics of the ML but also on the performance of the adjacent GP facility. For these two ML strategies, a second, frictional curve (dashed line) has been produced showing the speed-flow relationship for periods of time during GP congestion. The frictional curve is a function of both the non-friction curve and the flow rate. For two-lane ML facilities, the buffer-

separated facility shows an earlier drop in the speed-flow curve compared to the barrier-separated facility. No stripe-separated two-lane ML facilities were field observable.

5.4 Modeling of Cross-Weave Effect

5.4.1 Simulation Model Calibration

Simulation model calibration is crucial for realistic representations of simulated scenarios as well as reliable outputs. Calibration efforts are therefore required to ensure that the model output can replicate the observed field data. Driving behavior parameters need to be adjusted during the process to match the outputs with field conditions. Field data were collected at one access point along IH 635 in Dallas, Texas. The lane configuration sketch is shown in Figure 5.12. There are four GP lanes and one buffer-separated ML in the westbound direction of the IH 635. The data collection site is located just west of Midway Road entrance ramp. The ML is an HOV-2 lane. The ML is separated from the GP lanes by a double white line buffer, and it is illegal to cross the line. At the BOA (shown in Figure 5.12), the separation marking changes to dashed lines, and vehicles can ingress/egress to the ML. The BOA is 1,160 ft at this site and $L_{CW\text{-}Min}$ is 0 ft, which indicates that the opening starts immediately at the GP on-ramp. Cross-weave movements occur at this location as well, with ML-targeting vehicles coming from the Midway on-ramp needing to weave across multiple GP lanes to access the ML. In most designs, $L_{CW\text{-}Min}$ is often too long to be completely covered by one freeway surveillance camera. This makes it very difficult to observe lane changing behaviors of the cross-weave vehicles, although they are essential for simulation model calibration. However, the IH 635 site shown in Figure 5.12 has an unusual on-ramp position which is very close to the beginning point of the BOA. This configuration made it possible to

capture the entire freeway segment with one video camera placed on a downstream overpass (Figure 5.13 shows a snapshot from the camera). Cross-weave maneuvers were therefore extracted from the data for calibrating the model.

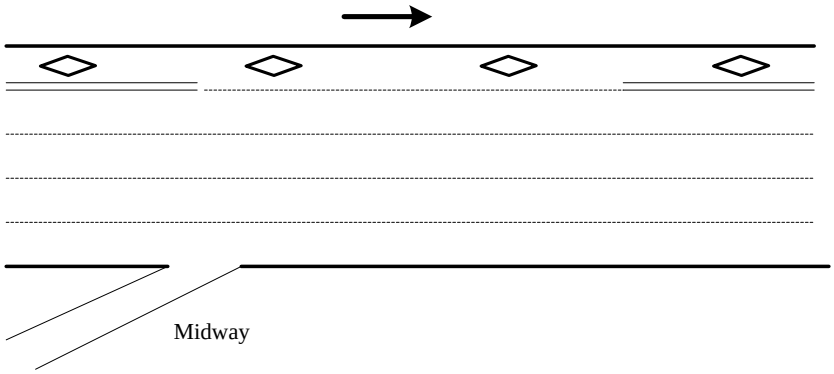

FIGURE 5.12 Lane Configuration of the ML Access Point at IH 635 Dallas, Texas

FIGURE 5.13 Video Image for IH 635 ML Access Point

Two 1-hour video recordings were evaluated for this location. The first dataset was during moderate traffic conditions on March 14, 2008 between 10:20 to 11:20 AM. The second dataset was collected during the high-volume afternoon peak period between 3:25 to 4:25 PM. For each dataset, origin-destination flows were extracted as well as the actual speed and the spatial distribution of lane changes. A VISSIM simulation model was developed for this site with many

virtual sensors deployed across lanes and over the entire segment for data collection and comparison purposes. The model was carefully calibrated based on the field observed speed and total lane changing activities. The spatial distribution of lane changes in the field was collected by a research team at the University of Texas at Arlington and was used for model calibration. The data consisted of the longitudinal location of each lane change from the GP lanes to the ML. The BOA was divided into 100-foot zones. The number of vehicles that changed lanes to the ML within each zone was collected for comparing with the simulated data for calibration. The detailed field data processing is described in Williams *et al.* (2010). Driver behavior parameters were adjusted through an iterative process until the difference from the reference data is relatively small (less than 10%). Several major parameters are adjusted according to the observed field data, including standstill distance, time headway, and maximum deceleration for lane changing. Also, other parameters, such as look back distance are modified individually for weaving areas. The detailed calibration process is described in Appendix A of this dissertation.

5.4.2 Simulation Scenario Setup

Different simulation scenarios were designed to test the cross-weave effect. The simulation network consists of a one-lane on-ramp and a multi-lane GP section. A BOA was set in the downstream section of the GP lane on-ramp to allow vehicle ingress/egress to the ML. To capture the effect of queues that formed on the APIA and to ensure adequate storage for entering demands, long approach links upstream of the entrance ramp were coded on the freeway mainline. Likewise, to ensure that the freeway traffic had adequate time to recover after clearing the weaving area, the link downstream of the access point opening area was also set sufficiently long. The configuration used in the simulation is shown in Figure 5.14.

One of the factors that varied significantly in the experimental design was the length of $L_{CW\text{-}Min}$ and $L_{CW\text{-}Max}$. Several combinations of the factors were identified from field data, and listed in Table 5.13. The design length for a BOA normally ranges between 1,300 ft and 2,000 ft. The simulation experiments used 1500 ft for the BOA for all cases and three different $L_{CW\text{-}Min}$ lengths (Case 1: 1,500 ft; Case 2: 2,000 ft; Case 3: 2,500 ft) to examine the impacts of $L_{CW\text{-}Min}$ on cross-weave behavior.

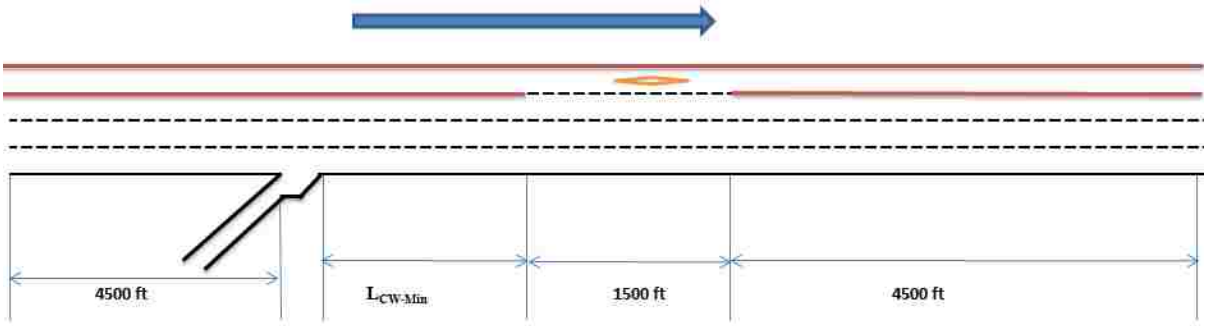

FIGURE 5.14 Configuration Used in VISSIM Simulation

TABLE 5.13 Field Data Reference for $L_{CW\text{-}Min}$ and $L_{CW\text{-}Max}$

Facility Name	$L_{CW\text{-}Min}$ (ft)	$L_{CW\text{-}Max}$ (ft)	Buffer Opening Area (ft)
I-394 EB, Minneapolis, Minnesota	2737	5082	2345
	2278	4623	2345
	1500	2984	1484
	2095	3577	1482
	2240	3722	1482
I-394 WB, Minneapolis, Minnesota	415	4044	3629
	2029	3226	1197
	1710	2907	1197
	3484	6462	2978
SR 167 NB, Seattle, Washington	2008	3460	1452
	2982	4434	1452
	2302	3798	1496
	2432	3928	1496
	2474	3951	1477
	4814	6191	1377
SR 167 SB, Seattle, Washington	3386	4842	1456
	4213	5669	1456
	3757	5304	1547
	2041	3588	1547
	2101	3593	1492
	2688	4180	1492

The cross-weave intensity is postulated to be a function of the number of necessary lane changes, the cross-weave demand, and the surrounding GP traffic. Therefore, when evaluating its operational impact on the GP lanes, various traffic demands on both the GP on-ramp and the approaching GP lanes need to be tested in the simulation experiment. GP lane demand varied from 1,600 pcphpl to 2,400 pcphpl in 100 pcphpl increments. Cross-weave demand from the GP on-ramp to the ML was tested for five different levels (100, 200, 300, 450 and 600 pcph). Three GP lane configurations (two-lane, three-lane and four-lane) were tested. The full sets of simulations were run without considering truck volume.

In the test scenario simulation model, virtual sensors were deployed in all GP lanes starting at the

ramp gore point and continuing through the end of the BOA to collect average speed and volume across all GP lanes. A spacing of 200 ft was configured between each set of sensors. Different vehicle types were also configured in the simulation model with the cross-weave flows labeled as "ramp". Therefore, the sensors could capture the frequency of each vehicle type at the cross section every 200 ft apart on a lane-by-lane basis. Lane change intensity could then be calculated at various points in the segment. Also within the GP segment before the BOA, the capacity reduction of the GP segment due to the cross-weave volume needs to be estimated. To achieve this, link evaluation was performed for the GP segment at a spacing of 500 feet. In other words, speed-flow-density data for the GP segment are aggregated in 500-foot segments. By regressing from the speed-flow curves using the link evaluation output, the capacity for each scenario could be determined and the CRF/CAF for various configurations can be estimated as well.

In VISSIM, traffic generation depends on the random seed number to use. By employing different random seeds, simulation results change due to the stochastic nature of the underlying algorithms. To capture this stochastic variability, multiple simulation runs for each scenario are necessary. Therefore, for each scenario, five different random seeds were selected, which sufficiently increased the sample of speed-flow data points. The integrated results from these simulation runs are considered reliable and unbiased, and are consistent with what an agency may obtain in the field from sensor data.

5.4.3 Simulation Result Analysis

From the simulation, traffic volumes and speeds were collected within the segment every 500 ft

apart in 15-minute increment. The speed-flow diagram can be drawn correspondingly and Van Aerde's curve fitting can be performed to determine the capacity of the GP segment (Van Aerde and Rakha, 1995). Figure 5.15 shows the speed-flow diagram for the four-lane GP scenarios with $L_{CW\text{-}Min}$ =1,500 ft, and cross-weave volumes ranging from 100 pcph to 600 pcph. Within each cross-weave setting, the GP mainline demand changes from 1,600 pcphpl to 2,400 pcphpl, such that a set of complete data points could be collected from the simulation.

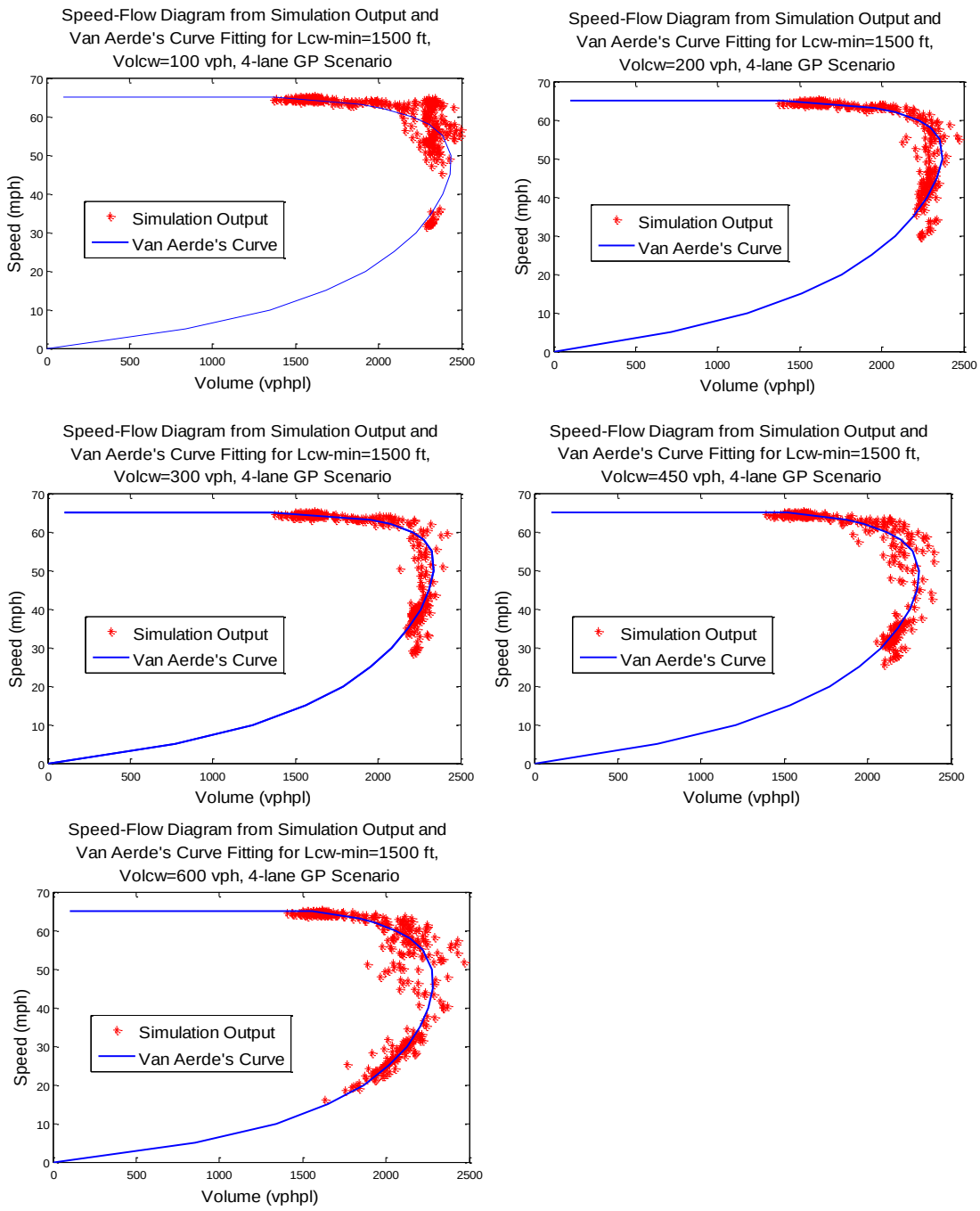

FIGURE 5.15 Speed-Flow Diagrams from Simulation Output and Van Aerde's Curve Fitting for 4-lane GP Scenarios

A base scenario with no cross-weave flow was analyzed. The capacity from the Van Aerde's regression is calculated to be 2450 pcphpl, which is only slightly higher than the HCM 2010

freeway capacity for a 70 mph free-flow speed and is considered an acceptable match with the HCM. The remaining scenarios with varying cross-weave demands expectedly resulted in lower capacities relative to the base. The CRF therefore can be expressed as a function of the base capacity C_{base} and the cross-weave capacity C_{cw} in Equation (5.5). Correspondingly, the CAF used in the HCM 2010 freeway facility chapter can be calculated as formulated in Equation (5.6).

$$CRF = \frac{C_{base} - C_{cw}}{C_{base}} \times 100\% \tag{5.5}$$

$$CAF = 1 - CRF \tag{5.6}$$

For each combination of cross-weave flow, number of lanes, and $L_{CW\text{-}Min}$, the capacity of the configuration is derived from the simulation model. The CRF for the combination is then consequently calculated. Figure 5.16 gives the graphical representation of the CRF for the 4-Lane GP scenarios. Note that as cross weave flow increases, the CRF increases as well. The general trend follows a logarithmic distribution. A longer $L_{CW\text{-}Min}$ would have less capacity reduction impact on the GP segment. Table 5.14 gives a complete result of the CRF for each configuration tested in the simulation model. Note that for the capacity calculated using the Van Aerde's model, all the calculated capacities were rounded to the nearest 5 or 0 in consideration of the underlying variability in the simulated speed-flow data. The results show reasonable trends since the CRF increases as the cross-weave flow increases, the $L_{CW\text{-}Min}$ decreases, and the number of GP lane increases. This result is as hypothesized, since as the cross-weave flow increases, more weaving would be generated within the GP segment, which brings more capacity disturbance to the area. With a longer weaving length ($L_{CW\text{-}Min}$), the cross-weave vehicles would have more time to position themselves onto the left-most lane to get into the ML. Therefore, the average LCI would be less intense and the CRF lower. Also, with fewer GP lanes, the number of lane changes required for the cross-weave flow would be correspondingly reduced, which also results in a lower

disturbance frequency on the GP segment.

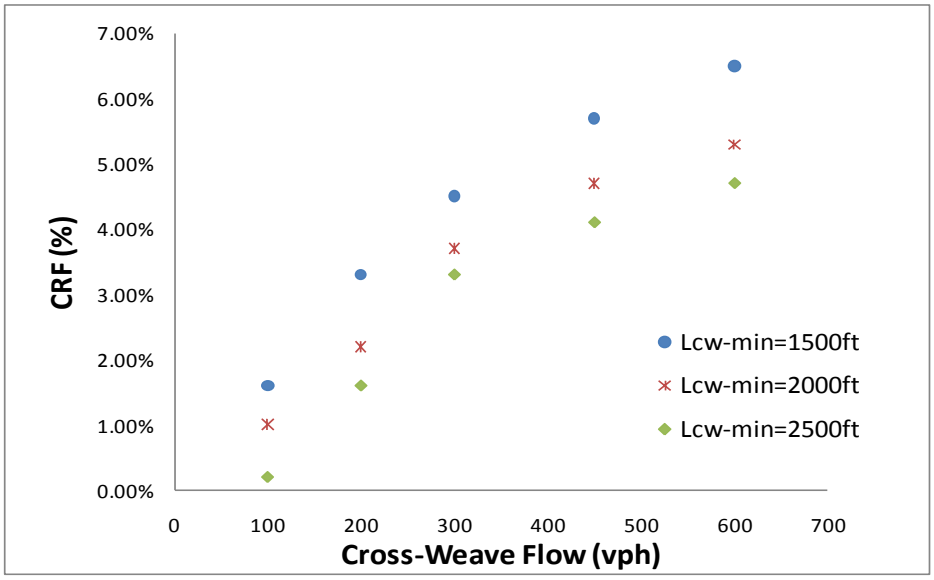

FIGURE 5.16 CRF as Response to Cross Weave Flow and Lcw-min under 4-Lane GP Scenarios

TABLE 5.14 CRF for Each Configuration Scenario

	$L_{CW\text{-}Min}$ (ft)	Cross-Weave Flow (pcph)				
4 GP Lanes		100	200	300	450	600
	1500	1.63%	3.27%	4.49%	5.71%	6.53%
	2000	1.02%	2.24%	3.67%	4.69%	5.31%
	2500	0.20%	1.63%	3.27%	4.08%	4.69%
3 GP Lanes	$L_{CW\text{-}Min}$ (ft)	Cross-Weave Flow (pcph)				
		100	200	300	450	600
	1500	1.22%	3.06%	3.88%	5.51%	6.12%
	2000	0.82%	2.04%	3.47%	4.29%	4.69%
	2500	0.20%	1.43%	2.65%	4.08%	4.29%
2 GP Lanes	$L_{CW\text{-}Min}$ (ft)	Cross-Weave Flow (pcph)				
		100	200	300	450	600
	1500	1.02%	2.65%	3.67%	5.10%	5.31%
	2000	0.61%	2.04%	3.06%	4.29%	4.90%
	2500	0.00%	1.22%	2.24%	3.27%	4.08%

To further investigate the capacity reduction due to various configurations, lane change intensity analysis was performed for different scenarios. Figure 5.17 demonstrates the cumulative number of lane changes profile for simulation scenarios with cross-weave flow of 300 pcph, and GP input demand of 2,400 pcphpl. The LCI is quite different for the three GP lane scenarios. With fewer

lanes, the LCI is less due to the lower number of lane change maneuvers required for the cross-weave flow. Figure 5.18 gives the same configuration comparison, except that the changing variable is the length of $L_{CW\text{-}Min}$. Note that the shorter $L_{CW\text{-}Min}$ results in more intense lane changing, however, the significance is not that prominent. Also with a longer $L_{CW\text{-}Min}$, the total number of lane changes is increased due to the fact that more vehicles would position themselves on the left-most lane to be ready to get into the ML at the BOA. However, if analyzing the LCI on the entire length of $L_{CW\text{-}Min}$, the difference between the three scenarios would be quite pronounced. The LCI (total number of lane changes/$L_{CW\text{-}Min}$) are 0.48 LC/ft, 0.39 LC/ft and 0.32 LC/ft for $L_{CW\text{-}Min}$ =1500 ft, 2000 ft, and 2500 ft, respectively.

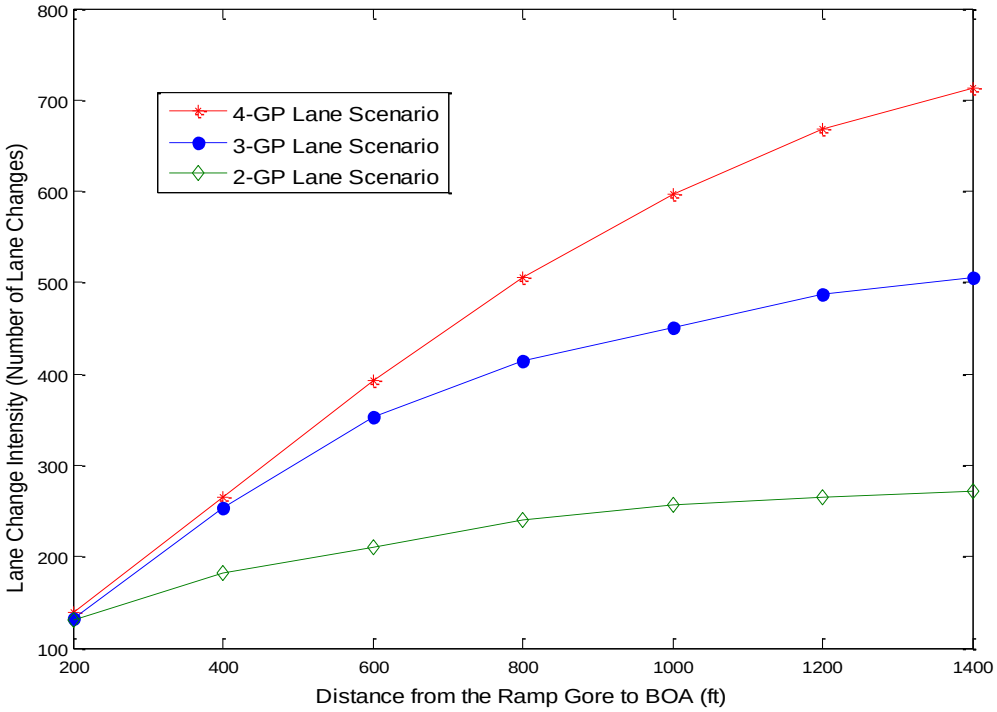

FIGURE 5.17 Cumulative Lane Change Intensity for Different GP Lanes Scenarios with Cross-Weave Flow 300 pcph, and GP Input Demand of 2400 pcphpl

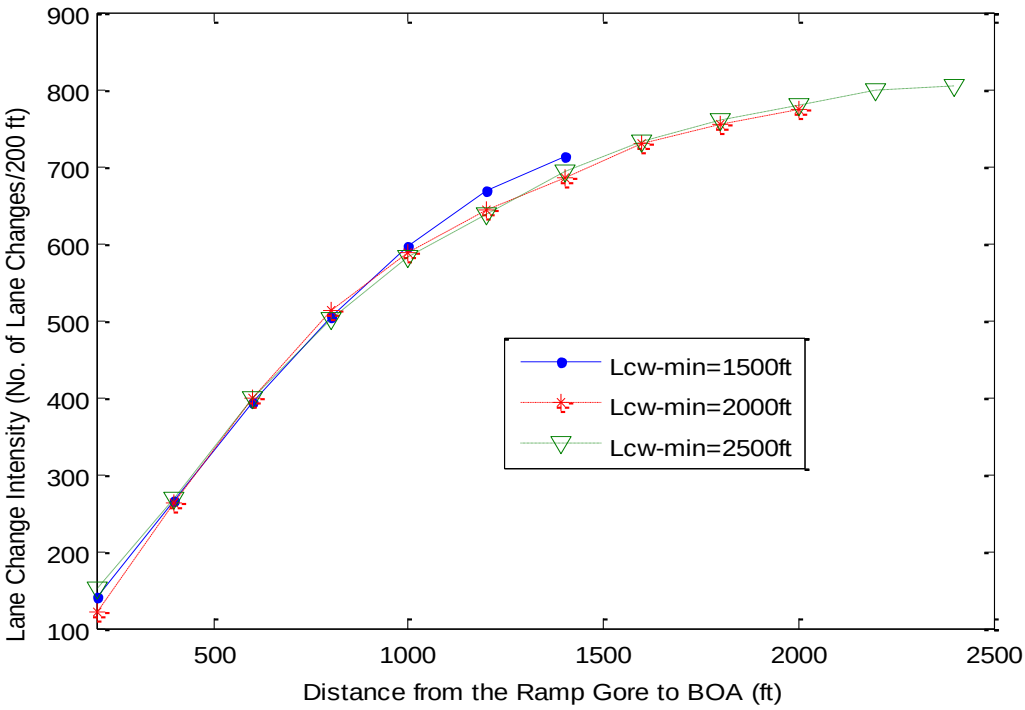

FIGURE 5.18 Cumulative Lane Change Intensity for Different $L_{CW\text{-}Min}$ Scenarios with Cross Weave Flow 300 pcph, and GP Input Demand of 2400 pcphpl

The calculated CRF was developed as a function of the number of GP lanes, cross-weave flows, and length of $L_{CW\text{-}Min}$. A regression model was performed to quantitatively establish the relation between the CRF and the other independent variables:

$$CRF(\%) = -8.957 + 2.52 \times \ln(CW) - 0.001453 \times L_{cw-min} + 0.2967 \times (No.\,of\ GP\ Lanes)$$

where CW is the cross-weave flow measured in pcph, $L_{CW\text{-}Min}$ is the length from the ramp gore to the beginning of BOA measured in ft, and number of GP lanes ranging from 2 to 4.

The regression result is shown in Table 5.15. All the independent variables yield a significant result at 95% confidence interval on the CRF, and the adjusted R-square value is 0.9837 which indicates an excellent fit.

TABLE 5.15 Linear Regression Output for CRF and the Corresponding Variables

Independent Variable	Estimated Parameter	T-statistic	P-Value
Constant (intercept)	-8.957	-24.063	0.000
ln(CW)	2.52	46.349	0.000
Lcw-min	-0.001453	-17.329	0.000
Number of GP Lanes	0.2967	7.075	0.001

5.5 Twin-Cell based Modeling Approach

5.5.1 Basic Segment Modeling Result

In the proposed traffic flow model on the basis of CTM, boundary conditions are specified by means of input and output cells according to Daganzo (1993). The output cell, functioning as a sink to absorb all the exiting traffic, has infinite size (set as 10,000,000 in this study). A source cell also with an infinite number of vehicles is set that would discharge into a "gate" cell of infinite size. This source cell functions as a valve that would release the inflow traffic at the default rate while holding the rest traffic flows that cannot enter the cell. The relevant parameters in the model were either taken from the empirical study or estimated based on the actual condition of SR 167 freeway sections (Liu *et al*., 2012).

With the developed HCM-based model, a numerical study is performed to observe the inflow patterns within the simulated freeway segment. For a simulation period of 100 time steps (1 hour period), the GP volume that enters into the segment is changed from 2000 to 2800 vphpl with a 200 vphpl increment for every 20 time steps (0.2 hour). The ML volume that is trying to enter the segment is set as 1800 vphpl constant for the entire period. Figure 5.19 shows the contour plot of traffic evolution (cell inflow) of the freeway segment for ML and GPLs, separately in both spatial

and temporal dimensions using the HCM-based approach. With the increase of the traffic flow trying to enter the GPLs, the GPLs are getting congested. After the 40th time step where the GP inflow (2400 vphpl) exceeds its capacity (2300 vphpl), the GP cells are unable to provide enough space for accommodating all the incoming vehicles. Therefore, for the rest of the simulation period, the largest flow that each cell could take is constrained to 23 veh/time step. For the ML cell, since it is affected by the status of the GP cell, it is noted that although the inflow into the ML is constant, the actual flow passed on to each cell indeed varies. Beginning at the 40th time step, the adjacent GP cell was detected to have a density higher than 35 vpmpl, and it thus imposed a frictional effect onto the ML. Correspondingly, the ML cell was shifted to the "friction state", where its cell capacity and maximum occupancy were decreased. The maximum inflow that it could take in for each cell is constrained to 16 veh/time step.

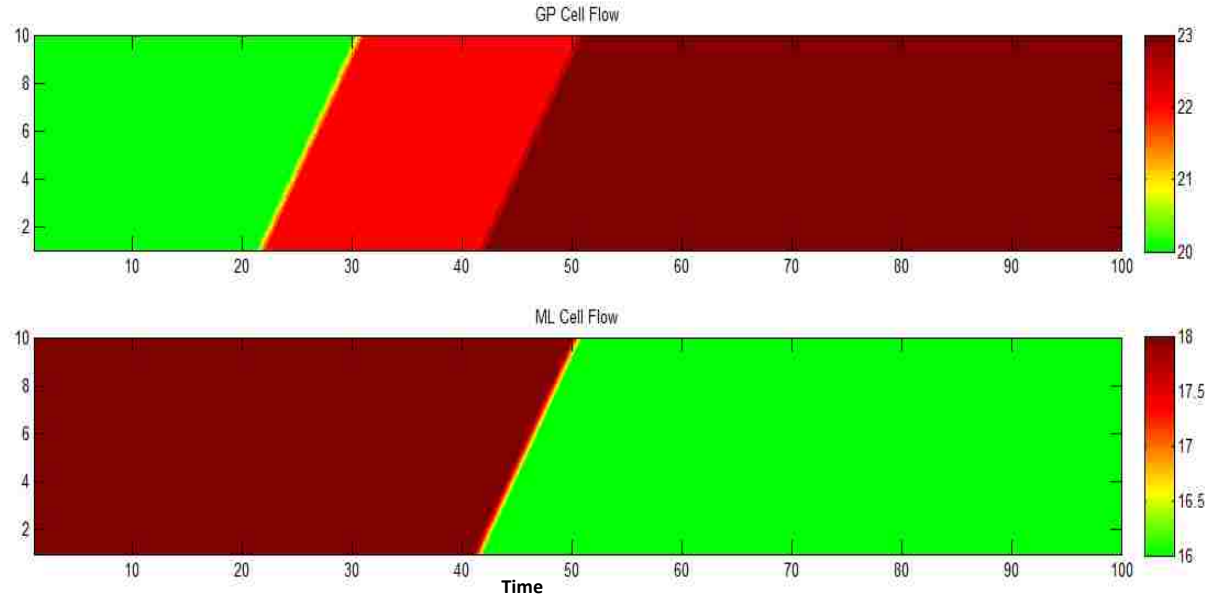

FIGURE 5.19 Temporal-Spatial Traffic Evolution using HCM-based Approach

To further model the freeway bottleneck scenario and better observe the process of onset, propagation, and dissipation of traffic congestion, a bottleneck GP cell (Cell 7) is set where the

cell capacity (maximum inflow for the cell) is dropped by 60% during Time Step 20 through 30 to simulate an incident scenario. The incident scenario is tested using both HCM-based and unsupervised machine learning-based approaches.

5.5.1.1 HCM-based Approach

For the HCM-based approach, the source inflows for GPL and ML are set as 2000 vphpl and 1800 vphpl, separately for the entire simulation period. Figure 5.20 shows the contour plot of traffic evolution pattern under the bottleneck scenario. Essentially, upon the formation of a bottleneck at Cell 7, queue begins to back up on GP upstream. After the bottleneck is cleared, the downstream cells are capable of absorbing the inflow traffic as much as they can that has been previously accumulated upstream. The ML cells performance is also impacted due to the bottleneck, which results in a speed reduction of up to 10%.

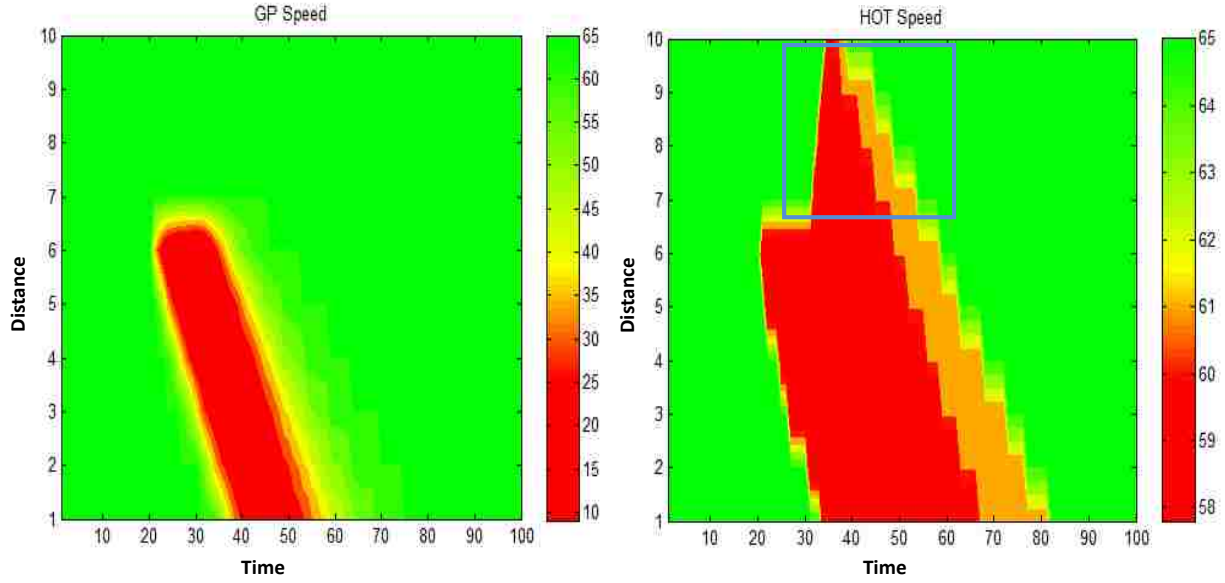

FIGURE 5.20 Temporal-Spatial Traffic Evolution under Bottleneck Scenario using HCM-based Method

5.5.1.2 Unsupervised Machine Learning Approach

As a comparison, unsupervised machine learning approach is applied to the same scenario to emulate the traffic flow patterns. Different from the HCM-based method, sensitivity analysis can be performed for different ML inflow demand, as the model assigns different frictions under various circumstances. Again GP has a constant demand of 2000 vphpl across the entire simulation period. Figure 5.21 shows the simulation result. For the GP cell occupancy (density) graph, both methods yield the same result as following the same progression logic. Particularly for the unsupervised machine learning approach, different ML demands are tested to examine how the ML is affected by the GP performance. When ML demand is 900 vphpl, the ML speed already has a 10% reduction (58 mph) even when no incident happens. Towards the end of the incident (30 time step), the speed is reduced to around 50 mph. When the ML demand increases to 1400 vphpl, the ML speed reduces to 56 mph when no incident is present, and the impact due to the GP incident is more pronounced and persistent.

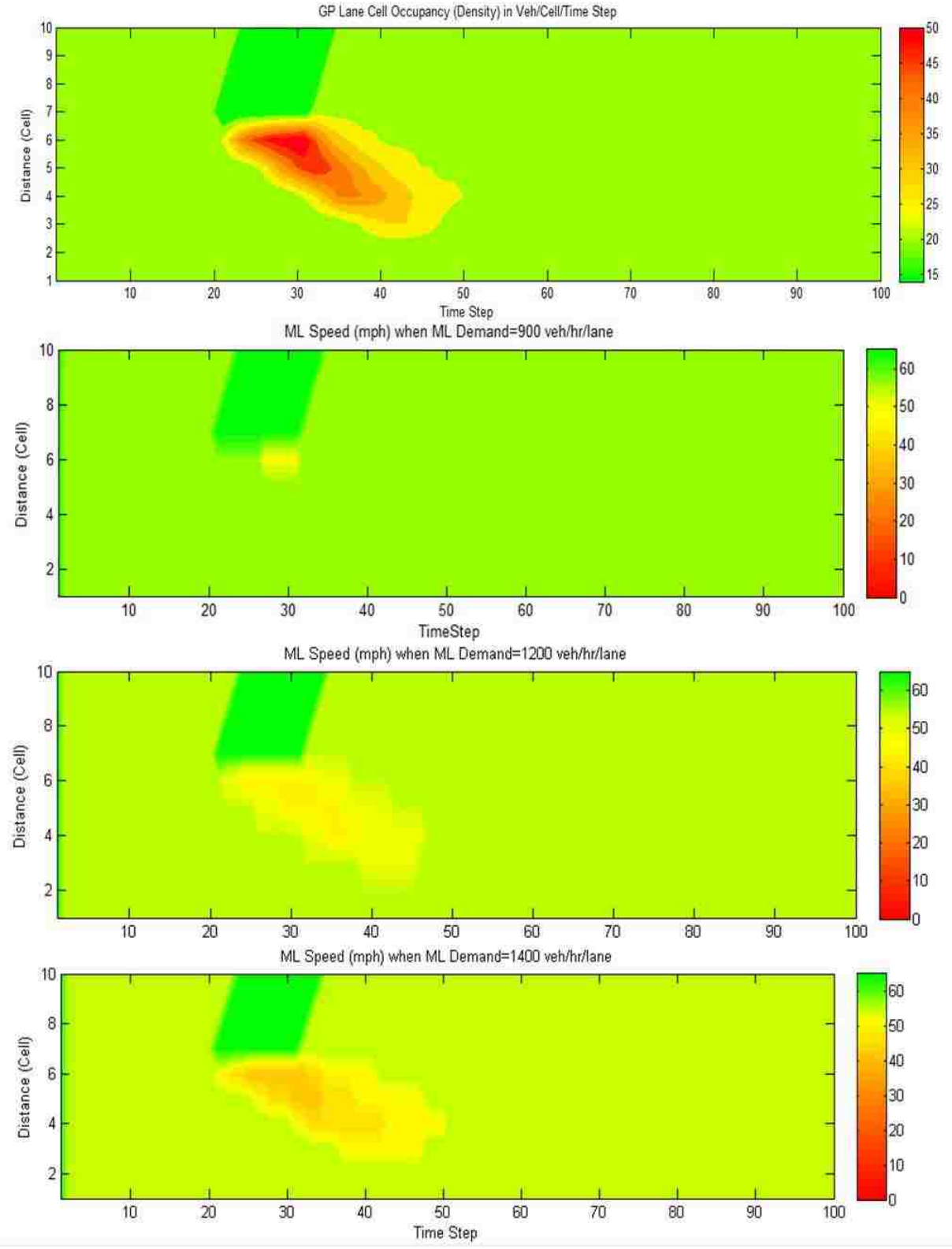

FIGURE 5.21 Temporal-Spatial Traffic Evolution under Bottleneck Scenario for Various ML Demand using the Unsupervised Machine Learning Method

5.5.1.3 Comparison of the Two Approaches for Basic Segment Modeling

It is therefore demonstrated that the developed traffic flow models on top of the original CTM are both capable of capturing the traffic evolution pattern on the current freeway segment as well as modeling the interaction between the GP lanes and its adjacent ML. Note from Figures 5.20 and 5.21, slight ML speed difference can be detected at the downstream of Cell 7 after the incident is cleared. The HCM-based model yields a lower speed shown in the highlighted region of Figure 5.20. That is because of the fact that the threshold for the friction state is set at 23 veh/cell/lane, and within that region, the GP upstream is still absorbing the traffic accumulated due to the incident. With different parameters setup, the traffic flow pattern can be varied under different traffic conditions. Therefore, when applying the proposed model for further applications, e.g. evaluate the effectiveness of traffic control strategies, careful calibration of the model is needed to determine the traffic flow parameters such as FFS, capacity, jam density, and friction threshold, such that meaningful inferences can be drawn for specific cases.

5.5.2 Weaving Segment Modeling

5.5.2.1 Numerical Example

A numerical study is presented to illustrate the vehicular procession at a weaving segment. Assume time step of 0.01 hour, cell capacity of 2400 vph, jam density of 140 vpm. With a FFS= 65 mph, the cell length is configured as 0.65 mile, and the maximum cell occupancy $N = 140 \times 0.65 = 91\ veh/cell$. The OD matrix is thus constructed as:

$$\begin{bmatrix} 12 & 4 \\ 6 & 18 \end{bmatrix} \tag{5.7}$$

$$\begin{aligned} \min(24, 91 - 0, 12 + 6) = 18 = O_1D_1 + O_2D_1 \\ \min(24, 91 - 0, 4 + 18) = 22 = O_1D_1 + O_2D_1 \end{aligned} \tag{5.8}$$

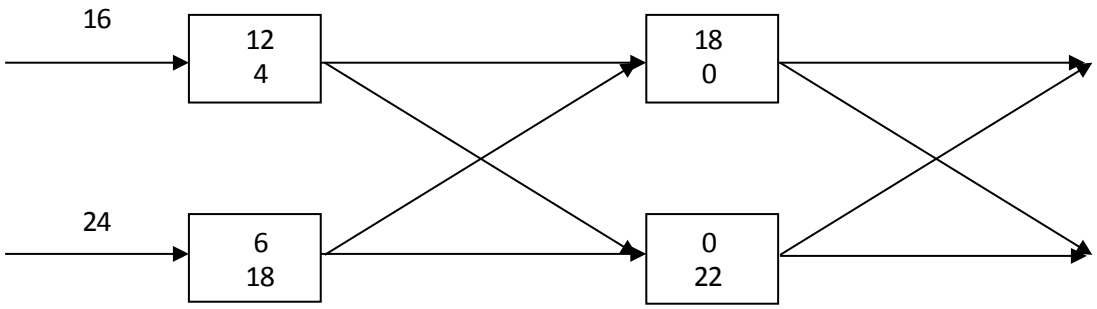

FIGURE 5.22 Numerical Example

This is the scenario where no congestion is formed at the weaving segment. When congestion happens, the downstream cell is restraining the demand from flowing in. At the next tick of clock, the question is about whether such restraint occurs at the downstream cell or the connecting link. It further comes to the reality that the link itself may have certain gauging functionalities, such that in the next tick of clock, it refrains the specific amount of traffic into the downstream cell. The following building block as shown in Figure 5.23 is constructed to describe the extended version of the weaving segment. Note that the lateral extension of the cells are imaginary, only serving as the function to gauge the specific portion of through/lane change traffic into the downstream cell.

Here we give explanation about why the cells are imaginary and have no storage capabilities. We prove this proposition by counterexample. If the mid-cells, as illustrated in Figure 5.23, have storage capabilities, then when a bottleneck is formed downstream, the traffic that cannot progress to the end cells will stay in the mid-cells. In reality, it would correspond to the situations where vehicles stop at the shoulder. This is neither true nor realistic for the existing travel behavior in the U.S. Also, If certain amount of traffic is stored in the mid-cells (e.g. at *cell a* in Figure 5.23), it reduces the actual demand that existed at the upstream (e.g. at *cell b* in Figure 5.23), which is also not a true reflection of the reality. Thus, the mid cells are only serving as a function of gauge for

splitting the through and lane change traffic. The computation of the mid-cells' properties can be completed during the single time step. The capacity of the mid cells is defined as:

$$Q_a = Q \times \frac{O_1D_2}{p \times O_2D_2 + O_1D_2} \tag{5.9}$$

$$Q_c = Q \times \frac{O_2D_1}{p \times O_1D_1 + O_2D_1} \tag{5.10}$$

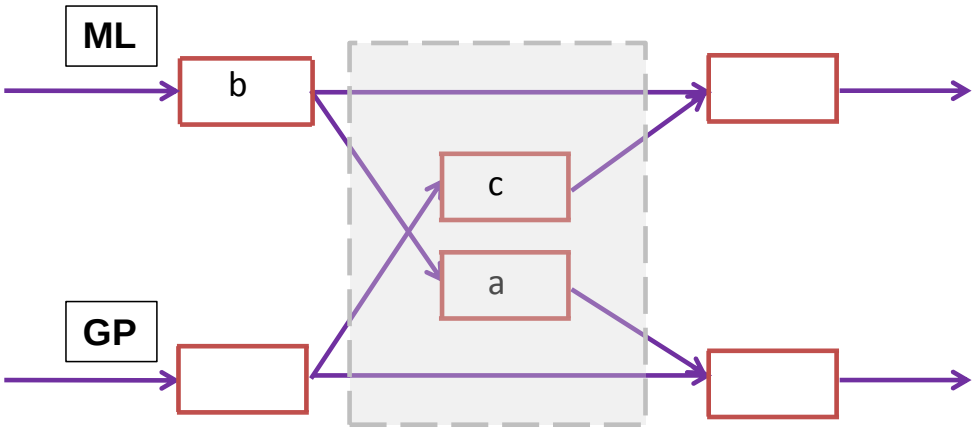

FIGURE 5.23 The Weaving Segment with Extended Lateral Building Blocks

CHAPTER 6 CONCLUSIONS AND FUTURE RESEARCH

With increasing concerns over environmental impacts and sustainable transportation systems, transportation agencies are seeking solutions for congestion mitigation other than the traditional roadway expansion. ML systems are a very effective way to optimize the utilization of freeway capacities. In the absence of a methodology for analytically evaluating ML facilities in the HCM, analysts typically reply on time-consuming and cost-ineffective simulation experiments. MLs encompass a series of operational strategies to efficiently manage the traffic demand by altering pricing, vehicle eligibility and access control. It thus is a concept so comprehensive with inclusion of a variety of components. Therefore, it is challenging to develop a methodological framework for analyzing the performance of ML facilities.

This study is determined to fill this gap. This research approaches the problem from the demand-and-supply perspective. For the demand-side, how people respond to tolling is systematically investigated using empirical data. By quantitatively assessing SOVs' travel pattern changes under various conditions, it is determined that frequent paid customers value travel time saving just as much as the infrequent paid customers. And the reason that some people use HOT lanes more than others may indeed lie in socio-economic differences such as income, lifestyle, and educational level. From the supply-side, an analytical methodology is developed for analyzing freeway facilities with ML and GP lanes operated in parallel. The dichotomy of design and behavioral attributes, as well as the interactions between the two lane groups are quantified via this research and fitted within the HCM methodology to accommodate both ML and GP facilities. On the basis of the developed methodology, a computational engine is developed to integrate, test and evaluate

the proposed approach by allowing users to input their own facility specifications. Furthermore, a twin-cell based modeling approach, by incorporating the finding from the proposed methodology, further extends the scope of conventional macroscopic simulation models (e.g. CTM) to the analyses of parallel facility on freeway.

The following sections first summarize research efforts and findings, followed by highlighting research contributions in resolving demand analysis, modeling methods, and performance evaluation. Finally, future research is discussed, including an in-depth study on demand estimation, over-saturated ML condition analysis, as well as further development of modeling techniques for traffic flow dynamics.

6.1 Summary of Research

6.1.1 Identify Incentives for SOVs to Use the HOT Lane Facilities

Sensor data along with transponder data were collected for SR 167 HOT lane system to capture detailed vehicle trajectory as well as the ambient traffic environment when the lane choices are made. We investigates, at a macroscopic level, how SOV demand on HOT lanes changes with toll rates and various traffic conditions. A logit-like model is applied to simulate the effect. It is found that SOV demand would mostly be affected by three factors: toll rate, travel time difference, and travel time reliability. A travel time reliability index was developed to measure the system reliability using a probabilistic approach, which was defined as the probability that a trip can be made successfully within a specified interval of time as a function of time of day. The model was applied to three different traffic phases: pre-congestion, congestion, and post-congestion. From the

model results, it was determined that for the pre- and post-congestion periods, the SOV demand was more affected by the system reliability and travel time savings, while during the congestion period, tolling functions as a signal to attract more traffic into the HOT lane so as to avoid downstream congestion. The results are important, as analysts are developing methods to better understand the effectiveness of HOT lane performance and the heterogeneity among SOV users. The findings suggest that, under different traffic conditions, SOV lane choices may be affected by different attributes. This consideration is important for optimal setting of tolling policies, which often overlook variation in users' concerns under various traffic conditions.

6.1.2 Methodological Framework for Analyzing the ML Facilities

MLs are considered an effective countermeasure against freeway congestion. A methodological framework along with a computational engine for the performance evaluation of freeway facilities with MLs is developed in this research. Major components of the framework are described in this study along with the detailed modeling and data process for deriving the components.

Parallel Lane Groups of MLs and GP Lanes

This research adopts the lane group concept widely used in the signalized intersection analysis in HCM 2010 to ascribe separate attributes to parallel ML and GP facilities, while retaining the ability to model a certain degree of interaction between the two. As widely observed, the ML and GP lane groups may have different geometric characteristics, such as number of lanes, lane width, segment types. They may also have distinctive behavioral and traffic attributes, such as FFS, segment

capacity, traffic demand, etc. Besides these dichotomies, the two lane groups would impose interaction onto each other under certain circumstances. For example, a congested GP lane may have an adverse frictional effect on the adjacent MLs. To accommodate all these features, the lane group concept is well-suited under the umbrella of a deterministic analytical framework for the two parallel facilities. The frictional effect was empirically derived from field collected data. It can be user-calibrated based on the types of physical separation, number of lanes, and FFS.

Unique Speed-Flow Features for Basic ML Segments

Speed-flow models for the basic ML segments are developed following the HCM 2010 methodology. The models were developed based on an extensive amount of traffic sensor data collected nationwide. Fifteen-minute speed and volume data were used for consistency with HCM 2010. Traffic behavior characteristics of various ML design and strategies were carefully identified and studied, and a total of 63,656 fifteen-minute data points were extracted from 10 different freeway facilities with MLs. Five basic ML segment types are proposed based on field observation, including Continuous Access, Buffer 1, Buffer 2, Barrier 1, and Barrier 2. Operational performance and traffic flow characteristics were analyzed from intensive data sites for each segment type. To this end, the speed-flow models for the five segment types were developed. It was found that the separation type and number of lanes distinguish the traffic flow behavior of ML facilities. The developed models also incorporated and quantified the frictional effect imposed onto the ML facilities when the GP lanes are congested.

Cross-Weave Effect Imposed onto the Parallel GP Lanes

As the adjacent ML facilities would be readily impacted by traffic conditions on the GP lanes, there is an interdependent effect with the GP lanes. For example, when the GP on-ramp traffic tries to weave-across multiple GP lanes over a relatively short distance to get into MLs, there is a capacity-reducing effect on the GP segments called cross-weave effect. This cross-weave effect is quantified in this study through a multi-scenario simulation model that is carefully calibrated using field collected video data. The simulation sensitivity is verified in that the capacity reduction in the simulation model is responsive to the cross-weave distance, cross-weave demand, and the number of GP lanes. As expected, the capacity reduction effect is more significant with shorter cross-weave distances, increased cross-weave demand, and the number of GP lanes. With these results, CRFs that are compatible with the deterministic analysis approaches in the HCM are developed in the study. The CRF is the percentage of capacity reduction compared to the base scenario where no cross-weave flow is present. CRFs are analogous to the CAF used in the HCM freeway facilities method. This feature quantitatively describes the ML cross-weave impact on the GP segment. It also allows for an appropriate integration of this phenomenon into the ML methodology developed under research project NCHRP 03-96 for evaluating the performance of freeway facilities with MLs.

6.1.3 Twin-Cell Modeling Approach for Parallel Freeway Facilities

Based on the finding from the analytical framework, it is necessary to develop a simulation model that is able to incorporate the frictional effect into modeling the ML facilities, and to extend the interaction concept into modeling traffic flow evolution on parallel freeway facilities. The existing simulation models do not have such a plug-in function for that. This research fulfilled the issue by

developing a twin-cell modeling approach. Two different methods are proposed for incorporating the frictional effect into cell-based traffic advancing logic. The first one is HCM-based approach, where piecewise functions are used to quantify the impact of GP congestion onto MLs. The second method is inspired by the concept of viscosity, which is widely used in hydraulic study and fluid theory. The frictional effect is quantified via data mining techniques and empirical data collected. The result is incorporated into a modified cell-based model for modeling the basic freeway segment, and empirical tests suggest that the ML travel condition is readily impacted by the GP lane congestion level as well as its own demand.

Meanwhile, the original CTM cannot model the weaving behavior due to its macroscopic nature. However, weaving is a critical component, especially for parallel freeway facilities, that affects the freeway performance. Therefore, a weaving model is developed to successfully model the vehicular interaction from a macro/meso perspective. A parameter p is used to calibrate the model by quantifying the drivers' aggressiveness. The cell-based mesoscopic simulation can therefore be extended to model the traffic dynamics on the freeway facilities with more than one lane group. It also fills the gap in the existing research by modeling the weaving behavior from a macroscopic perspective.

6.2 Research Contribution

Such a modeling framework will be very valuable in guiding the practitioners for evaluating the ML performance at a facility level and hence leveraging the benefits in both short term and long term. In the short term, the framework and the theoretical basis in this research will enhance academic understanding and field practice in the following aspects:

- Provide prototype analysis of the SOV demand in response to tolling and ambient traffic conditions, and discover the hidden parameters that get people into making specific lane choice;
- Develop modules within the framework for quantifying the characteristics of ML facilities, including ML speed-flow relationship, the frictional effect of adjacent lane traffic speed, the adjustment for cross-weave effects, and the development of side-by-side facility-wide ML and GP performance measures;
- Allow users to evaluate the performance of MLs using the developed computational engine to determine the feasibility of ML implementation, identify existing ML operational issues, as well as to assess different operational strategies or ML configurations; and
- Bring new insights to the weaving analysis of macroscopic/mesoscopic simulation models, and extend the knowledge for the evaluation of parallel facilities on the freeway.

In the long run, the proposed methodology is sensitive to different GP and ML segment types (basic, weaving, etc.) and separation styles (none, buffer, barrier), and is capable of analyzing extended facilities across multiple time periods. It will hopefully radiate the benefits beyond ML facilities to other network-wide analysis, especially the ones with the components of ITS strategies,

such as Integrated Corridor Management (ICM), connected vehicle, or Active Traffic Management (ATM), etc. This study will lay a solid foundation for those related research as a roadway analytical framework, which not only interoperates various datasets, operational strategies, and roadway conditions, but also enables the computational capabilities, to support project appraisal and decision making for ML related investment and policy shaping.

6.3 Future Research

The shear number and complexity of the considerations (from both supply and demand sides) that go into the development of ML system have increased. As can be foreseen in the near future (some of them are being implemented right now), MLs are and will be operated part time on shoulders, continuous access between HOT lane and GP lanes, that have left-hand exits, and that start on one freeway and end on another freeway, etc. This study sets the milestone for future research and practices in ML analysis. However, the implementation and evaluation of MLs is a complex issue that involves people from all walks of life. Several areas that warrant further study and investigation are identified:

- Future research should explore congested ML facilities, with a special emphasis on queuing patterns at intermittent access points, and queue spillback allocation between ML and GP lanes.
- Future research should investigate the beginning and end point designs of ML facilities. Variations in the design of these termini are expected to impact operations of the overall facility, and future research should explore what design aspects minimize the turbulence created at these locations.

- Future research should tie the operational HCM methodologies with demand-estimation procedures. Since many ML facilities in the US feature a congestion-pricing component, the distribution of corridor demands between ML and GP lanes has been shown sensitive to pricing. While the HCM is traditionally not focused on demand estimation (demand is generally treated as an input), a closer scrutiny on the supply and demand tradeoffs is needed for ML design and operations.
- Future research should take a more detailed look at special configurations of ML access points. In addition to the lane-change or weaving access mentioned above, grade-separated ramp access points also warrant further scrutiny, especially ramps to and from single-lane ML facilities. The methodology for merge and diverge sections in the HCM generally assumes a ramp-influence-area (RIA) of two lanes, and it is likely that ramps on single-lane facilities have different operational attributes.
- Future research should take a field data-based approach to estimating capacity-reducing effects of ML cross-weave maneuvers on the GP lanes. The simulation-based approach taken in this research showed the hypothesized sensitivity, but this should be confirmed by field data.
- Future research should investigate, from the planning and policy perspective, why and how certain design decisions are made, especially why certain design options are considered but rejected. It will provide valuable information to today's designers of ML systems and provide insights into the new critical research that is needed to provide a foundation for key design decisions that are being made.
- Finally, future research should focus on studying the multi-regime macroscopic fundamental diagram (MFD), and the necessity for including those models into the updates of modeling the traffic flow dynamics of freeway networks.

REFERENCES

Athol, P. (1965). Interdependence of Certain Operational Characteristics Within a Moving Traffic Stream. In *Highway Research Record,* 72, pp. 58–87.

Asakura, Y., and Kashiwadani, M. (1999). Road Network Reliability Caused by Daily Fluctuation of Traffic Flow. *Proceedings of the 19th PTRC Summer Annual Meeting,* Brighton, United Kingdom.

Alecsandru, C.D. (2006). *A Stochastic Mesoscopic Cell Transmission Model for Operational Analysis of Large-Scale Transportation Networks.* Ph.D. Dissertation. Louisiana State University.

Brilon, W., Geistefeldt, J., Regler, M. (2005). Reliability of Freeway Traffic Flow: A stochastic Concept of Capacity, *Proceedings of the 16th International Symposium on Transportation and Traffic Theory*, pp. 125 – 144, ISBN 0-08-044680-9.

Bloomberg, L., and Dale, J. (2000). Comparison of VISSIM and CORSIM Traffic Simulation Models on a Congested Network. *Transportation Research Record: Journal of the Transportation Research Board*, Vol. 1727, pp. 52-60.

Brownstone, D., and Small, K. A. (2005). Valuing Time and Reliability: Assessing the Evidence from Road Pricing Demonstrations. *Transportation Research Part A*, Vol. 39, No. 4, pp. 279–293.

Cassidy, M.J., Jang, K. and Daganzo, C.F. (2010). The Smoothing Effect of Carpool Lanes on Freeway Bottlenecks. *Transportation Research Part A* 44(2), pp. 65–75.

Carson, J.L. (2005). *Monitoring and Evaluating Managed Lane Facility Performance*. Publication No: FHWA/TX-06/0-4160-23. Federal Highway Administration.

Chang, M, Wiegmann, J., Smith, A., and Bilotto, C. (2008). A Compendium of Existing HOV Lane Facilities in the United States. *Report No. FHWA-HOP-09-030*.

Chen, A., Yang, H., Lo, H. K., and Tang, W. H. (2002). Capacity Reliability of a Road Network: an Assessment Methodology and Numerical Results. *Transportation Research Part B,* Vol. 36, pp. 225–252.

Daganzo, C. F. (1993). The Cell Transmission Model: A Dynamic Representation of Highway Traffic Consistent with the Hydrodynamic Theory. *Transportation Research Part B.* Vol 28, No 4. pp 269-287.

Daganzo, C.F. (1995). The Cell Transmission Model, Part II: Network traffic. *Transportation Research Part B* 29(2), pp. 79–93.

Dahlgren, J. (1999). High Occupancy Vehicle/Toll Lanes: How Do They Operate and Where Do They Make Sense? *California PATH Working Paper* UCB-ITS-PWP-99-8.

Federal Highway Administration (FHWA). (2012). Managed Lanes. Retrieved from: http://ops.fhwa.dot.gov/freewaymgmt/managed_lanes.htm.

Government Accountability Office (GAO) of the United States. (2012). *Traffic Congestion: Road Pricing Can Help Reduce Congestion, but Equity Concerns May Grow*. Report to the Subcommittee on Transportation, Housing, and Urban Development and Related Agencies, Committee on Appropriations, House of Representatives.

Gomes, G., May, A., and Horowitz, R. (2004). Congested Freeway Microsimulation Model Using VISSIM. *Transportation Research Record: Journal of the Transportation Research Board*, Vol.

1876, pp. 71-81.

Ghosh, A. (2001). *Valuing Time and Reliability: Commuters' Mode Choice from a Real Time Congestion Pricing Experiment*. Ph.D. dissertation. University of California, Irvine.

Goodall, N., and Smith, B. L. (2010). What Drives Decisions of Single-Occupant Travelers in High-Occupancy Vehicle Lanes? Investigation Using Archived Traffic and Tolling Data from the MnPASS Express Lanes. In *89th Annual Meeting of the Transportation Research Board*, Washington, D.C.

Geistefeldt, J. (2010). Consistency of Stochastic Capacity Estimation. In *the 89th Annual Meeting of Transportation Research Board,* Washington D.C., Paper No. 10-3042.

Guin, A., Hunter, M., and Guensler, R. (2008). Analysis of Reduction in Effective Capacities of High Occupancy Vehicle Lanes Related to Traffic Behavior. *Transportation Research Record: Journal of Transportation Research Board*, 2065, pp 47-53.

Han, C.-P., and Li, J. (2009). Evaluating Estimation Techniques of Transportation Price Elasticity. In *Transportation Research Record: Journal of the Transportation Research Board*, No. 2115, pp. 94–101.

Jang, K., and Cassidy, M, J. (2012). Dual Influences on Vehicle Speed in Special-Use Lanes and Critique of US Regulation. *Transportation Research Part A*, Vol. 46, No. 7, pp. 1108–1123.

Jang, K., J. Suh, M Park, and H Yeo. (2013). Synchronized Speed Reductions in Contiguous High-Occupancy Vehicle Lanes. In *92nd Annual Meeting Transportation Research Board*, Washington D.C.

Kaplan, E.L. and Meier, P. (1958). Nonparametric Estimation from Incomplete Observations. *Journal of the American Statistical Association*, 53, 457-481.

Kuhn, B., Goodin, G., Ballard, A., Brewer, M., Brydia, R., Carson, J., Chrysler, S., Collier, T., Fitzpatrick, K., Jasek, D., Toycen, C., and Ullman, G. (2005). *Managed Lanes Handbook*, Federal Highway Administration.

Kwon, J., and Varaiya, P. (2008). Effectiveness of California's High Occupancy Vehicle System. *Transportation Research Part C* 16. pp 98-115.

Lighthill M. J. and Whitham J. B. (1955). On Kinematic Waves. I: Flow Movement in Long Rivers; II: A theory of traffic flow on long crowded roads. *Proceedings of the Royal Society A* 229, pp281-345.

Liu, X., Wang, Y., Schroeder, B., and Rouphail, N. (2012). Quantifying Cross-Weave Impact on Capacity Reduction for Freeway Facilities with Managed Lanes. *Transportation Research Record: Journal of the Transportation Research Board*. No. 2278. pp. 171-179.

Liu, X., Zhang, G., Lao, Y., and Wang, Y. (2012). Modeling Traffic Flow Dynamics on Managed-Lane Facility: Approach Based on Cell Transmission Model. *Transportation Research Record: Journal of the Transportation Research Board*. No. 2278. pp. 163-170.

Liu, X., Schroeder, B., Thomson, T., Wang, Y., Rouphail, N., and Yin, Y. (2011). Analysis on Operational Interactions between Freeway Managed Lanes and Parallel General Purpose Lanes. *Transportation Research Record: Journal of Transportation Research Board.* Vol 2262, pp 62-73.

Liu, X. Zhang, G., Lao, Y. and Wang, Y. (2011). Quantifying the Attractiveness of High Occupancy

Toll Lanes with Traffic Sensor Data under Various Traffic Conditions. *Transportation Research Record: Journal of the Transportation Research Board*. Vol 2229. pp 102-109.

Liu, X., Zhang, G., Wu, Y., and Wang, Y. (2010). Analyzing System Performance for Washington State Route 167 High-Occupancy Toll (HOT) Operations. In *89th Annual Meeting of the Transportation Research Board,* Washington, D.C.

Minderhoud, M. M., Botma, H., and Bovy, P.H.L. (1997). Assessment of Roadway Capacity Estimation Methods. In *Transportation Research Record: Journal of Transportation Research Board*, No 1572, pp 59-67.

Menendez, M. and Daganzo, C.F. (2007). Effects of HOV Lanes on Freeway Bottleneck. *Transportation Research Part B*, Vol. 41, No. 8, pp. 809-822.

Martin, P., Perrin, J., Lambert, R., and Wu, P. (2002). *Evaluate Effectiveness of High Occupancy Vehicle (HOV) Lanes*. Utah Department of Transportation Report No. UT-03.26.

Nee, J., Ishimaru, J., and Hallenbeck, M. (1999). *Evaluation Tools for HOV Lane Performance Monitoring,* Washington State Transportation Center, Washington State Department of Transportation Report No: WA-RD 473.2.

Orange County Transportation Authority (OCTA). 91 Express Lanes 2010-2011 Annual Report. Retrieved from http://www.91expresslanes.com/pdf/91elannual11.pdf

Obenberger, J. (2004). Managed Lanes: Combining Access Control, Vehicle Eligibility, and Pricing Strategies Can Help Mitigate Congestion and Improve Mobility on the Nation's Busiest Roadways. *Public Roads,* Vol. 68, No. 3, pp. 48-55.

Park, B., and Qi, H. (2005). Development and Evaluation of a Procedure for the Calibration of Simulation Models. *Transportation Research Record: Journal of the Transportation Research Board*, Vol. 1934, pp. 208-217.

POET-ML Users Guide and Methodology Description. (2008). *POET-ML Purposes*, Retrieved from http://ops.fhwa.dot.gov/publications/fhwahop09031/purpose.htm.

Roess, R. (2011). Speed-Flow Curves for Freeways in the Highway Capacity Manual 2010. In *Transportation Research Record: Journal of the Transportation Research Board*, No. 2257, pp. 10-21.

Rodrigues, J., Kawamura, K., and Samimi, A. (2008). FREQ Simulation and Ramp Meter/HOV bypass Optimization for the Northwest Study Area. *Transport Chicago 2008*. Illinois Institute of Technology.

Rakha, H. and Arafeh, M. (2009). Calibrating Steady-State Traffic Stream and Car-following Models using Loop Detector Data. *Transportation Science,* DOI: 10.1287/trsc.1090.0297.

Schrank D., Eisele, B, and Lomax, T. (2012). *TTI's 2012 Urban Mobility Report Powered by INRIX Traffic Data*. Texas A&M Transportation Institute.

Schroeder, B., Aghdashi, S., Rouphail, N., Liu, X., and Wang, Y. (2012). Deterministic Approach to Managed Lane Analysis on Freeways in a Highway Capacity Manual Context. *Transportation Research Record: Journal of Transportation Research Board*. Vol 2286, pp. 122-132.

Song, H., and Smith, B. L. (2009). Empirical Investigation of the Impact of High Occupancy-Toll Operations on Driver Behavior. In *88th Annual Meeting of the Transportation Research Board*,

Washington, D.C.

Steinmetz, S. S. C., and Brownstone, D. (2005). Estimating Commuters' "Value of Time" with Noisy Data: A Multiple Imputation Approach. *Transportation Research Part B*, Vol. 39, pp. 865–889.

Thomson, T., Liu, X., Wang, Y., Schroeder, B., and Rouphail, N. (2012). Operational Performance and Speed-Flow Relationships for Basic Managed Lane Segments. *Transportation Research Record: Journal of Transportation Research Board*. Vol 2286. pp. 94-104.

Tu, H., Van Lint, H., and Van Zuylen, H. (2005). Real-time Modeling Travel Time Reliability on Freeway. In *Advanced OR and AI Methods in Transportation*, Proceedings of the 16th Mini-EURO Conference and 10th Meeting of EWGT, pp. 540–546.

Texas Transportation Institute (TTI). (2001). *Current State-of-the-Practice for Managed Lanes*. Texas Department of Transportation.

Tian, Z., Urbanik, T., Engelbrecht, R., and Balke, K. (2002). Variations in Capacity and Delay Estimates from Microscopic Traffic Simulation Models. *Transportation Research Record: Journal of the Transportation Research Board*, Vol. 1802, pp. 23-31.

Transportation Research Board (TRB). (2010). Highway Capacity Manual (HCM) 2010. 5th edition. Washington, D.C.

Van Lint, J. W. C., and Van Der Zijpp, N. J. (2003). Improving a Travel-Time Estimation Algorithm Using Dual Loop Detectors. In *Transportation Research Record: Journal of the Transportation Research Board*, No. 1855, pp. 41–48.

Van Aerde, M. and Rakha, H. (1995). Multivariate Calibration of Single-Regime Speed-Flow-Density Relationships. In *Proceeding of IEEE Vehicle Navigation and Information Conference (VNIS),* pp.334–341.

Varaiya, P. (2005). What We've Learned About Highway Congestion. *Access*. 27, pp 2-9.

Vo, P. (2008). *Capacity Estimation of Two-Sided Type C Weaves on Freeways*, Ph.D. dissertation, University of Texas at Arlington.

Williams, J., Mattingly, S. and Yang, C. (2010). *Assessment and Validation of Managed Lanes Weaving and Access Guidelines*. FHWA/TX-09/0-5578-1.

Washington State Department of Transportation (WSDOT). (2012). *SR 167 HOT Lanes Pilot Project Fourth Annual Performance Summary*. Retrieved from http://www.wsdot.wa.gov/NR/rdonlyres/2DA072CA-7D4A-4876-A58B-64DBE152D48D/0/SR167_AnnualPerformanceSummary_080812_web.pdf.

Wang, Y., and Nihan, N. L. (2000). Freeway Traffic Speed Estimation with Single-Loop Outputs. In *Transportation Research Record: Journal of the Transportation Research Board,* No. 1727, pp. 120-126.

Wang, Y., and Nihan, N. L. (2003). Can Single-Loop Detectors Do the Work of Dual-Loop Detectors? *Journal of Transportation Engineering*, Vol. 129, No. 2.

Wang, Y., Liu, X., Rouphail, N., Schroeder, B., Yin, Y., and Bloomberg, L. (2012). Analysis of Managed Lanes on Freeway Faiclities. Final Report for NCHRP 03-96. Web-Only Document 191. Retrieved from http://onlinepubs.trb.org/onlinepubs/nchrp/nchrp_w191.pdf

Williams, G. (2011). *Data Mining with Rattle and R*. Springer, New York.

Williams, J., Mattingly, S., and Yang, C. (2010). *Assessment and Validation of Managed Lanes Weaving and Access Guidelines*. FHWA/TX-09/0-5578-1.

Yu, R., Zhang, G., and Wang, Y. (2009). Loop Detector Segmentation Error and Its Impacts on Traffic Speed Estimation. In *Transportation Research Record: Journal of the Transportation Research Board, No. 2099,* pp. 50–57.

Zhang, G., Yan, S., and Wang, Y. (2009). Simulation-based Investigation on High Occupancy Toll (HOT) Lane Operations for Washington State Route 167. *ASCE Journal of Transportation Engineering*. Vol. 35, No. 10, pp. 677-686.

REPRINT PERMISSIONS

Permissions have been granted by the publishers to reuse the contents in the papers listed below in this dissertation:

Xiaoyue Liu, Yinhai Wang, Bastian Schroeder, and Nagui Rouphail. Quantifying Cross-Weave Impact on Capacity Reduction for Freeway Facilities with Managed Lanes. *Transportation Research Record: Journal of the Transportation Research Board*. *No. 2278*, pp. 171-179. Copyright, National Academy of Sciences, Washington, D.C., 2012.

Xiaoyue Liu, Guohui Zhang, Yunteng Lao, and Yinhai Wang. Modeling Traffic Flow Dynamics on Managed-Lane Facility: Approach Based on Cell Transmission Model. Transportation Research Record: Journal of the Transportation Research Board. *No. 2278*, pp. 163-170. Copyright, National Academy of Sciences, Washington, D.C., 2012.

Timothy Thomson, **Xiaoyue Liu**, Yinhai Wang, Bastian Schroeder, and Nagui Rouphail. Operational Performance and Speed-Flow Relationships for Basic Managed Lane Segments. *Transportation Research Record: Journal of Transportation Research Board*. *No. 2286*, pp 94-104. Copyright, National Academy of Sciences, Washington, D.C., 2012.

Bastian Schroeder, Seyedbehzad Aghdashi, Nagui Rouphail, **Xiaoyue Liu**, and Yinhai Wang. Deterministic Approach to Managed Lane Analysis on Freeways in a Highway Capacity Manual Context. *Transportation Research Record: Journal of Transportation Research Board*. *No. 2286*, pp 122-132. Copyright, National Academy of Sciences, Washington, D.C., 2012.

Xiaoyue Liu, Bastian Schroeder, Timothy Thomson, Yinhai Wang, Nagui Rouphail, and Yafeng Yin. Analysis of Operational Interactions Between Freeway Managed Lanes and Parallel General Purpose Lanes. *Transportation Research Record: Journal of the Transportation Research Board*. *No. 2262*, pp 62-73. Copyright, National Academy of Sciences, Washington, D.C., 2011.

Xiaoyue Liu, Guohui Zhang, Yunteng Lao, and Yinhai Wang, Quantifying the Attractiveness of High Occupancy Toll Lanes with Traffic Sensor Data under Various Traffic Conditions. *Transportation Research Record: Journal of the Transportation Research Board*. *No. 2229*, pp 102-109. Copyright, National Academy of Sciences, Washington, D.C., 2011.

APPENDICES

Appendix A

Simulation Model Calibration for Evaluation of the Cross-Weave Effect

A VISSIM simulation model has been developed to investigate how the cross-weave flow would impact the GP lane operational performance. Cross-weave flow refers to those vehicles get on rightmost GP lane from an on-ramp and change multiple GP lanes to enter the ML. Cross-weave data extracted from the University of Texas at Arlington (UTA) video footage collected from IH 635 in Dallas, Texas were used for the calibration of the simulation model. The site with the extracted ground-truth data is on the WB IH 635 with four GP lanes and one buffer-separated HOV lane. An aerial photograph of this site from Google map and a schematic layout of site configuration are shown in Figure A-1.

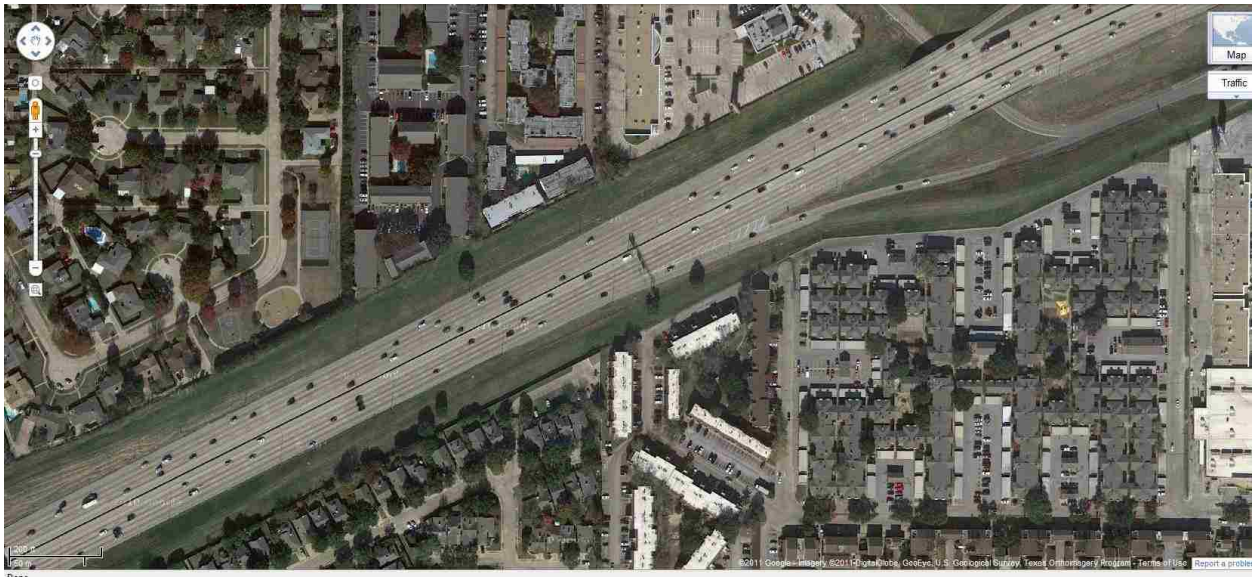

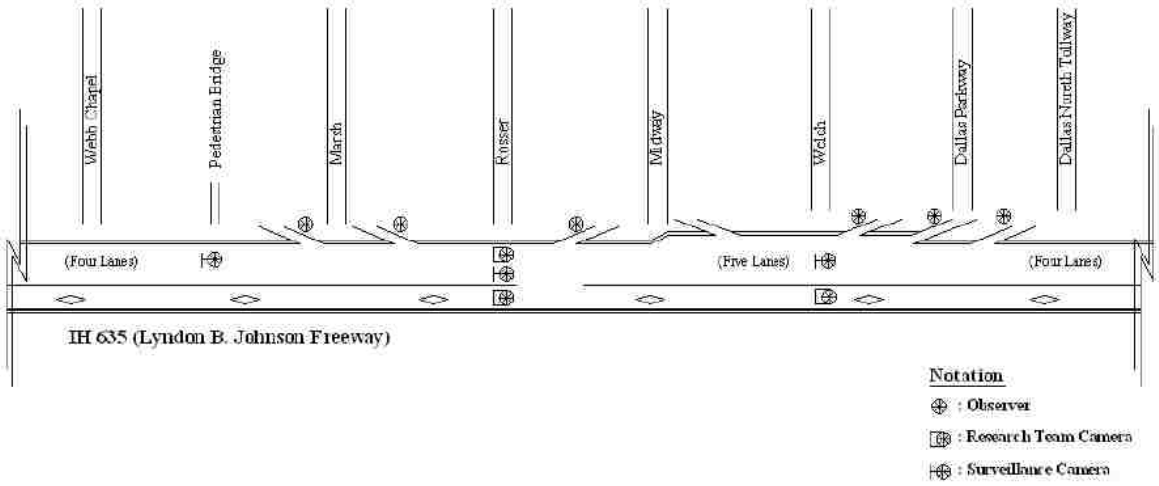

FIGURE A-1 Aerial Photograph and Schematics of Site Configuration

The access point of this data site is 1160 feet long. There is a pedestrian bridge at the downstream end of the access point, which allowed a camcorder to be set up to record traffic along the entire access point. A sample image of the video data is shown in Figure A-2.

FIGURE A-2 Sample Image from Video Data at IH 635 Access Point

Two one-hour video datasets were collected at this site:

− Friday, March 14, 2008, 10:20 a.m. to 11:20 a.m.

− Friday, March 14, 2008, 3:25 p.m. to 4:25 p.m.

The late morning dataset represents a moderate flow condition, while the late afternoon dataset shows an instance of heavy flow condition. The video datasets were processed to count the throughputs of GP and HOV lanes, respectively, and lane changes between the lane groups. Speed data were also collected from the same video by randomly selecting vehicles in each lane and recording their travel times as they travelled the entire length of the access point (1,160 ft).

Simulation Model Build-up

The research team relied on the UTA collected free-flow speed data to revise the distribution of desired speeds of cars and trucks in VISSIM. A RADAR gun was used to collect the speed information by randomly targeting vehicles that were not directly following other vehicles in the light traffic condition. We used the UTA collected speed data to revise the desired speeds in the VISSIM configuration. The revised distributions of desired speeds for cars and trucks were coded in VISSIM as shown in Figure A-3.

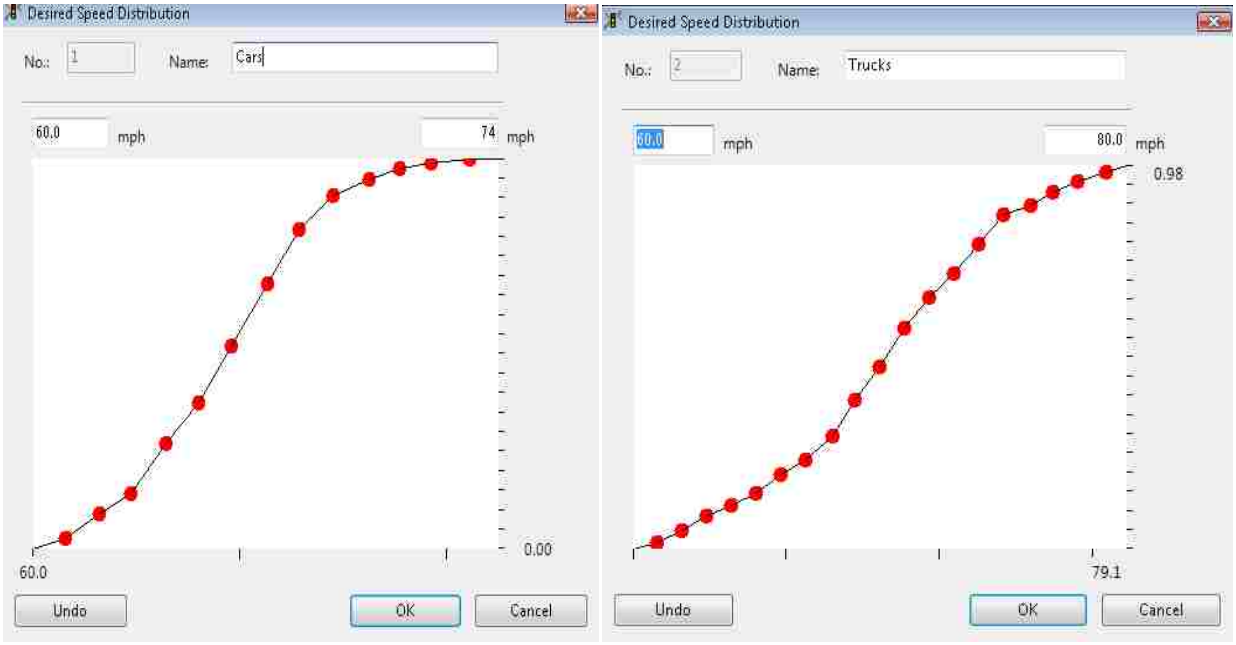

FIGURE A-3 Distributions of Desired Speeds for Cars and Trucks

For the convenience of calibration, three vehicle classes/types were defined including HOV, Car (SOV), and Truck as shown in Figure A-4. The vehicle composition includes GP traffic, Ramp Traffic, and HOV traffic.

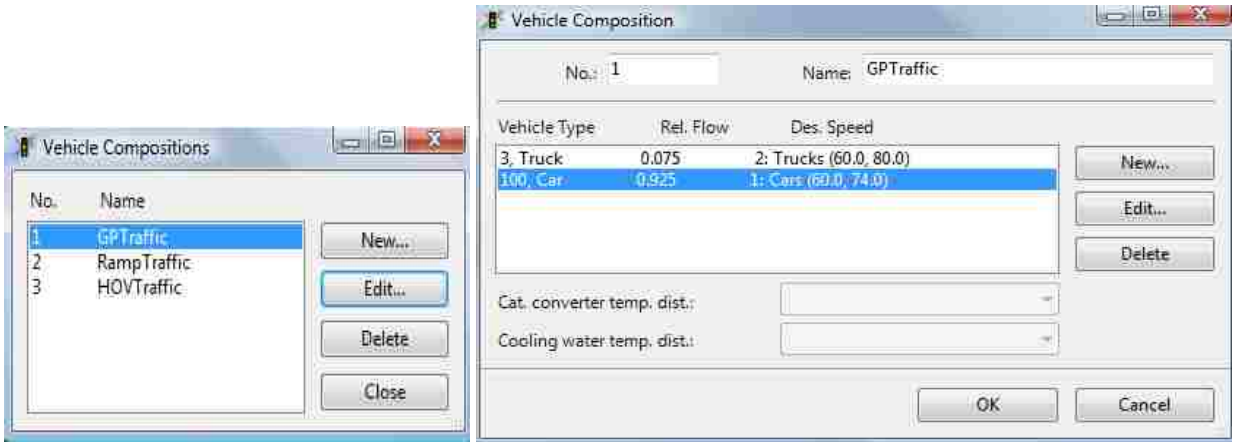

FIGURE A-4 Vehicle Composition

Using the processed video data, the Origin-Destination (OD) information was collected and aggregated at 10-min intervals to facilitate the routing input in VISSIM. The processed data are summarized in Figure A-5.

	Approaching Volume (vphpl)								Speed (mph)	
	GP	HOV	Ramp	Lane Change from GP Into HOV (veh/hr)	Lane Change from Ramp Into HOV (veh/hr)	Lane Change Out of HOV (veh/hr)	Lane Change Total (veh/hr)	Lane Change Intensity (veh/hr/100ft)	AVG GP	HOV
10:20 AM-10:30 AM	1650	300	894	132	18	60	210	18	61.4	68.9
10:30 AM-10:40 AM	1622	354	720	156	0	90	246	21	62.7	68.2
10:40 AM-10:50 AM	1650	378	822	156	0	84	240	21	62.6	66.8
10:50 AM-11:00 AM	1578	372	816	90	18	54	162	14	63.3	67
11:00 AM-11:10 AM	1589	420	870	108	0	66	174	15	63.1	65.9
11:10 AM-11:20 AM	1692	402	960	108	12	36	156	13	60.8	63.4
3:25 PM- 3:35 PM	1679	996	996	222	36	108	366	32	30.6	56.5
3:35 PM- 3:45 PM	1818	1212	996	300	60	132	492	42	33.7	56.5
3:45 PM- 3:55 PM	1725	1290	1002	246	72	210	528	46	27.8	49.4
3:55 PM- 4:05 PM	1598	1176	996	246	60	162	468	40	25.5	49.3
4:05 PM- 4:15 PM	1541	1518	996	222	60	312	594	51	23.2	45.2
4:15 PM- 4:25 PM	1625	1260	1002	144	24	204	372	32	25.6	45.9

FIGURE A-5 Processed Video Data from IH 635, Dallas, Texas

The simulation model was built following the network layout shown in Figure A-1 and configured using the data described above. The parameters considered in the calibration process are listed as

follows:

Lane-changing Parameter

- Lane change
- Maximum deceleration for the current vehicle
- Maximum deceleration for trailing vehicles
- Waiting time before diffusion
- Safety distance reduction factor

Car-following parameters

- Standstill distance (CC0)
- Headway time (CC1)
- Following variation (CC2)
- Threshold for entering “following ” mode (CC3)
- “Following” thresholds (CC4 and CC5)

Figure A-6 shows the values used for the simulation models.

Parameter	Description	Default	Range	
			Minimum	Maximum
p_1	Lane Change	656 feet	1500	5000
p_2	Max. deceleration for own vehicle	-13.1 ft/sec^2	-20	-11
p_3	Max. deceleration for trailing vehicle	-9.8 ft/sec^2	-17	-8
p_4	Waiting time before diffusion	60 sec	2	30
p_5	Safety distance reduction factor	0.6	0.0	0.8
p_6	CC0 (Standstill distance)	4.9 feet	4	10
p_7	CC1 (Headway time)	0.90 sec	0.7	1.3
p_8	CC2 (Following variation)	13.1 feet	10	35
p_9	CC3 (Threshold for entering "following" mode)	-8.00	-15	-5

p_{10}	CC4 (Negative "following" threshold)	-0.35	-2.4	-0.2
p_{11}	CC5 (Positive "following" threshold)	0.35	0.2	2.4

FIGURE A-6 Parameters Description

Several indicators were selected for the calibration quality assessment, including:

- Cumulative number of vehicles entering the ML from the GP lanes and from the Midway ramp at Z4, Z7 and Z10 (the exact location of zones Z4, Z7, and Z10 can be found in Figure A-7);
- Number of vehicles entering the section from GP mainline to exit to the MLs;
- Number of vehicles entering the section from ML to exit to the GP lanes; and
- Speed in GP lanes

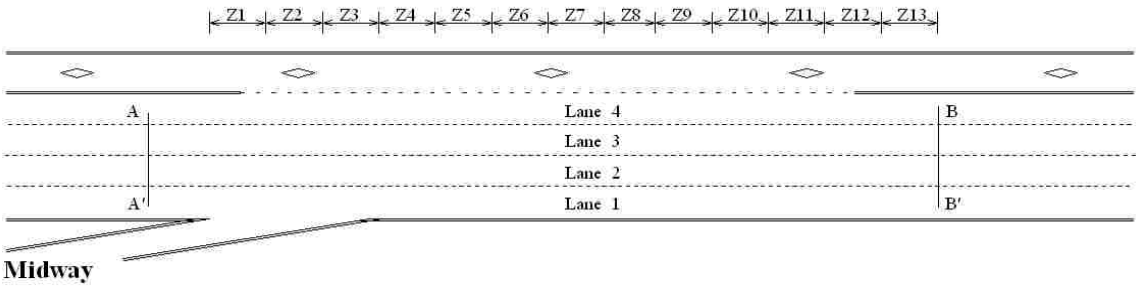

FIGURE A-7 Schematic of Configuration for the UTA Data Collection Site

A snapshot of the simulation model is in Figure A-8.

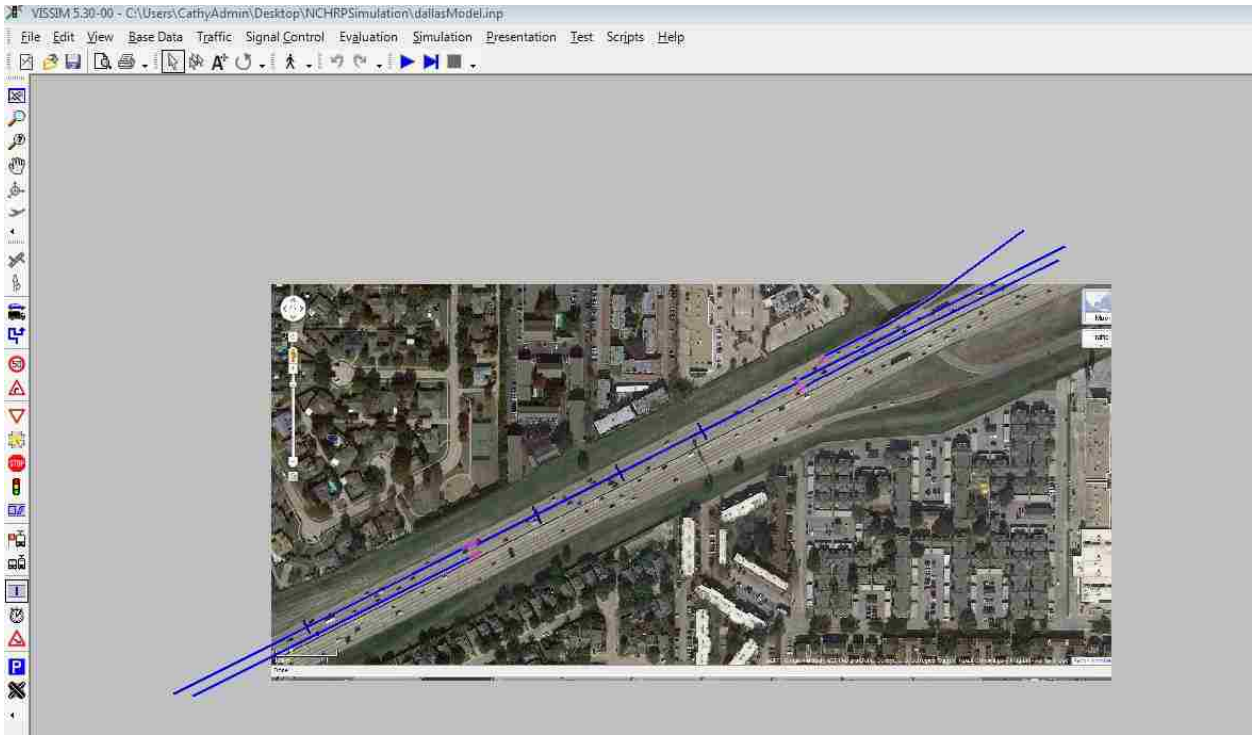

FIGURE A-8 VISSIM Simulation Model

Calibrated Model

The calibrated simulation model parameter values are shown in Table A-1 below:

TABLE A-1 Calibrated Parameters using the Dallas Dataset

Parameter	P1	P2	P3	P4	P5	P6	P7	P8	P9	P10	P11
Default	656	-13.1	-9.8	60	0.6	4.9	0.9	13.1	-8.0	-0.35	0.35
Calibrated	1750	-16	-13	12	0.4	6.0	1.3	16	-7	-1.5	1.5

Definitions of the parameters can be found in Figure A-6. Three simulation experiments were conducted with different randomly selected random seeds (42, 19, and 76) for each run. The calibration quality indicators were then averaged through the three simulation runs as show in Table A-2 and Table A-3 for moderate traffic flow and heavy traffic flow, separately.

TABLE A-2 Calibration Quality Indicators Comparison for Moderate Traffic Flow

Measurements	Entering ML from GP and Ramp			No. of HOV Leaving in GP					
	Z4	Z7	Z10	10-min	20-min	30-min	40-min	50-min	1 hour
Field Data	68	91	108	10	15	14	9	11	6
Simulated Data after Calibration	67	95	108	12	17	15	10	11	6

Measurements	No. of HOV Entering from GP leaving in HOV lanes					
	10-min	20-min	30-min	40-min	50-min	1 hour
Field Data	25	26	26	18	18	20
Simulated Data after Calibration	25	26	24	25	16	19

Measurements	Average Speed			
	L1	L2	L3	L4
Field Data	57.1	62.7	63.5	65.9
Simulated Data after Calibration	53.2	57.5	58.2	63.9

TABLE A-3 Calibration Quality Indicators Comparison for Heavy Traffic Flow

Measurements	Entering ML from GP and Ramp			No. of HOV Leaving in GP					
	Z4	Z7	Z10	10-min	20-min	30-min	40-min	50-min	1 hour
Field Data	146	198	235	18	22	35	27	52	34
Simulated Data after Calibration	152	203	234	19	23	32	26	54	41

Measurements	No. of HOV Entering from GP leaving in HOV lanes					
	10-min	20-min	30-min	40-min	50-min	1 hour
Field Data	43	60	53	51	47	28
Simulated Data after Calibration	39	52	49	53	47	27

Measurements	Average Speed			
	L1	L2	L3	L4
Field Data	22.6	27	29.3	32.3
Simulated Data after Calibration	25.3	32.7	35.2	28.7

Simulation Modeling and Calibration Summary

The UTA research team has used this Dallas dataset to build VISSIM simulation models to quantify the weaving effect at the buffer opening area of the HOV facility. They built two different simulation models, one for moderate traffic condition and the other for heavy traffic condition. However, a properly calibrated model should be responsive to various traffic conditions. Therefore, in this study, one simulation model was developed and one set of parameter settings was used to account for all traffic conditions. The simulation results were validated using the ground-truth data manually extracted from the UTA video data. As shown in Tables A-2 and A-3, the simulated results match the observed data reasonably well, indicating that the calibration result is quite satisfactory. The calibrated simulation model was successfully used for the cross-weave analysis in this study.